Flinders
UNIVERSITY

# Biocompatibility and Applicability of Silk Nano-Diamond Films in Wound Healing

*Submitted to the Collage of Science & Engineering for partial fulfilment of credits needed to complete B Engineering (Biomedical) (Honours), M Engineering (Biomedical)*


Author: *Alex Daniel Matušica*

Academic Supervisor: *Youhong Tang*

Project Supervisors: *Dr. Christina Bursill, Dr. Achini Vidanapathirana*

# Declaration

I, Alex Daniel Matušica, hereby declare that this work does not include any images, text or other materials that are no my own, to the best of my knowledge, unless otherwise referenced in text.

All experiments were conducted in accordance to the South Australian Government Animal Welfare Act 1985 and The Best practice methodology in the use of animals for scientific purposes 2017.(Legislation Revision and Publication Act, 2017; NHMRC, 2002)

Ethics: SAM363

**Author:** Alex Daniel Matušica **Signature:**  **Date:** 21/10/19

# Abstract

Wound healing is one of the most important and complex biological processes, with a currently unmet demand for clinical therapies to combat the prevalence of wound healing complications, specifically in patients with diabetes mellitus.(Brem and Tomic-Canic, 2007) Biomaterial scaffolds are a promising avenue for effective wound healing therapies by promoting cell proliferation and vascularisation through integration with the body's own tissue.(Vepari and Kaplan, 2007) The degradability and biocompatibility of silk firoin (SF) makes it a suitable biomaterial for a variety of medical applications, and its effects on accelerated wound healing are cited.(Zhou et al., 2019) A hybrid material of electro-spun silk fibroin impregnated with 100μm Nano-diamonds (NDSF) is investigated for its biocompatibility and wound healing promotion using a humanised mouse model. The characteristic nitrogen vacancy ($NV^-$) centre in specific diamonds opens the door to biosensing through magnetic resonance techniques, and potential diagnostics of wound parameters such as temperature and pH with different methods.(Schrand et al., 2009) This investigation firstly analyses the wound healing promotion of SF in the Murine wound healing model to approximate the human healing equivalent, and then compares results to the NDSF hybrid. Wound closure was measured over a 10-day experiment in addition to doppler blood flow analysis at day 3, 7 and 10 of the experiment. The doppler measurements gave a quantifiable indication of blood perfusion at surface capillaries and vasculature to correlate with influx of cells at the wound milieu. Further histology was used to analyse the wound cross sections for the level of inflammatory infiltrate (granulation zone) as a further indicator of biocompatibility. The results showed that in general the SF scaffold improved the rate of wound healing over the 10-day experiment as compared to control, and the NDSF hybrid did not exhibit the same effect compared to control. Blood perfusion at the wound site exhibited no significant correlation between the presence of treatment vs control. Area calculations of granulation zones in scavenged wound tissue suggest no significant correlation between the presence of either material and the level of inflammatory infiltrate.

# Acknowledgements

I would like to acknowledge the following people for continued guidance, support and contribution for the duration of the project.

Dr. Youhong Tang and Dr. Javad Tavakoli for providing academic support throughout the investigation process and guiding the project in the appropriate direction.

Dr. Christina Bursill and Dr. Achini Vidanapathirana for project support and direction during practical components such as surgical intervention and histology.

Prof. Brant Gibson for support and collaboration and Dr. Asma Khalid for fabricating materials used for the study, and continued collaboration.

# Contents

# Table of Figures

# Introduction

Diabetes mellitus affects approximately 1.7M Australians with a healthcare expenditure upwards of 1.5B. (Australian Institute of Health and Welfare, 2013) The delaying effect diabetes has on wound healing is significant, and diabetic foot ulcers (DFUs) can occur due to unregulated blood sugar, poor blood flow, cigarette and alcohol abuse, nerve damage and a variety of other factors.(Pendsey, 2010) DFU's are characterised by infection, ischemia and neuropathy at the wound site.(Pendsey, 2010) Neuropathy can be the result of damaged intrinsic innervations to the foot muscles reducing natural mobility, shifting foot pressures and manifesting bony prominences leading to tissue breakdown.(Pendsey, 2010) Peripheral vascular diseases (PVD) in diabetic patients are known to occur prematurely, and are mainly attributed to coronary artery disease.(Pendsey, 2010) The resulting ischemia reduces blood perfusion in lower extremities, limiting nutrient supply and waste removal at the site of wounds.(Brem and Tomic-Canic, 2007) Foot infection can go unnoticed in neuropathic patients due to reduced sensation, and the infection can spread to other compartments of the foot.(Pendsey, 2010) Prolonged infection can onset osteomyelitis which is the result of deep tissue infection into the bone marrow.(Pendsey, 2010) DFUs occur in approximately 15% of all diabetes patients, of which 84% will require lower-limb amputation due to healing complications.(Brem and Tomic-Canic, 2007) The rise in diabetes puts increased demand on new and innovative wound healing therapies to be developed that can promote tissue regeneration. Biomaterial scaffolds are heavily researched as a temporary extracellular matrix to replace lost or damaged tissue at the wound milieu.(Boughton and Mclennan, 2013) The important considerations for designing biomaterial scaffolds are to ensure biocompatibility and mitigate the foreign body response, whilst providing a platform for physiological stress transfer, porosity for vascularisation and promotion of immune cell activity. (Boughton and Mclennan, 2013) Given that the scaffold is replacing the ECM, it must attempt to replicate the physical and mechanical properties for acceptance and integration with the body's own tissue.(Boughton and Mclennan, 2013) Proteolytic degradation is an important property of biomaterial scaffolds to ensure the material is completely replaced by biological tissue, and the by-products are expelled from the body.(Howard et al., 2008) The ideal case is a match in the rate of material degradation and tissue growth to prevent the scaffold from acting as a physical barrier, however this is a continuing challenge considering the differing rates of growth between tissues in vivo.(Howard et al., 2008) The field of tissue engineering employs these fundamental scaffold design principles to develop specific scaffolds seeded with pre-programed stem cells.(Howard et al., 2008) Tissue engineering opens the door to potential

re-growth of any tissue within the body, given the appropriate bio-resorptive scaffold and programmable stem cells from the patient's body.(Howard et al., 2008) The implications are enormous, however the issue remains that each case is patient specific, and no perfect biomaterial exists in a standardised form.(O'Brien, 2011) Topical administration of SF has exhibited accelerated healing in mice in comparison to the natural alternative, and the benefits of SF in wound healing are known.(Kumari et al., 2013; Tahir et al., 2017; Vasconcelos et al., 2012) Specifically, SF is known to proteolytically degrade in vivo, provide physical cues on surrounding cells, promote vascularisation and re-epithelialisation, and reduce bleeding due to inherent levels of potassium.(Kumari et al., 2013; Vepari and Kaplan, 2007) By extracting silk from the cocoon of a silkworm, the solution can be electro-spun to produce films consisting of fibres of differing diameters depending on spin parameters, and the β-sheet crystallisation can be selectively induced to control the structure and mechanical properties. (Zhou et al., 2019) By controlling electrospinning parameters the produced films can have tuneable degradability, porosity and fibre thickness to suit the desired environment for integration.(Zhou et al., 2019) Hybrid film materials containing SF have been investigated for their wound healing acceleration potential, some conjugated with naturally derived compounds to replenish depleted stores at the wound site.(Arai et al., 2004; Vasconcelos et al., 2012) An interesting component of film design is that degradation can be coupled with growth factor release, or release of other pre-cursors which may be depleted in chronic non-healing wounds to facilitate the process.(Han and Ceilley, 2017) One interesting space currently being investigated in biotechnology is the use of nitrogen vacancy ($NV^-$) point defects in nano-diamonds (NDs) for biosensing, bio-probing and a variety of other biomedical applications.(Schrand et al., 2009) The unique physical structure of these diamonds exists in an optically and magnetically significant charge state, allowing magnetic resonance techniques to manipulate quantum information and observe the response to determine information on the external environment.(Schrand et al., 2009; Zhang et al., 2018) Several research groups worldwide have been experimenting with these specific NDs and exploit them in different ways to quantify environmental parameters such as electric field strength, temperature and pH.(Fujisaku et al., 2019; Hayashi et al., 2018; Neumann et al., 2013; Sekiguchi et al., 2018) The point defect in these NDs also gives them the ability to fluoresce when excited by the appropriate optical energy, which allows them to be used as target cell markers and fluorescent bio-probes for in vivo applications.(Khalid et al., 2014) There is clear potential for NDs in the medical industry given that they are non-cytotoxic and biocompatible, coupled with the potential for diagnostics or imaging.(Khalid et al., 2014) The unique physical structure of NDs also allows them to be used for protein, hormone or cell

locating through surface modification, useful in combination with fluorescence to identify and destroy target compounds such as cancerous cells.(Schrand et al., 2009)

This investigation discusses the findings from a biomaterial scaffold wound healing study, which focusses on utilizing some of the known properties of SF in healing promotion. Khalid et al., (2014) have developed a silk fibroin nano-diamond hybrid (NDSF) material much like the one investigated here. The findings were that the presence of silk almost doubled the number of emission counts from the $NV^-$ centre, and a mouse study revealed that the NDSF film was non-cytotoxic.(Khalid et al., 2014) Given that the presence of silk significantly improves the number of emission counts during ND fluorescence, the imaging potential of the material is greater in comparison to pure NDs.(Khalid et al., 2014) An NDSF scaffold like the one produced by Khalid et al., (2014) has been used for this investigation, electro-spun by Dr. Khalid & Prof. Gibson for a pilot wound healing study. The non-cytotoxicity of the NDSF material has been validated by Khalid et al., (2014), however given the imaging and diagnostic potential of NDs coupled with the healing acceleration achieved by topical silk administration, it is an important next step to investigate the implications for wound healing.(Khalid et al., 2014) The electro-spun films are of two kinds, pure methanol treated SF, and a methanol treated NDSF hybrid with impregnated 100μm NDs. The two materials are used as treatments in a humanised wound healing model in rodents, the Murine model, which approximates the human equivalent by preventing the contractile wound healing function in rodents and allowing healing strictly through re-epithelization and new cell growth.(Dunn et al., 2013) The effects of SF wound films in a humanized rodent model have not yet been investigated, and although the benefits have been cited, previously used rodent models are poor human comparisons due to discrepancies in the wound healing process.(Dunn et al., 2013) Thus, by observing the effects of SF in this model, local effects can be better compared to the human equivalent and may give new insight into the magnitude of healing acceleration for human wounds. These results act as a bench mark for the SF action and allow a basis for comparison when analysing the effects of NDSF treatment in the same model. The biomaterial scaffolds are not cell seeded, that is, the effects on healing acceleration are studied as purely attributed to the material properties and cellular interactions.

# Literature Review

## Wound Healing Overview

Wound healing in the body is an intricate biological process which is fundamentally described by four overlying phases: Hemostasis, Inflammation, Proliferation and Remodelling.(Guo and DiPietro, 2010) The time period and sequencing of overlapping chronological healing phases has a large impact on successful remodelling and maturation.(Guo and DiPietro, 2010) Therefore, acute natural healing wounds can transition to chronic non-healing wounds due to prolongation or interruption during the four phases, often disease related, such as diabetic ischemia or neuropathy complications.(Guo and DiPietro, 2010)

Hemostasis is immediately onset following cutaneous laceration with preceding vascular constriction, clot formation and release of growth factors and pro-inflammatory cytokines.(Guo and DiPietro, 2010) Transforming growth factor (TGF-$\beta$), epidermal growth factor (EGF), fibroblast growth factor (FGF) and platelet-derived growth factor (PDGF) are released at the wound site for bleeding control and to facilitate important reactions during the Hemostasis phase.(Guo and DiPietro, 2010) Hemostasis must immediately control bleeding through vasoconstriction, platelet aggregation and formation of fibrin to prevent blood loss.(Guo and DiPietro, 2010)

The Inflammatory stage is onset by wound site infiltration of neutrophils, lymphocytes an macrophages.(Guo and DiPietro, 2010) Neutrophil release facilitates the removal of cell debris and the inflammatory infiltrate collectively promotes release of lysosomes and reactive oxygen species.(Gonzalez et al., 2016) Macrophages initiate cytokine release at the wound site for leukocyte activation and apoptotic cell clearance in the premature wound.(Guo and DiPietro, 2010) Macrophages induce phenotypic transitions in apoptotic cells which promotes keratinocyte, fibroblast and angiogenesis activity for tissue remodelling(Guo and DiPietro, 2010). Macrophage activity at the wound site mediates the transition from the inflammation phase into tissue Remodelling, for a normal biological wound healing process.(Guo and DiPietro, 2010)

T-lymphocyte influx at the wound occurs after macrophage and inflammatory cell infiltration, and the highest concentration is observed during early remodelling.(Guo and DiPietro, 2010) Although the action of T-lymphocyte infiltration is not conclusive, studies suggest delayed release or low concentrations at the wound site contribute to impaired wound

healing. (Guo and DiPietro, 2010) Dendritic epidermal T-cells (DETC) are known to preserve tissue integrity, defend pathogen invasion and regulate inflammation upon activation.(Guo and DiPietro, 2010) DETC activation is facilitated by damaged keratinocytes and produce (FGF-7), insulin-like growth factor-1 and keratinocyte growth factors to aid cell survival and proliferation of keratinocytes.(Guo and DiPietro, 2010) Interactions between keratinocytes and DETC is known to help maintain wound healing, hence keratinocyte proliferation and wound closure are delayed as a result of defective or lacking DETC at the wound milieu.(Guo and DiPietro, 2010)

The proliferative phase is characterised by re-epithelialisation and construction of an early phase extracellular matrix.(Guo and DiPietro, 2010)

Fibroblasts and endothelial cells aid in collagen production, formation of capillaries, granulation tissue, glycosaminoglycan and proteoglycan production at the wound site.(Guo and DiPietro, 2010) Glycosaminoglycans and proteoglycans are important structural components of the ECM, and the remodelling phase of the ECM can last several years.(Guo and DiPietro, 2010) The ECM synthesis attempts to replicate the pre-trauma microarchitecture of tissue and increase the vascular density.(Guo and DiPietro, 2010)

## pH in Wound Healing

It is known that the pH value of a wound governs important biochemical reactions throughout the healing timeline, and consequently pH information is an important diagnostic tool.(Schneider et al., 2007) Although pH is recognized as a clinically significant marker, the actual variance in relation to time is complicated and influenced heavily by patient specific endogenous and exogenous factors.(Schneider et al., 2007) pH is defined as the negative logarithm of hydrogen ions H+ present in solution at the site (pH=log(H+)) ranging 0-14.(Schneider et al., 2007) Metabolic activity within the wound at different time points has peak activity at specific pH values corresponding to active proteins.(Schneider et al., 2007) Under normal conditions, the pH of skin is between 4-6 (acidic) controlled by keratinocyte fatty acid secretion and the lactate-bicarbonate buffer system which in turn is influenced by anatomical location and age.(Schneider et al., 2007) Wounds disrupt the acidic pH of skin, exposing the internal pH of 7.4 resulting in candida bacteria colonisation due to the alkaline pH of the wound milieu.(Schneider et al., 2007) Therefore, application of acidic agents to the wound site cause a diminished bacterial load at the skin interface, however the connection between bacterial colonisation and delayed healing is not conclusive, although, presence is known to delay healing of chronic wounds.(Schneider et al., 2007) Therefore, reducing wound

pH is a clinically practiced concept for therapeutic measures regarding wounds, for prevention of staphylococcus aureus colonisation, which is similar to the body's natural physiological wound healing mechanism.(Schneider et al., 2007) Chronic wounds have been recorded to have a pH in the range of 7.15-8.9, therefore the length of time in which the wound milieu remains in this alkaline state governs the transition from an acute to chronic wound.(Gethin, 2007) Schneider et al., (2007) has produced an elegant graph explaining the pH variations in chronic and acute wounds shown in Figure 1 - pH in Acute and Chronic Wounds (Schneider et al., 2007).

**This image has been removed due to copyright restrictions.**

*Figure 1 - pH in Acute and Chronic Wounds (Schneider et al., 2007)*

From the data, there are distinct differences in the pH fluctuation for acute and chronic wounds, hence pH as a diagnostic tool is useful and significant for proceeding intervention.

# Temperature in Wound Healing

Temperature plays an important role in the wound healing process, specifically for optimal function of epithelial cell, neutrophil and fibroblast activity.(McGuiness et al., 2004) Sub core body temperatures at the wound milieu impact the healing rate and efficiency of the wound via reduced collagen deposition, slow epithelial repair and inflammatory cell and fibroblast influx.(McGuiness et al., 2004) Impedance or delay of these biological processes contributes to increased risk of infection and results in a ~2.6 day increase in hospital time for patients in comparison to patients with near core-body temperatures at the wound milieu.(McGuiness et al., 2004) Through in-vitro experimentation it has been determined that the critical temperature at which these cellular processes are impeded is 33°C.(McGuiness et al., 2004) Additionally, an improvement in healing has been exhibited by warming the wound site toward core temperatures increasing blood flow, immune cell function, deposition of collagen and partial pressure of oxygen supplied.(McGuiness et al., 2004) The literature suggests that wound healing is optimal at normal core body temperatures of 36°-38°C, with delayed healing onset by temperatures outside this range.(McGuiness et al., 2004) For these reasons, it seems logical that wound temperature is an important clinical parameter for assessing the state of a patient wound. Standard clinical practice is to utilize wound dressings to elevate wound temperature through heating and to aid the process with therapeutic agents.(McGuiness et al., 2004) Wound dressings which successfully maintain the milieu at core temperatures have shown an 108% increase in epidermal layer cell division.(McGuiness et al., 2004) However, the influence of periodic wound cleansing and dressing changes on temperature is significant,

as investigated by McGuiness et al., (2004). With little change in ambient temperatures of between 18-24°C,(McGuiness et al., 2004) McGuiness et al., (2004) found that out of 44 patients with trauma or surgical debridement originating wounds, the average dressing surface temperature was 29.5°C for a variety of commonly used dressings.(McGuiness et al., 2004) The temperature of the wound bed directly after dressing removal yielded an average below 33°C (32.6°C) with a range of (25.3-37.3°C).(McGuiness et al., 2004) Furthermore, routine saline cleansing of the wound resulted in an additional drop of 2°C, collectively giving an average temperature drop of 2.7°C from the dressing surface value.(McGuiness et al., 2004) Previous studies suggest that once core temperatures are recovered at the wound bed following a dressing change, it takes 3-4 hours for leucocyte activity and cell division to resume, which is significant when considering periodic changes to accommodate varying wound types.(McGuiness et al., 2004) Hence, it is beneficial to identify novel methods of wound cleansing and therapeutics that mitigate these processes.

# Current Wound Healing Therapies

## Dressings and ointments

Wound infection is a complication of untreated or non-healing wounds with a bacteria threshold of $10^5$ being recognised clinically as the onset of infection and healing impedance.(Han and Ceilley, 2017) Silver has been an agent used in wound dressings for over 2000 years due to its antimicrobial properties for the prevention of further bacterial colonisation.(Han and Ceilley, 2017) Although the benefits of silver are recognised in bacterial growth impedance, recent studies suggest that silver sulfadiazine has no significant effect on overall wound healing due to the high concentration required for continuous release to maintain efficacy.(Han and Ceilley, 2017) Iodine based compounds are also used for clinical wound healing therapy with a significant amount of data supporting its benefits for small wounds, however for larger wound areas toxicity becomes a concern.(Han and Ceilley, 2017) Antibiotic ointments are used for topical application at wound sites, however several studies suggest that periodic administration results in patient discomfort with potential dermatitis and antibiotic resistance with results no better than cases of single use administration.(Han and Ceilley, 2017) Due to the uncertain significance of topical antibiotics for prevention of infection in clinical settings, it is often used to target already infected wounds and not necessarily as a preventative measure.(Han and Ceilley, 2017) Debridement is an important practice in wound care through surgical mechanisms or enzymatic methods in order to expose

viable tissue and remove impeding damaged tissue from the wound site to prevent accelerated infection.(Han and Ceilley, 2017) Exposure of the viable tissue allows the un-impeded and well perfused viable tissue to proliferate and repopulate the tissue milieu.(Han and Ceilley, 2017) The application of maggots to a wound site is a procedure recently investigated due to the simultaneous effect of mechanical and enzymatic debridement in addition to eliminating pathogens and promoting fibroblast proliferation, however further research is needed for its conclusive overall effect.(Han and Ceilley, 2017)

Moist wound dressings provide low oxygen tension environments by occlusion, promoting hypoxia inducible factor-1 and facilitating re-epithelialization.(Han and Ceilley, 2017) Dry wound dressings inhibit autolytic debridement at the wound milieu in addition to potentially causing further tissue damage on removal do to adherence to the wound tissue.(Han and Ceilley, 2017) The aims of a moist dressing are to have low adherence, be semipermeable to water and air vapour whilst inhibiting fluid and pathogens.(Han and Ceilley, 2017) Hydrophilic dressings (hydrocolloids and hydrogels) exploit the tendency to remain moist over long time periods whist removing additional exudate, however hydrocolloids are known to have low permeability to air and consequently are generally not used for exudate wounds.(Han and Ceilley, 2017) Exudative wounds are often treated with hydrogels for increased moisture in addition to alginate dressings (seaweed derived) which are known to have high water absorption.(Han and Ceilley, 2017) Therapeutic foams are also helpful to increase moisture and bypass the increased tissue damage associated with wound dressing replacement.(Han and Ceilley, 2017) Collagen based products are an alternative therapy which directly influences the wound milieu by attracting important cells and diminishing free radicals and proteases.(Han and Ceilley, 2017) Recent remedies for would healing have involved anti-microbial doping of moist dressings such as hydrogels or even foams to target the issue of biofilm production.(Han and Ceilley, 2017) Biofilms are created by pathogen adherence creating a barrier between the wound and therapeutic dressing, resulting in reduced antibiotic efficacy and prolongation of the inflammatory phase in healing.(Han and Ceilley, 2017) The benefits of antimicrobial dressings can be mostly exploited in chronic pressure ulcers as opposed to acute cases.(Han and Ceilley, 2017)

## Skin substitutes

Skin substitutes for wound therapy are used for grafts, commonly from autologous sources to prevent a foreign body response to non-native tissue.(Han and Ceilley, 2017) A recently developed material from infant foreskin tissue uses fibroblasts to activate growth factors, cytokines, glycosaminoglycans and collagen for healing promotion.(Han and Ceilley, 2017) A

cultured skin Apligraft is another allogenic therapy which replaces the traumatised dermal layer in patients containing bovine collagen and keratinocytes which integrates well with native wound tissue. (Han and Ceilley, 2017) The material has shown to increase blood flow to the site up to 70% and is a treatment used for DFUs to combat ischemia. (Han and Ceilley, 2017) Nevertheless, the cultured Aligraft is a costly venture for patients and is therefore not a solution for all patients.(Han and Ceilley, 2017) The alternative Omnigraft is effective for burn victims and consists of collagen, glycosaminoglycans and chondroitin-6 sulphate which has shown to increase wound closure up to 50% in comparison to standard care.(Han and Ceilley, 2017) However, these substitutes are not the most economic option and require heavy processing and preparation, and thus used for severe cases in patient chronic wounds. (Han and Ceilley, 2017)

## Negative pressure therapy (NPT)

This method of wound therapy uses a device to moisten the environment whilst simultaneously pressuring the wound for facilitated closure, optimising blood flow and removing exudates.(Han and Ceilley, 2017) NPT exhibits reduced rates of infection for treated chronic wounds.(Han and Ceilley, 2017) In comparison with traditional wound dressings, NPT is costly and requires almost daily maintenance for replacement of the foam dressing and evacuation tube.(Han and Ceilley, 2017) Nevertheless, the benefits of NPT are seen in acute care burn units and volume reduction of the wound, simplifying any proceeding surgical intervention.(Han and Ceilley, 2017)

## Growth Factors

Growth factor therapy is a chronic wound therapy which attempts to facilitate the process through replenishment of depleted growth factors and pre-cursors at the site, for it is known that chronic wounds exhibit depleted levels of tumor necrosis factor-α, fibroblast growth factor , vascular endothelial growth factor and transforming growth factor-β.(Han and Ceilley, 2017) Application of Insulin-like growth factor-1 has shown good results for treatment of chronic wounds in addition to other literature showing the benefits of other hormones or cytokines for treatment of these conditions.(Emmerson et al., 2012; Lima et al., 2012) However, standardization of this type of treatment in a clinical setting is difficult given the variation in experiments conducted in literature, making it difficult to correlate results, growth factor used and ideal scenario.(Han and Ceilley, 2017) Becaplermin is one commercially available platelet derived growth factor based gel used for treatment of wounds.(Han and Ceilley, 2017)

## Hyperbaric Oxygen

Hyperbaric oxygen therapy involves systemic oxygen delivery by placing patients in a chamber on the basis that this method facilities fibroblast proliferation, angiogenesis and immune function.(Han and Ceilley, 2017) However, local delivery does not yield the same effects and the hyperbaric oxygen chamber therapy side effects can be severe; oxygen toxicity induced seizures and myopia.(Han and Ceilley, 2017)

## Tissue Scaffolds

Material scaffolds for soft tissue repair are a promising avenue for treatment of lesions and chronic wounds by mimicking dermis structure and function. (Boughton and Mclennan, 2013) Common practice for biomaterial scaffold therapy is to produce biocompatible scaffolds with bioactive molecules such as growth factors or collagen for extracellular matrix (ECM) replacement.(Boughton and Mclennan, 2013) It is important for the scaffold to act as a temporary ECM in addition to promoting growth, immune cell infiltration and cell proliferation.(Boughton and Mclennan, 2013) The formation of new tissue at the site of trauma can also be coupled with bioresorption of the scaffold such that the structure is completely replaced by the body's own tissue.(Boughton and Mclennan, 2013) Fluid exchange and cell integration is also important for regeneration and remodelling of the ECM.(Boughton and Mclennan, 2013) The scaffold should ideally provide a framework that protects new tissue against infection, elasticity and compression whilst being integrated with surrounding tissue.(Boughton and Mclennan, 2013) Encouragement of new cell growth and vascularisation are key attributes which can determine the success regeneration. (Boughton and Mclennan, 2013) The scaffold should also act to minimise the foreign body response and be accepted by the immune system.(Boughton and Mclennan, 2013) Given that the aim of the scaffold is to behave as a temporary ECM, physiological stress should be transferred between the material and surrounding tissue such that the body accepts it as a temporary ECM and integration is improved.(Boughton and Mclennan, 2013) Material selection is an important consideration for the scaffold to prevent bacterial colonisation whilst allowing nutrient delivery for cells and removal of waste products.(Boughton and Mclennan, 2013) Due to the substantial demands for a successful biomaterial scaffold, continuing research aims to identify the most suitable scaffold materials for specific types of trauma, to ensure that the presence of the material itself does not begin to inhibit the healing process by a mismatch of degradation to proliferation or adverse effects.(Vepari and Kaplan, 2007) Some FDA approved allogeneic skin substitute scaffolds for dermal repair are already available, which utilize either natural cell-derived materials or scaffolds designed specifically to mimic the ECM for bodily

acceptance.(Boughton and Mclennan, 2013) However, given the DNA mismatch between the seeded allogeneic cells and the patient, the immune response can be significant and rejection is a possibility.(Lakkis and Lechler, 2013)

## Silk Fibroin

Silk fibroin is an organic protein and the characteristics are suitable for a variety of medical applications, such as gels, films, sponges biosensors and tissue scaffolds in regenerative medicine.(Vepari and Kaplan, 2007) Natural silk fibre is comprised of proteins fibroin and sericin, which both contain the same 18 amino acids in different concentrations.(Cao and Wang, 2009) Fibroins make up the core of silk fibres and are encased in sericin which is a hydrophilic protein which adheres two fibroin fibres.(Cao and Wang, 2009) The fibroin molecule contains a crystalline component of 2/3 and an amorphous component of 1/3, with the crystalline portion creating antiparallel β-sheet formations which contribute to the mechanical properties of silk fibres.(Cao and Wang, 2009)

Silk fibroin (SF) exists in two stable secondary structures, a random-coil amorphous structure (Silk I) and an antiparallel β-sheet structure (Silk II).(Cao and Wang, 2009) The β-sheet crystallisation of Silk II is formed through hydrogen bonds between neighbouring peptide chains.(Cao and Wang, 2009) SF can be extracted directly from a silkworm cocoon through protein extraction and then used for electrospinning.(Zhou et al., 2019) The amorphous SF structure can be easily converted to the β-sheet structure through methanol or potassium chloride treatment, with one side containing glycine originating hydrogen side chains and the other side occupied by alanine originating methyl side chains.(Vepari and Kaplan, 2007) The hydrogen and methyl groups of opposing sheets form an interface of stacking crystals, with van der Waals interactions and strong hydrogen bonds rendering the $\beta$-sheet structure thermodynamically stable.(Vepari and Kaplan, 2007).

In vivo, the silk $\beta$-sheet structures biodegrade primarily into nanofibrils and then nanofilaments by protease XIV, with the number of $\beta$-sheets being positively correlated to degradability resistance.(Numata et al., 2010) Silk biomaterials are heavily investigated due to the inherent properties of flexibility, proteolytic biodegradability, non-cytotoxicity, biocompatibility and ability to immobilize growth factors through amino acid side change alteration.(Vepari and Kaplan, 2007) Silk scaffold design must consider physical cues on neighbouring cells, cell adhesion, facilitation of angiogenesis through porosity and immune acceptable, and scaffold degradation rate to compliment new tissue growth.(Vepari and

Kaplan, 2007) The mechanical properties of silk can be seen in Figure 2. This **image has been removed due to copyright restrictions.**

Figure 2 - Mechanical Properties of Silk (Vepari and Kaplan, 2007).

**This image has been removed due to copyright restrictions.**

*Figure 2 - Mechanical Properties of Silk (Vepari and Kaplan, 2007)*

Chemical modification of silk fibres through amino acid side chains is common practice to alter the surface structure for target cell recognition, immobilization of growth factors in vivo or mineralization.(Vepari and Kaplan, 2007) The benefits of electrospinning SF solutions are tuneable degradability through structure modification, tuneable porosity to facilitate vascularisation and tuneable mechanical properties for interactions with native cells.(Zhou et al., 2019) The spin parameters dictate the outcomes of the fabricated scaffold, and due to the versatility possible with electrospinning techniques, this method of scaffold design is continually researched.(Zhou et al., 2019)

# Relevant studies

Tahir et al., (2017) investigates the wound healing effects of topically administered spider silk on a full thickness wounds in mice over a 20-day period. The spider silk treatment was compared against topically administered povidone-iodine, honey and turmeric as therapeutic agents.(Tahir et al., 2017) The treatments were administered once every two days for each group of five animals, and a sterile bandage was then used to cover the area.(Tahir et al., 2017) Wound area measurements were performed every two days to determine the level of closure and the results showed that the administration of silk caused ~95% closure in 14 days as opposed to 20 days for natural wound healing.(Tahir et al., 2017) The silk treatment also outperformed the honey and turmeric treatments which exhibited healing around 18 days.(Tahir et al., 2017) Another study conducted into the effects of silk fibroin (SF) and elastin (EL) hybrid scaffolds on burn wounds by Vasconcelos et al., (2012) suggests that the addition of elastin had remarkable healing results.(Vasconcelos et al., 2012) The study was conducted on full thickness in-vitro skin substitutes (EpidermFT) with three concentration ratios, pure silk fibroin, 80/20 SF/EL and 50/50 SF/EL.(Vasconcelos et al., 2012) The most successful treatment was the 50/50 SF/EL scaffold which exhibited improved wound healing in comparison to pure silk and the 80/20 SF/EF material.(Vasconcelos et al., 2012) Topical spider silk treatment for wound healing is a procedure practiced in India, and a rat study

conducted by Kumari et al., (2013) further demonstrates the benefits of silk administration in comparison to povidone-iodine and natural wound healing. Histological analysis revealed reduced scabbing and ulcer formation in addition to accelerated wound healing for the silk group as opposed to control.(Kumari et al., 2013) The presence of vitamin K in natural silk is thought to contribute to enhanced blood clotting and reduced bleeding.(Kumari et al., 2013) Gil et al., (2013) found that silk biomaterials with epidermal growth factor and silver sulfadiazine exhibited accelerated wound healing in a rodent model in addition to higher rates of re-epithelialisation, collagen synthesis, dermis formation and reduced scar tissue in comparison to control and hydrocolloid dressing.

## Nano Diamonds & Optically Detected Magnetic Resonance

Some of the inherent properties of fluorescent Nano-Diamonds(NDs) have resulted in recent interest within the scientific community over the last decade.(Schrand et al., 2009) NDs with a nitrogen vacancy (NV) centre consist of a substitutional nitrogen atom within the carbon lattice.(Schrand et al., 2009) This unique structure of NDs allows for single photon emission of up to $10^7$ counts per second with optical excitation, and stable emission at room temperature.(Schrand et al., 2009) The NV point defects in NDs can exist in two magnetically and optically separate charge states, neutral ($NV^0$) and negatively charged ($NV^-$).(Zhang et al., 2018) The negatively charged NV state is of particular interest due to its strong optical signal through quantum information processing.(Zhang et al., 2018) ND's characteristic nitrogen vacancy (NV) centre, in addition to non-cytotoxicity and high biocompatibility, allows them to be exploited in a wide range of biomedical application such as sensing, pH-controlled drug delivery and imaging.(Schrand et al., 2009) NDs can also be synthesized artificially within a laboratory at low cost through detonation synthesis.(Schrand et al., 2009) Due to surface reactions with synthesized NDs, they have been used in some cases as biomedical probes, sensors and additives for intensification of other components in vivo.(Schrand et al., 2009) Purified NDs have the capability of normalizing blood pressure, aid in cancerous conditions and detoxify the gastrointestinal tract.(Schrand et al., 2009) The unique surface structure of NDs has several unpaired electrons rendering them capable of binding with free radicals in blood and tissues which are associated with serious illnesses.(Schrand et al., 2009) The large specific surface area coupled with high affinity allow NDs to easily absorb proteins and other molecules in the body.(Schrand et al., 2009) The large surface area of NDs has an inclination to absorb and attach to bacteria and viruses destroying them.(Schrand et al., 2009) During purification and modification of NDs in synthesis, several oxygen functional groups are developed on the surface resulting in

hydrophilicity promoting aqueous dispersion.(Schrand et al., 2009) These synthesis and purification techniques allow NDs to be sterilized safely for medical purposes at high temperatures, and stored in liquid nitrogen without impacting the crystalline structure. (Schrand et al., 2009) ND surface structure modification is special tool that allows integration with other matrices to allow binding with selected biological materials, such as target proteins, hormones, enzymes, DNA, antigens, or drugs.(Schrand et al., 2009) The optical properties of NDs allow them to be used for detection and imaging for both in-vitro and in-vivo applications with and without surface modification.(Schrand et al., 2009) Non photobleaching florescence is achieved by optical illumination of NDs for cell or biological molecule detection and tracking without damage to living cells.(Schrand et al., 2009) The high biocompatibility, non-cytotoxicity and photobleaching immunity of NDs is converse to alternative nanoparticles used for imaging such as organic dies, quantum dots and fluorescent proteins.(Khalid et al., 2014) Another avenue for NDs in biomedical applications is wear resistant coatings for metallic impact coatings through tuneable surface roughness and hardness, reducing the friction coefficient of articulating surfaces.(Schrand et al., 2009) Tuneability of the surface microarchitecture also allows NDs to be used for polishing hard and soft surfaces.(Schrand et al., 2009)

The $NV^-$ defect in diamond is exploited for its unique optical and magnetic properties in optically detected magnetic resonance imaging (ODMRI).(Zhang et al., 2018) When the NV centre is illuminated by a green laser ( $\lambda \approx 532$nm) this causes red fluorescence ( $\lambda \approx 650$-850nm) as electrons release photons of energy to the environment.(Zhang et al., 2018) Due to the unique characteristics of the ND the NV centre electron spins behave independently of the surrounding lattice allowing long coherence times in which the phase of quantum spins remains predictable.(Zhang et al., 2018)

By referring to Figure 3, an explanation of the events within the NV centre can be derived. The excited state $|e\rangle$ exists 1.945eV from the ground state $|g\rangle$ corresponding to a frequency of 2.87GHz between the $m_s=0$ and $m_s=\pm 1$ substrates.(Zhang et al., 2018) When exposed to an external magnetic field in ODMR, NV electrons act as dipoles aligning themselves parallel (low energy $\alpha$ spin state) or anti parallel (high energy $\beta$ spin state) and there is a Zeeman shift.(Zhang et al., 2018) The Zeeman shift is the energy difference between electrons in $\alpha$ and $\beta$ spin states and increases proportionally with magnetic field strength.(Zhang et al., 2018) Green laser light with a photon energy of 2.4eV ( $\lambda \approx 532$nm) excites ground state $|g\rangle$ electrons to the excited $|e\rangle$ state giving them 1.945eV of energy, with excess energy

contributing to NV centre vibrational motion.(Zhang et al., 2018) Vibrational energy transfers to excited electrons disperses within the lattice quickly, whilst electronic energy (13ns lifetime) is converted to single photon emissions upon ground state transition from the excited state.(Zhang et al., 2018) The 13ns lifetime of excited electrons facilitates several cycles of excitation/emission upon laser pumping, with a $10^7$ red photons/second emission achievable from a single NV centre.(Zhang et al., 2018)

**This image has been removed due to copyright restrictions.**

*Figure 3 - NV Centre Energy State Diagram (Zhang et al., 2018)*

Green photons move electrons in the ground state to the excited state (green arrow) and fall back to the ground state releasing red photons (red arrow) whist preserving their spin state in the external magnetic field.(Zhang et al., 2018) The long lived spin state $|s\rangle$ is populated only through non-radiative transitioning, whereas green illumination results in favoured population of the $m_s$=0 ground state.(Zhang et al., 2018)The probability of $|e\rangle$ to $|s\rangle$ transitioning is in increased when the NV centre exists in the $m_s$=±1 state as opposed to the $m_s$=0 ground state.(Zhang et al., 2018) Therefore, the average fluorescence observed is reduced by NV centres in the $m_s$=±1 state as a result of electrons existing for long time periods in the $|s\rangle$ state – the non-radiative transition.(Zhang et al., 2018) The significance of this is that through optical pumping the NV centre can be physically transformed to the $m_s$=0 state, and the resulting average florescence is significantly less in comparison to the $m_s$=±1 state.(Zhang et al., 2018) The inhabitancy of $m_s$=0 and $m_s$=±1 substrates can be changed with microwave pumping of 2.87GHz in ambient conditions, however this resonant frequency is temperature dependent.(Zhang et al., 2018) It is known that the resonant frequency of the NV centre is dependent on the external magnetic field, electric field and temperature, allowing either one of these parameters to be identified through keeping the others constant.(Hayashi et al., 2018)

Sekiguchi et al., (2018) was able to utilize NDs to determine the temperature inside a single-cell with ±1° resolution, demonstrating that the thermosensing capabilities are not influenced by environmental pH, cellular interactions, ion concentrations or any other environmental factors. The ODMR technique was employed to identify the characteristic fluorescence intensity dip upon microwave pumping relative to resonant frequency, which is attributed to environmental temperature.(Sekiguchi et al., 2018) An analysis of temperature sensing using ODMR techniques is further explored by Neumann et al., (2013), discussing future developments in biomedical probes and thermosensing nano-scale devices. A recent study

produced by Fujisaku et al., (2019) found that the T1 relaxation times of electron spins in NDs coated in an ionic layer of carboxyl groups are dependent on environmental pH. Consequently Fujisaku et al., (2019) was able to create a nanoscale pH sensing device by experimentally determining the relationship between electron relaxation time T1 and the pH value. This is a remarkable outcome of continuing research into nanoscale biosensing using the unique properties of NDs and based on recently published techniques on temperature and pH sensing the outcomes will continue to be observed in the biomedical field.

## Research Gap

Nano diamonds (NDs) and silk fibroin (SF) are both cited to be biocompatible and non-cytotoxic by extensive literature, as the application of both has been studied for a variety of medical applications.(Vepari and Kaplan, 2007; Zhu et al., 2012) Given the prevalence of diabetes mellitus (DM) across the globe and DM facilitated chronic wound development in lower limb ulceration, there is a necessity to investigate potential therapies to accommodate failed wound healing in DM patients to improve mortality rates overall.(Guo and DiPietro, 2010) The known benefits of SF as a biomaterial and the biosensing potential of NDs make the combination an interesting hybrid to investigate for the production of a therapeutic wound dressing which promotes healthy wound healing in patients.(Arai et al., 2004; Guo and DiPietro, 2010) SF is already cited to have success as a wound dressing and the systemic and local effects of NDs have been investigated by literature, hence there is motivation to initially investigate how the hybrid combination behaves in in-vivo wound healing conditions to assess its potential as a therapeutic wound dressing. There is currently no literature which underlines the biocompatibility and inflammatory cell behaviour in response to a hybrid of NDSF used in wound healing. The motivation for the SF component stems from extensive literature citing its successful use in tissue engineering applications, where the immune response is controlled, and the material is accepted.(Cao and Wang, 2009) Additionally, electrospinning SF allows for $\beta$-sheet crystallinity in addition to methanol or potassium chloride induced polymorphism to increase resistance to bioresorption, consequently the SF scaffold can be selectively tuned to degrade at an appropriate rate for its application, e.g. tissue scaffold, suture, drug delivery vehicle.(Vepari and Kaplan, 2007) This aspect makes SF appealing as the primary scaffold for a therapeutic wound dressing, given that bioresorption can be tuned to match the rate of angiogenesis and re-epithelialization of the wound site to prevent its presence becoming a barrier to wound closure.(Vepari and Kaplan, 2007) The concept of degradation re-epithelialization matching is heavily researched in tissue engineering applications in order to ensure the scaffold provides temporary and sufficient

support as an artificial ECM to act as a medium for new cell growth.(Howard et al., 2008) However one of the largest challenges faced in the field of regenerative medicine is achieving versatility with temporary scaffolds, as expected.(Howard et al., 2008) The scaffold must satisfy the role of the original lost ECM for its targeted tissue, and mechanical properties between different biological hard and soft tissues vary greatly.(Howard et al., 2008) As a result successful scaffolds used in regenerative medicine are tailored solutions to both the individual patient physiology (such as bone microarchitecture) and target tissue for regeneration.(Howard et al., 2008) The use of SF in a wound dressing application somewhat mitigates the difficulty of degradation re-epithelialization matching because the material does not need to function mechanically as a strong temporary versatile ECM which must satisfy a variety of mechanical properties governed by target regeneration tissue.(Howard et al., 2008) The SF wound dressing must temporarily function as a replacement dermis ECM by promoting angiogenesis through porosity and physical ques.(Howard et al., 2008)

# Aims

The aim of the study conducted is to validate the biocompatibility of SF scaffolding, which is heavily supported by the literature, in addition to measuring the biocompatibility of a new silk-fibroin Nano-diamond hybrid scaffold (NDSF) never before investigated for its biocompatibility in a wound healing model.(Altman et al., 2003; Cao and Wang, 2009; Kaplan et al., 2010; Lindsay S. Wray et al., 2011; Wang et al., 2006; Yang et al., 2007) It is known that the $NV^-$ centre characteristic of ND's opens the door to biosensing through magnetic resonance techniques.(Khalid et al., 2014; Sekiguchi et al., 2018) The theory behind testing the biocompatibility of the NDSF hybrid scaffold is that if no adverse effects are observed throughout, and the healing rate is comparable to that of pure methanol treated SF scaffolds, the results can be used to validate the hybrid as viable for further study to exploit the benefits of individual constituents. Several parameters are considered throughout experimentation in order to ultimately help asses biocompatibility, in addition to using the SF scaffolds as a base for comparison. The most fundamental of parameters tested is wound area closure in the wound healing model employed, in addition to blood perfusion and inflammatory cell infiltrate at the site. The collaboration of these parameters both on a specimen and sample level are analysed in order to draw the most relevant observations and suggested outcomes. Given the preliminary research conducted on NDSF scaffolds by Khalid et al., (2014) this project serves as a further investigation into the material to lay the next foundation for

continuing research into potential benefits. The long-term goals of the wound healing research of the material are predicated on the results and observations of this study, in order to pave the correct path for applications of this material. By applying the experimental wound healing methodology to both SF and NDSF methanol treated scaffolds, there is a basis for comparison by virtue of extensive silk based biomaterials literature.(Altman et al., 2003; Cao and Wang, 2009; Wang et al., 2006) Preliminary aims for the wound healing study are to establish similarities in the roles of NDSF and SF scaffolds in wound healing using the established Murine model.(Dunn et al., 2013)

# Theoretical Methodology

The method of execution for the biocompatibility study is to employ an adapted Murine wound healing model by Dunn et al., (2013) on a sample size of *n* *C*57BL/6J adult mice over a period of 10 days with day 0 referencing the day of surgery. The Murine mouse model exhibited in Figure 4 entails the surgical procedures, measurement techniques and criteria to monitor wound closure of two lacerations made on the posterior of a rodent above the Spinotrapezius, Latissimus dorsi or External oblique muscle regions governed by specimen anatomy upon intervention.(Dunn et al., 2013) The most influencing discrepancy between human and mouse wound healing is that mouse wounds heal predominantly through contraction of the panniculus carnosus (lacking in humans), converse to re-epithelialization, angiogenesis and cell proliferation which are the main healing processes observed in human wounds.(Dunn et al., 2013; Scherer et al., 2008) For a valid comparison of human wound healing to that of a mouse, the contraction is inhibited in this model permitting wound healing through re-epithelialization, angiogenesis and cell proliferation only, to mimic the human equivalent.(Dunn et al., 2013) In order to account for significant specimen variability, the model employs both a control and treatment wound on each mouse allowing normalization of treatment results with control data from the same specimen.(Dunn et al., 2013) Hair covering the dorsum of the mouse must first be removed using a shaver and hair removal cream to expose smooth skin and assist in surgery.(Dunn et al., 2013) Two circular incisions are marked out using a biopsy punch (suggested 5mm) on each side of the midline for guidance, after swabbing the region with alcohol.(Dunn et al., 2013) The biopsy markings are carefully followed removing two circles of skin by pinching the centre and pulling upwards using forceps.(Dunn et al., 2013) The model incorporates silicon fixtures to the wound's surrounding skin held static through an adhesive skin-silicon barrier by superglue, and

further held in place by sutures as exhibited in Figure 4. Furthermore, a layer of clear Opsite dressing is adhered to the top of the silicone ring, reducing the likelihood of pathogens entering the wound during the 10 day experiment.(Dunn et al., 2013) Following surgery the wound diameter is measured on the x, y and diagonal axes daily such that the three diameter measurements can be averaged to calculate an average daily wound area using $A = \pi r^2$ for each wound for each mouse.(Dunn et al., 2013)

**This image has been removed due to copyright restrictions.**

*Figure 4 - Murine Model Procedure (Dunn et al., 2013)*

# Practical Methodology

The first biocompatibility study using the Murine model had a sample size of $n$=7 C57BL/6J adult mice, with three mice receiving the SF treatment and 4 receiving the NDSF treatment to the right wound. The electrospinning parameters of treatment scaffolds used are shown in Table 1 - Scaffold Spin Parameters:

| | **Concentration and Electrospinning Parameters for Methanol Treated SF & NDSF Films Using Disc Collector** | | | | | | |
|---|---|---|---|---|---|---|---|
| | **SF Concentration** | **ND Volume** | **Polyethylene Oxide (Polymer) Concentration** | **Needle to collector potential (kV)** | **Collector Distance (cm)** | **Collection Rate (ml/min)** | **Collection Time (Hrs)** |
| **SF** | **3ml (6.5-7%)** | **-** | **0.5ml (5%)** | **12** | **12** | **0.04** | **1.15** |
| **NDSF** | **3ml (6.5-7%)** | **150µL** | **0.7ml (5%)** | **12** | **12** | **0.04** | **1** |

*Table 1 - Scaffold Spin Parameters*

The SF and NDSF films were sliced using a 4mm diameter biopsy punch to produce the circular films observed in the Appendix Treatment Films. An important note to consider is that the electro-spun films were methanol treated to promote β-sheet crystallinity and thus increase the degradation time, which is an important factor in the success of scaffold facilitated wound healing.(Altman et al., 2003) The non-methanol treated films resulted in a ~5 minute degradation time in a bath of phosphate-buffered saline (PBS), which can produce no

measurable benefit to the wound healing process given that the superficial wounds tested take days to demonstrate quantifiable closure.(Dunn et al., 2013) It is important to note that the treatment films were adhered to thin glass panels, and in order to separate them from the glass they were submerged in a bath of PBS prior to surgery. Given the structure of the films, the 4mm diameter scaffolds were sliced in the bath by positioning the film against the edge of the wall. The films, and hence scaffolds, have a natural tendency to fold over themselves when not submerged, hence in order to combat this phenomenon, both control and treatment wounds had 10μL of PBS added to the wound surface, such that the meniscus on the right wound would allow the scaffold to unfold. Prior to surgery the mice were shaved, and hair removal cream was applied to expose the smooth skin. It is important to thoroughly wash the cream off to remove it as an interfering factor in wound closure, additionally the mice themselves clean excess hair. Silicone rings of 15mm diameter with 6mm circles cut out from the centre are then adhered to the skin with superglue adhesive aligning the fresh wound with the cut-out. Sutures are evenly spaced around the ring for a better fixture and to reduce risk of scratching removal. A layer of Opsite is placed on the silicone ring to prevent pathogens entering the wound and interfering. Each specimen is weighed, measured for wound closure, and injected with 10μL of buprenorphine daily in order to reduce irritability and scratching. The daily wound calculations are performed by calculating the wound diameter with 0.25mm resolution using medical callipers, in three different axes, the x, y and z (diagonal) and averaging the circle area ($A = \pi r^2$). Doppler measurements are taken at the 3,7- and 10-day time periods to hopefully observe blood perfusion at crucial time points throughout the experiment. The mice are fed a diet of Mazrui mouse food and tap water over the length of the experiment, with a 16hour day 8hour night cycle.

# Biocompatibility Study

The Murine model theory was applied to the 7 specimens in the first study, with 3 mice receiving the SF treatment and 4 receiving the NDSF treatment, as shown in appendix Biocompatibility Study 1# Images. One day prior to the surgery day the specimens had their fur shaven and removed with Nair hair removal cream, to completely remove the interference of fur during the delicate surgery. The hair removal phase is done one day prior to surgery so the mice are given ample time to clean themselves of excess hair and be as clean as possible for the procedure. On the surgery day the laboratory work space was cleaned thoroughly with F10 for hygiene and infection control, along with all surgery tools and equipment necessary

for the procedure. Prior to surgery, the mice were placed in an induction box which has an influx and 4% isoflurane to anesthetize the animal prior to surgery such that there is loss of consciousness and reflexes are supressed. In order to ensure the animal is sufficiently anesthetised, pain relaxes on the hind legs are checked to insure there is no response. The mouse is weighed on a pair of scales to monitor percentage fluctuations over the length of the experiment and intervene if significant fluctuation is observed over the course of the experiment. After several minutes inside the induction box, the animal is moved onto the workbench placing the mouth in a nose cone with a continuous supply of 2.5% isoflurane. Pain reflexes are checked a second time and a heat mat is placed underneath the animal to maintain core body temperature during surgery. A 6mm biopsy punch is used to mark the bare skin in the areas of incision, on the right and left side of the midline, as a guide for the surgical scissors. The bare skin is wiped with betadine prior to incision for sterility, then forceps are used to pinch the centre of each marked biopsy punch to make a 'lip' of skin for the first cut with surgical scissors. Once the first cut is made on the lip to the muscle fascia layer, one of the scissor heads is placed underneath the skin such that the circle of skin can be removed. The skin layer is carefully removed being conscious of not cutting into deep tissue or severing blood vessels. Once both control and treatment wounds are cut to the appropriate depth, the treatment is ready to be applied. Both SF and NDSF electro-spun films are adhered to thin glass films and must be submerged in a bath of PBS in order to separate each film from the glass slide. Using the contours of the PBS bath tray, 4mm circles of film are cut using a 4mm biopsy punch pressed against the edge (3×4mm SF, 4×4mm NDSF). The flat end of the forceps is used to scoop the appropriate treatment film to prevent folding, and place directly onto the surface on the right mouse wound. The left and right wounds of each mouse are topically given10μL of PBS as a control using a 1ml syringe. Two 1.5mm silicone rings are cut and a 6mm biopsy punch is used to remove the centre of the ring to align with each animal wound. Super Glue is carefully applied in droplets on one side of the silicone ring around the centre cut and then with forceps placed on the animal such that the 6mm hollow centre aligns with the wound, being careful to not get glue on the wound surface and cause closure interference. The silicone ring is held against the skin for 30 seconds making sure the ring is securely adhered to the bare skin to prevent contraction of the panniculus carnosus. Once each ring is adhered to the skin surrounding each wound, a 4-0 gage non-degradable medical suture is used to stitch the top skin layer to the silicone in several evenly spaced points around the circumference of each silicone ring to further prevent contractional wound healing. Careful consideration is put into not touching the wound surface with medical equipment or displacing the treatment film. Once the sutures are secured and tightened, an Opsite film layer

is required to prevent pathogens from entering the wound during the 10-day experiment. Two 1.5mm diameter circular Opsite films are cut from a sheet, using needle nose forceps to carefully place them on top of each silicone ring and align them correctly, with no air bubbles allowing fluids to enter or exit between the outside world and the wound. The specimen is then injected with its daily dose of 10µL of buprenorphine subcutaneously to supress irritability and scratching. The initial wound measurements are performed and recorded on Day-0 of a printed and laminated data table, taking x, y and z diameter measurements with a resolution of 0.25mm using callipers. Once the surgery is complete, isoflurane supply to the nose cone is stopped and the animal is carefully placed inside a mat heated recovery cage until full consciousness is regained and the animal can be returned to its original cage. The procedure is repeated for each specimen applying and documenting the appropriate treatment to the right wound. The mice are monitored daily for weight and wound area (taking x, y and z measurements) in addition to administration of 10µL of buprenorphine with a 27G needle once anesthetized. Furthermore, the adhesion of the silicone and suture stitches are checked to ensure skin is not free to move and interfere with wound healing. If a suture is missing or skin is loose, the appropriate combination of Super Glue and sutures are applied to re-secure the skin in a splinted open position around the wound.

For the purpose of this investigation, laser doppler perfusion analysis was performed at day 3,7 and 10 of the experiment for each animal to analyse blood perfusion in each wound for comparison. Laser doppler velocimetry operates on the principle of the doppler shift, whereby the frequency of a signal is altered by reflection off a moving object.(Micheels et al., 1984; Pettker and Campbell, 2018) When the known frequency of a monochromatic laser light is directed at some acute angle onto an area of blood flow, the velocity of that blood changes the irradiating frequency according to Equation 1 - Doppler Shift.

$$f = \left(\frac{c}{c \pm v_s}\right) f_0$$

$$\textit{Where } c \textit{ is the speed of light}$$

*Equation 1 - Doppler Shift*

The modified frequency of laser light reflects off the source of changing velocity and is received and interpreted by the observer, or source of monochromatic laser light.(Giordano, 2009) Knowing the angle of incidence, the reflection angle of the laser can be found, and the reflected signal can be interpreted by a processor on the observer side.(Giordano, 2009) By knowing the frequency of the signal sent by the observer, and calculating the frequency of

the reflected signal, the frequency shift is used to determine the velocity of the moving body of blood.(Giordano, 2009) The plus-minus term in Equation 1 - Doppler Shift depends on whether the body is moving toward or away from the observer.(Giordano, 2009) Blood perfusion is measured by calculated microcirculation in capillaries and vessels, where a single laser beam performs an x-y scan in rows moving across the specimen.(Micheels et al., 1984) MoorLDI software interprets the doppler image showing a heat map of the scanned area, allowing a flux measurement of a chosen area to be performed using the software.

On the final day of the experiment, final weights and measurements are recorded for each specimen prior to culling. A cardiac puncture is performed on each specimen to extract a blood sample for further immune cell concentration analysis. Surgical tools and work areas are thoroughly cleaned with F10 prior to the procedure. Prior to the cardiac puncture procedure, the animal must be heavily anesthetized, firstly in the induction box and then under the nose cone with a continuous supply of 7% isoflurane. Once the animal is unconscious and non-responsive to pain stimuli, it is positioned faceup on the dorsum, such that the chest cavity faces upwards. The entire underside of the body is wiped with F10 for sterilization, prior to surgery. In order to expose the heart, the skin underneath the rib cage is pinched with forceps and sharp surgical scissors are used to cut the skin lip, making a 45° angle between the underside of the scissors and the table top. A second cut is made directly upward toward the head of the mouse, to the base of the sternum exposing the internal organs. Once the organs are exposed, the beating heart is located on the relative right side of the midline underneath the ribcage. In order to extract the maximum volume of blood, the heart must be carefully punctured on the underside side with an 18G needle, and then by pulling back the syringe blood will begin to slowly fill the syringe cavity until all the blood is extracted and the handle will pull forward on release due to negative pressure inside the cavity. The most important part of the procedure is to ensure the needle does not traverse the heart completely, because a secondary puncture will cause blood to leak out into the body cavity. Once the blood is extracted, the contents of the syringe are injected into a blood collection tube and placed immediately on ice. Once blood has been harvested and the animal is culled, the isoflurane supply is cut off and the specimen is placed dorsum-up on a dissection tray for the wound tissue to be harvested. Using a 6mm biopsy punch, a circular mark is made on the skin surrounding each semi-healed wound, and surgical tools are used to extract each 6mm circle of wound tissue. The wound tissue circle is cut in half using a scalpel, making sure to separate the centre of the wound evenly between the two halves. One half of the wound tissue is further cut into two even quarters. All wound tissue pieces are carefully placed into separate sample

containers and submerged in dry ice immediately for freezing. One all the samples have been harvested, the bodies are disposed of, the tissue-half samples are placed in a 5°C fridge temporarily, and the tissue quarters are put in a -80°C freezer for preservation, and the blood samples are stored in a 5°C fridge temporarily. On the same day, the blood samples are centrifuged at 40,000 rpm for 5 minutes in order to separate the plasma from the red blood cells of each sample. Using a micro pipet, the surface layer of plasma is collected independent of red blood cells, transferred to a collection container and moved to the -80°C storage freezer. The semicircle half wound tissue is used for microtome slicing and cell staining to analyse cell types in the wound cross section, whilst one quarter of each wound tissue is put aside for RNA analysis and another quarter for protein analysis later. The blood plasma of each animal is collected so that future inflammatory cell concentrations can be analysed as another indicator of treatment biocompatibility.

Within a few days of the final experiment day and tissue harvestation, the stored tissue halves are embedded in paraffin wax using small metal mouldings and carefully placing the tissue halves upright such that the wound cross section is touching the base of the moulding. Forceps are used to hold the tissue in position while hot wax is poured into the moulding, the underside of the metal mould is then placed in contact with a 0°C surface causing the wax to solidify from the bottom upwards. Once the wax has solidified the tissue into place the forceps are removed, and a plastic casing is placed on the top of the mould where the wax is still in liquid form. Once the cool surface solidifies the entire volume of wax in the moulding, the porous plastic casing is adhered into the wax and the entire wax block can be removed from the metal mould. The wax moulds from each tissue-half sample can then be safely stored at room temperature and the tissue is preserved and ready for histology. In order to get a cross section of each wax embedded tissue sample, a microtome is used to slice several 10micron thick layers of the embedded sample and place them on a glass slide for cell staining. The microtome has an adjustable slicing width, and in order to get a complete cell cross section the first few slices are discarded to account for the contours of the half-wound not aligning with the flat wax surface. Once the initial layers are discarded, the slices which contain complete cell cross sections are carefully placed in a bath of 50°C water allowing any creasing in the wax slice to be straightened out. Once straightened out, three cell slices are carefully placed on a glass slide for collection, from each wax mould. It is important to be conscious of microtome slicing and make sure the cell is kept intact and not torn as a result of the slicing, because cell information is lost, and staining will be inconclusive. Once three samples of each cell cross section are collected on individual glass slides, the slides are placed upright in a

drying rack to drain excess water. Once dry, the glass slides are put into a 60°C oven for 24hours in order to preserve the cell samples on each slide and remove excess wax from the embedding procedure. After 24hours the slides are removed from the oven and can be stored safely at room temperature.

For the purpose of this investigation, the staining performed was a simple hematoxylin and eosin stain, (H&E) to identify the nuclei and cytoplasmic cells within each cross section. (Fischer et al., 2008) H&E staining involves submerging the glass slides in a series of solutions to re-hydrate dried cell samples, stain the nuclei and then de-hydrate them for preservation, according to the following procedure.

Hydrate

- Xylene – 6 min
- 100% Ethanol – 2 min
- 95% Ethanol – 1 min
- 70% Ethanol – 1 min
- Running tap water – 1 min

Stain

- Meyer's Haematoxylin
- Tap water – 3 dips
- 0.3% Acid Alcohol – 2 dips
- Scott's Blueing – 1 min
- Tap water – 3 dips
- Eosin – 1 min
- Tap water – 3 dips

Dehydrate

- 70% Ethanol – 1 min
- 95% Ethanol – 1 min
- 100% Ethanol – 2 min
- Xylene – 2 min
- Leave samples to dry
- Mount in DPX

Once the slides are dry, a small drop of DPX is placed on top of each cell on the slide and a glass cover slip is put on top of the DPX, to provide a medium for light microscopy and analysis without air bubbles.

During the first experiment with an $n=7$, complications arose in relation to the animals used in the study. The 7 mice were separated over 3 cages to minimise fighting by separating alpha males. However, during the experiment, there was unfortunately an unusual amount of rivalry between mice of the same cage, which resulted in regular fighting between the animals. The Appendix Biocompatibility Study 1# Images demonstrates some of the results of continual fighting between the specimens, regardless of the daily buprenorphine injections to soothe irritability. Given that in many cases some of the silicone fixtures has been completely removed from the specimen, the decision was later made to disregard the results of this initial study as the results are not reliable. Removal of the silicone fixtures removes the inhibition of contractile healing, and thus the wound healing model moves further from the human equivalent. Mice wounds heal at a much faster rate due to the contraction mechanic, and consequently even short periods of time can make a large impact on the healing rate. Once fixtures are removed the healing process no longer approximates that of humans, and the humanized model falls apart. In order to produce reliable and valid results the fixtures must remain on the animal for the length of the experiment to ensure the wound healing is the result of new cell growth and not another mechanism. Nevertheless, the results of study 1 have been included in the appendix for the readers interest - Biocompatibility Study 1# Images. The biocompatibility study was repeated with an $n=8$, with 4 mice receiving the SF treatment and 4 receiving NDSF, as shown in Appendix Biocompatibility Study 2# Images. In order to produce conclusive, reliable and valid results precautions were taken to ensure no mistakes were made during experimentation, and each specimen was assigned a personal cage to eliminate fighting. The same surgical, measurement and histological procedures were followed as outlined previously.

# Results

One of the primary outputs for the biocompatibility study is the daily wound area measurements taken of each wound for each specimen. The wound closure data provides a comparison for control vs treatment wound closure for each mouse. Figure 5 - Wound Closure shows a MATLAB plot of the wound closure for each specimen over the repeated 10-day experiment.

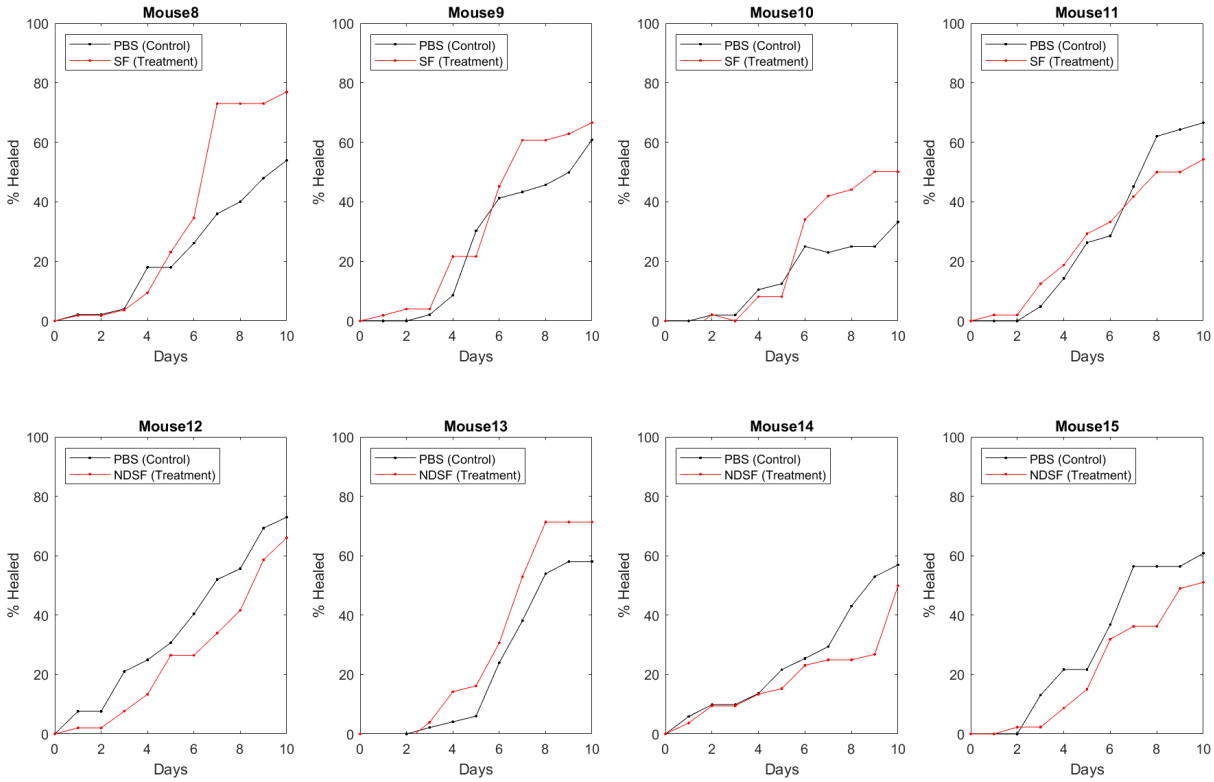


*Figure 5 - Wound Closure*

As exhibited by the data in the Figure 5 - Wound Closure ¾ animals in the SF group showed improved healing for the treatment relative to their controls, which validates the literature.(Altman et al., 2003; Cao and Wang, 2009; Kaplan et al., 2010; Lindsay S. Wray et al., 2011; Sugihara et al., 2000; Wang et al., 2006) Conversely, ¾ animals in the NDSF group showed impaired healing for the treatment in comparison to their controls. For Mouse 8, 9 and 10 in the SF group, the healing rate for both control and treatment appear to be very similar for the first 5 days after which the SF wound begins to overtake the control around the same time point. This is an interesting result as it may suggest that the 'buffer time' required for the SF scaffold to begin facilitating the healing process is around 5 days, after which the SF wound on these specimens is continuously smaller in comparison to the control until the end of the experiment. The benefit of the control wound in this healing model is the ability to compare each treatment wound against its control, which helps account for the drastic variability between different animals. Mouse11 in the SF group has the control and treatment wounds heal at almost the same rate for the first 7 days of the experiment, after which the control wound overtakes the treatment. It is important to notice that no wound in either group was able to heal above 80%, which indicates that if the experiment were to be repeated over a longer time period such that 100% healing was achieved, the results may have varied. For the NDSF group, Mouse12, 14 and 15 had their control wounds heal at a faster

rate and to a higher percentage in comparison to the treatment. On first inspection this indicates that the presence of the NDs did contribute negatively to the wound closure of these animals. Furthermore, much like the wound closure observed in Mouse9, 10 and 11, Mouse14 and 15 only healed to around the 60% mark after the 10-day experiment. This is a considerable observation as it suggests that only part of the whole picture is exhibited here. The highest percentage of wound closure overall is demonstrated by Mouse8, 12 and 13 coming close to 80% closure of the initial surgical wound. Given the small sample size of each group and healing percentage, it is difficult to conclusively say that the healing rate of each wound will remain constant as exhibited at day 10, overlaps may occur changing the overall result, however it is clear that the SF treatment shows a positive result. Tahir et al., (2017) conducted a similar study into the effects of topically administered spider silk on wound closure in a mouse model, with ~75.5% closure for control and ~96% closure for treatment after a 20-day period. Notably, the initial wounds were ~1cm$^2$ and the mouse model differs from the one conducted here by lack of wound splinting to precent contractile wound healing in the rodent. Given this information it is difficult to make a speculation on the appropriate time for complete wound closure of SF treated wounds given that the model used here is humanised. Nonetheless, the study conducted by Tahir et al., (2017) supports the overall results found from the SF group in this investigation, that the presence of SF did in fact improve wound closure. The significance of using the humanised Murine model is that observed effects can be better correlated to the potential effect in humans. Hence, it is necessary for more research to be conducted on topical SF administration using the humanized model for better transferrable conclusions. An important consideration is that due to the area measurement technique used for the wounds, some error is present when approximating the wound area as a perfect circle.

Unfortunately, there is little to no literature which studies the impact of topical NDs on wound healing, making it difficult to correlate the results seen here. However, the data suggests that the beneficial effects of SF on wound closure are supressed due to the presence of NDs. Nonetheless, more studies need to be conducted on the systemic and local effects of NDs for topical administration under these conditions. For a better interpretation of the wound closure measured in each animal, MATLAB code was generated to approximate the trend of each healing scatter plot as a logistic model, allowing an analysis of healing rate – as shown in Appendix MATLAB Code. Figure 6 - Logistic Models for Treatment Wounds and Figure 7 - Logistic Models for Control Wounds show the approximated logistic model for each wound in each specimen.

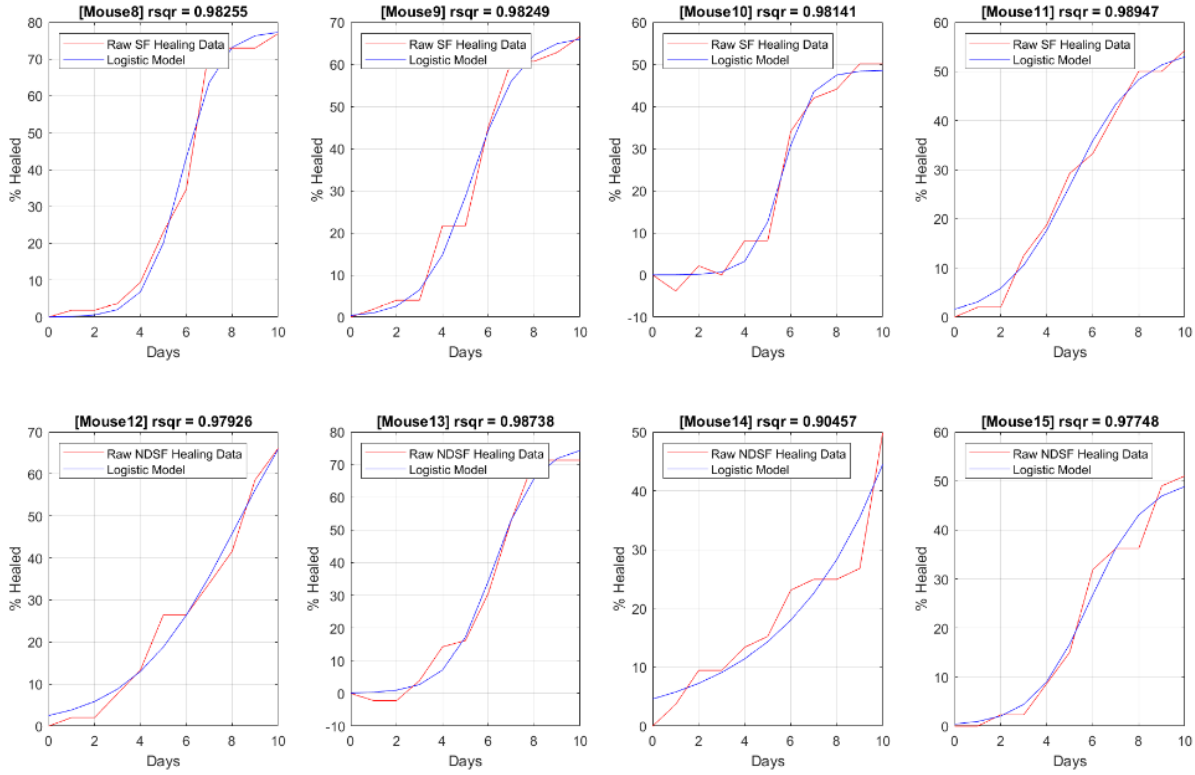


*Figure 6 - Logistic Models for Treatment Wounds*

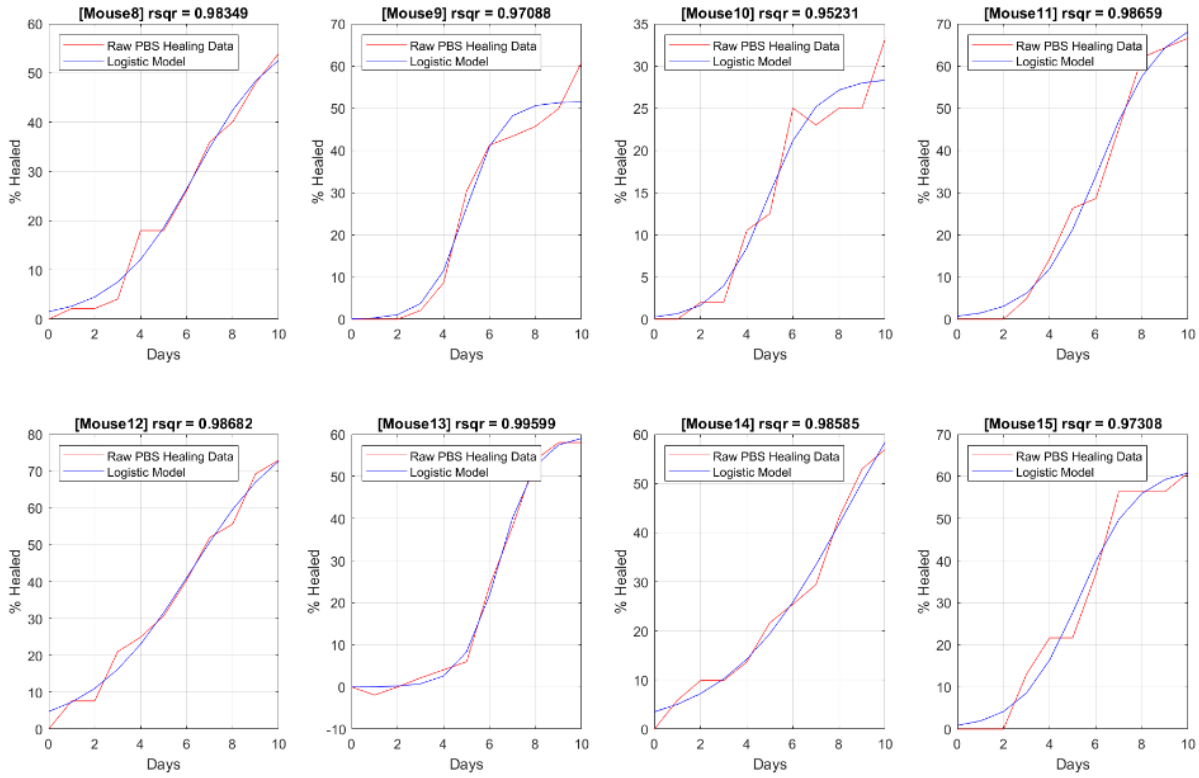


*Figure 7 - Logistic Models for Control Wounds*

The r-squared values suggest that the model is an appropriate fit to represent the healing trends measured. By differentiating the modelled equations in MATLAB, a theoretical healing rate graph can be generated for each animal, as observed in Figure 8 - Average Rate of Healing.

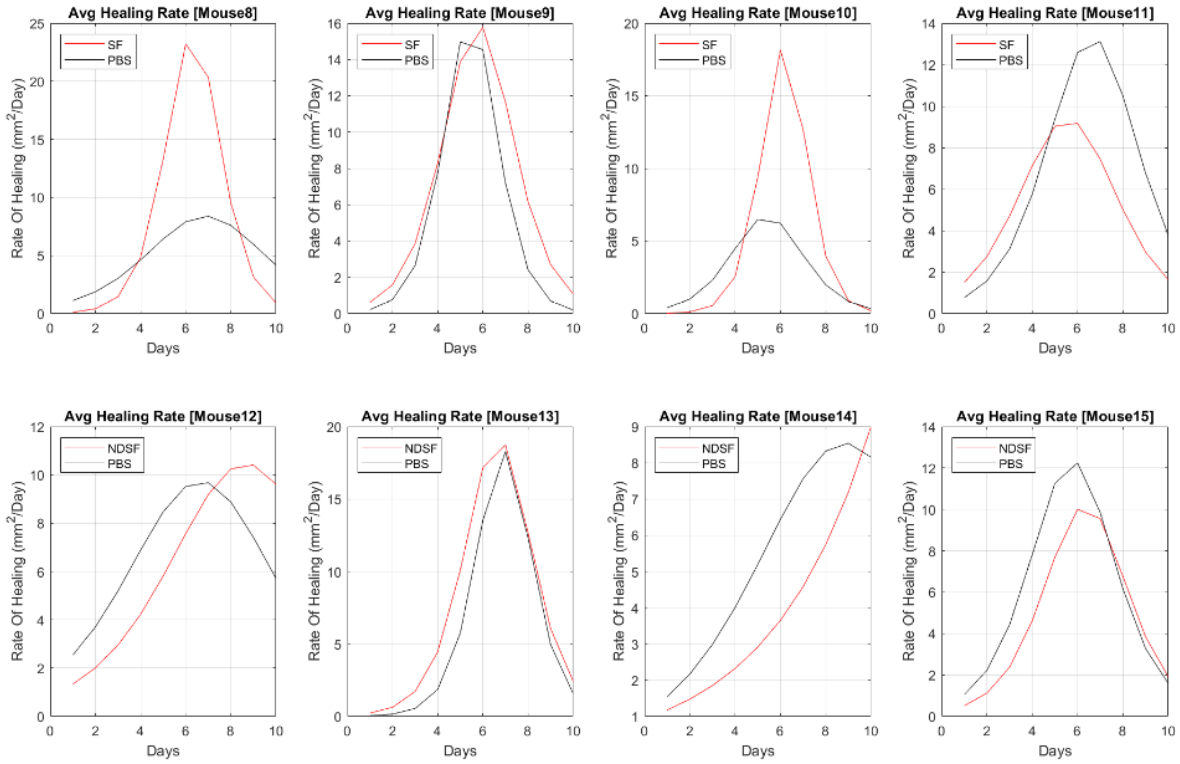


*Figure 8 - Average Rate of Healing*

An interesting observation when comparing the SF treatment healing rate to the relative control is that the presence of the SF did not change the time at which peak healing rate was achieved, but simply increased the healing rate over the length of the experiment, for mice 8, 9 and 10. A similar situation is observed in the NDSF group where both control and treatment peaks for healing rate occur around the same time. For the SF group, the peak healing rate is consistently around the 6-day mark for both treatment and control. Mouse11 shows a higher peak healing rate for the control wound which is consistent with the control healing to a higher percentage after the 10 days. Relationships between wounds in the NDSF groups are less consistent, and this is partially influenced by the approximative model used to generate the graphs. For Mice 12,13 and 14 the peak healing rate of both control and treatment is after the 6-day mark, which is interesting considering that there is expected consistency between controls of different animals. The discrepancies between the healing characteristics of control wounds in different animals highlight the importance of having a control wound in each animal, such that the treatment wound data can be normalised by the control to account for

some of the variability between specimens. Interestingly, the peak healing rate for control in Mouse8, 11, 12 and 13 is consistent at day 7, however the significance of this is supressed due to the small sample size used. Overall the logistic model appears to best represent the trend of healing data observed over the 10-day period.

The wound blood perfusion was analysed at day 3, 7 and 10 of the experiment using laser doppler velocimetry, exhibited chronologically in Figure 9 - Doppler Measurements Day 3, Figure 10 - Doppler Measurements Day 7 and Figure 11 - Doppler Measurements Day 10.

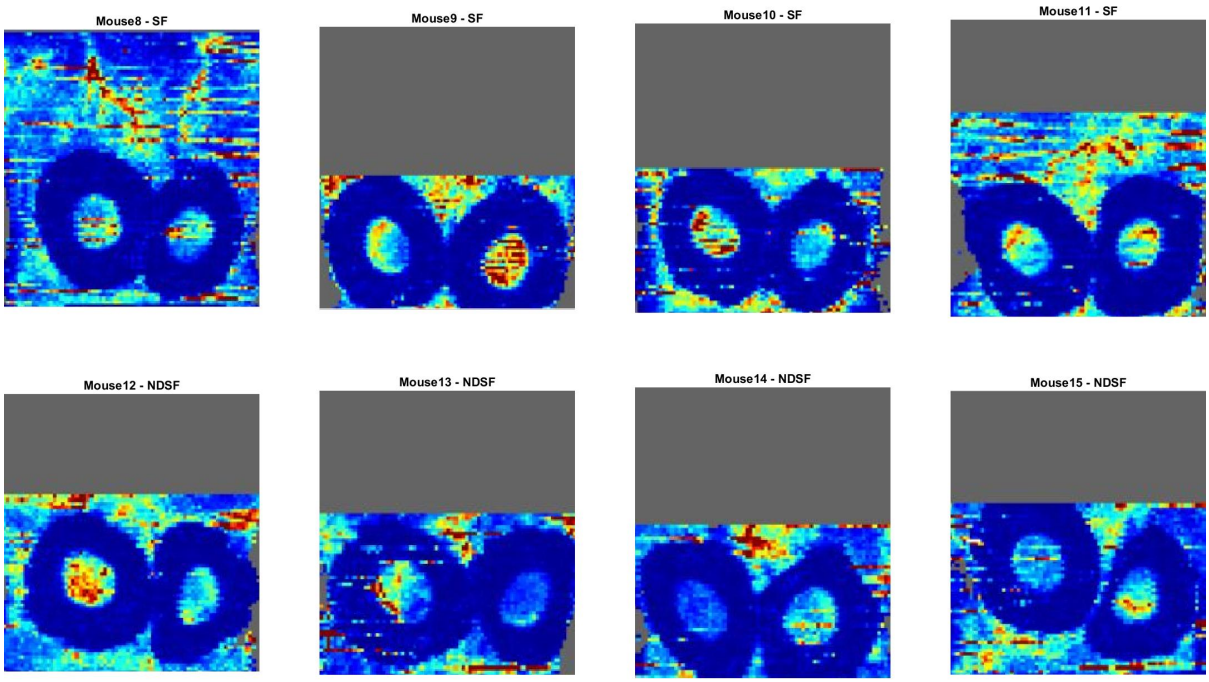


*Figure 9 - Doppler Measurements Day 3*

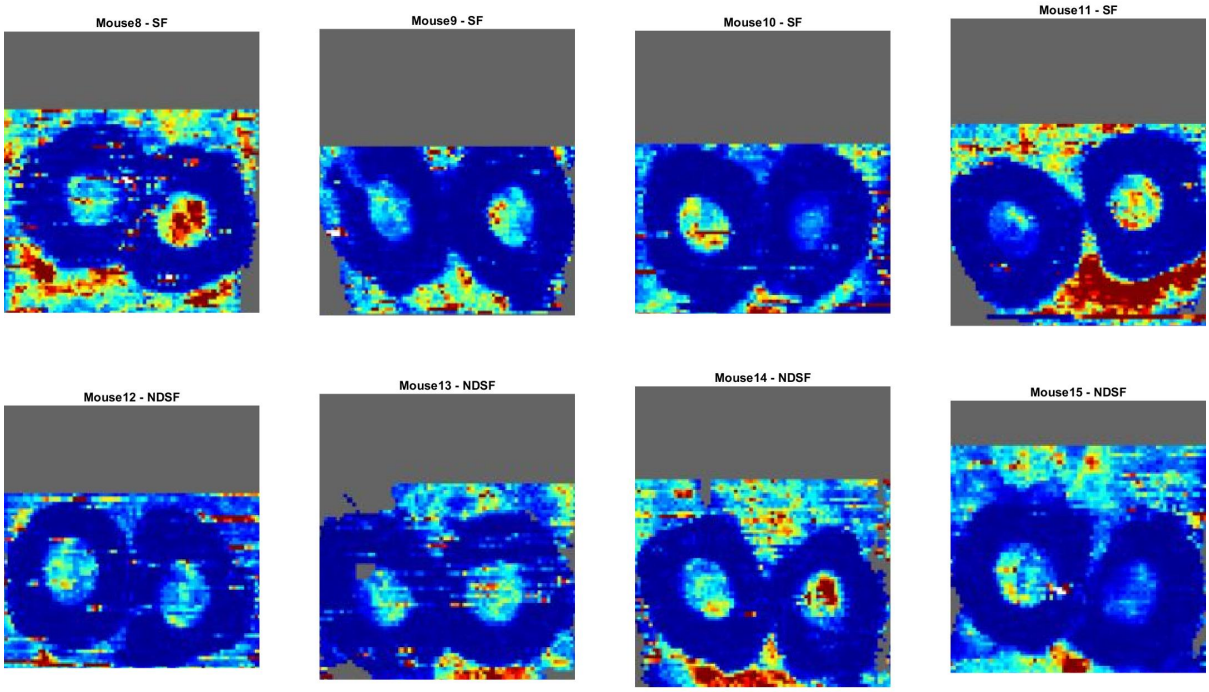


*Figure 10 - Doppler Measurements Day 7*

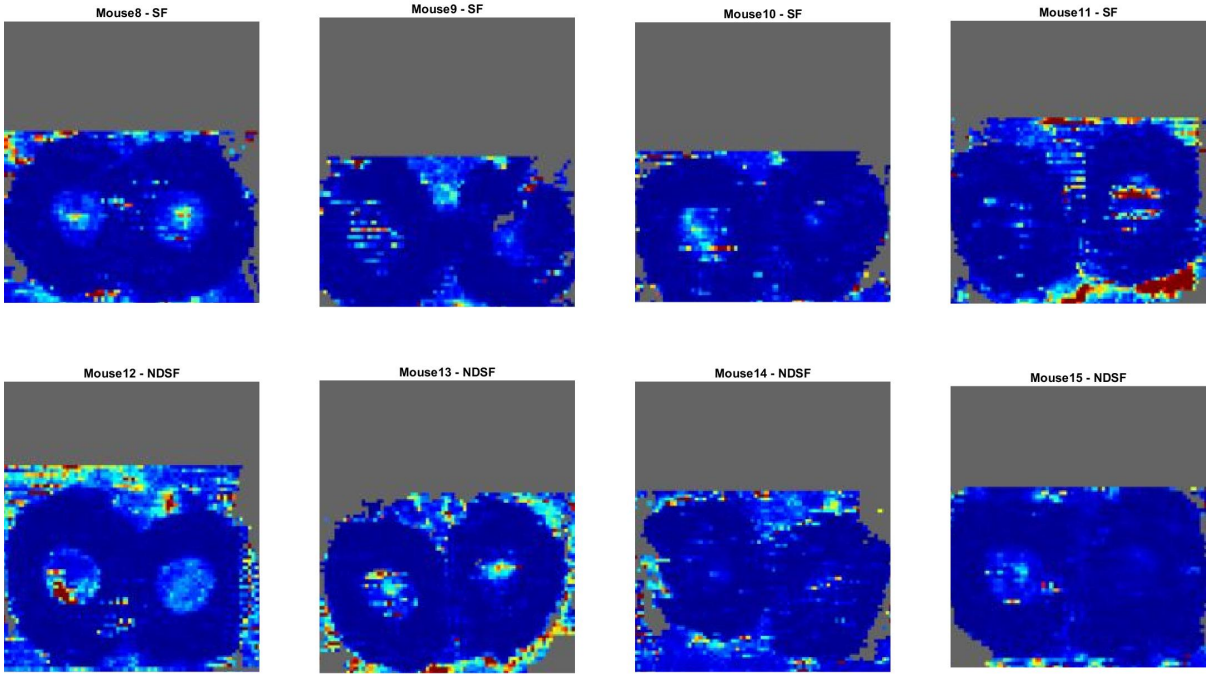


*Figure 11 - Doppler Measurements Day 10*

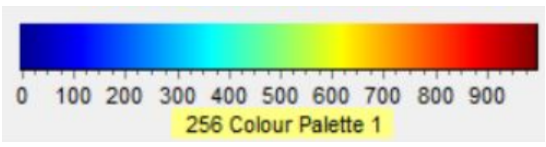

The doppler images were analysed using moorLDI software and a colour pallet correlating to the intensity of blood perfusion seen at the skin surface. The silicone rings of each animal appear as dark blue rings on the doppler images due to the laser not being able to detect blood flow through the barrier. A larger average intensity, or flux value, at the wound site suggests that more immune activity is occurring in this region due to the relative increased blood perfusion to supply the wound area with vital growth factors, cytokines and hormones. A consistent relative increased flux at one wound for each animal in the group suggests a correlation. As expected, the highest perfusion values seen occur at the 3- and 7-day marks where the most activity is occurring within the wound. The flux intensity at day 10 suggests that the immune response on the surface is decreasing due to partial healing. By referring to Figure 9 - Doppler Measurements Day 3, it appears that there is no correlation between treatment wounds in their respective groups. Similarly, it is difficult to form a correlation between the intensity values observed in Figure 10 - Doppler Measurements Day 7. The mean flux value at each wound is quantified using the moorLDI software by selecting the region of interest within the silicone rings, and from this information Figure 12 - Average Blood Perfusion can be generated using MATLAB.

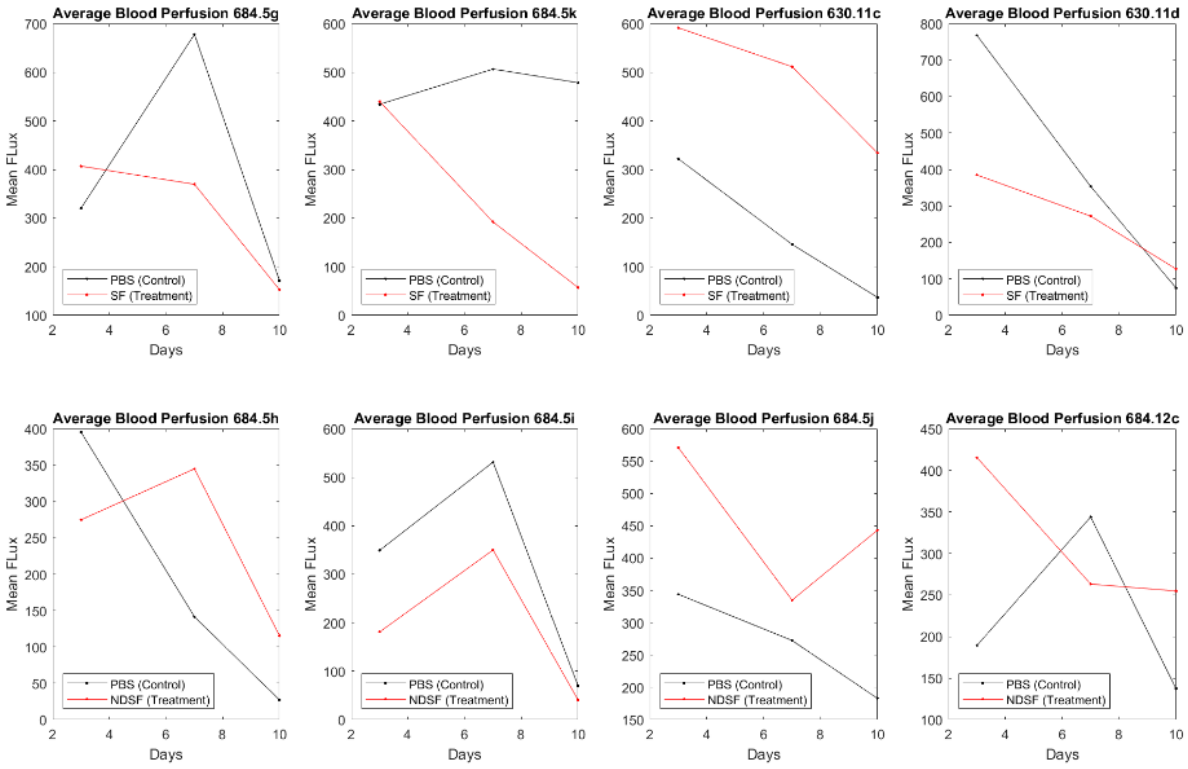


*Figure 12 - Average Blood Perfusion*

By analysing the mean flux values for different wounds in each group, it appears as though there is no apparent correlation for the 3, 7- and 10-day measurements. This further demonstrates the significance of variability in animal specimens and suggests that other physiological and exogeneous factors contributed to the high variation seen in results. In order to better understand the perfusion behaviour of the treatment wounds, the treatment flux values are normalized by the control values on the same day finding the ratio of treatment flux to control flux, therefore the difference between mean flux on the treatment side and control side can be better represented for each animal. Figure 13 - Doppler Perfusion Ratio plots the average flux value of treatment wound for each animal normalized by the flux value of the control wound on the same measurement day.

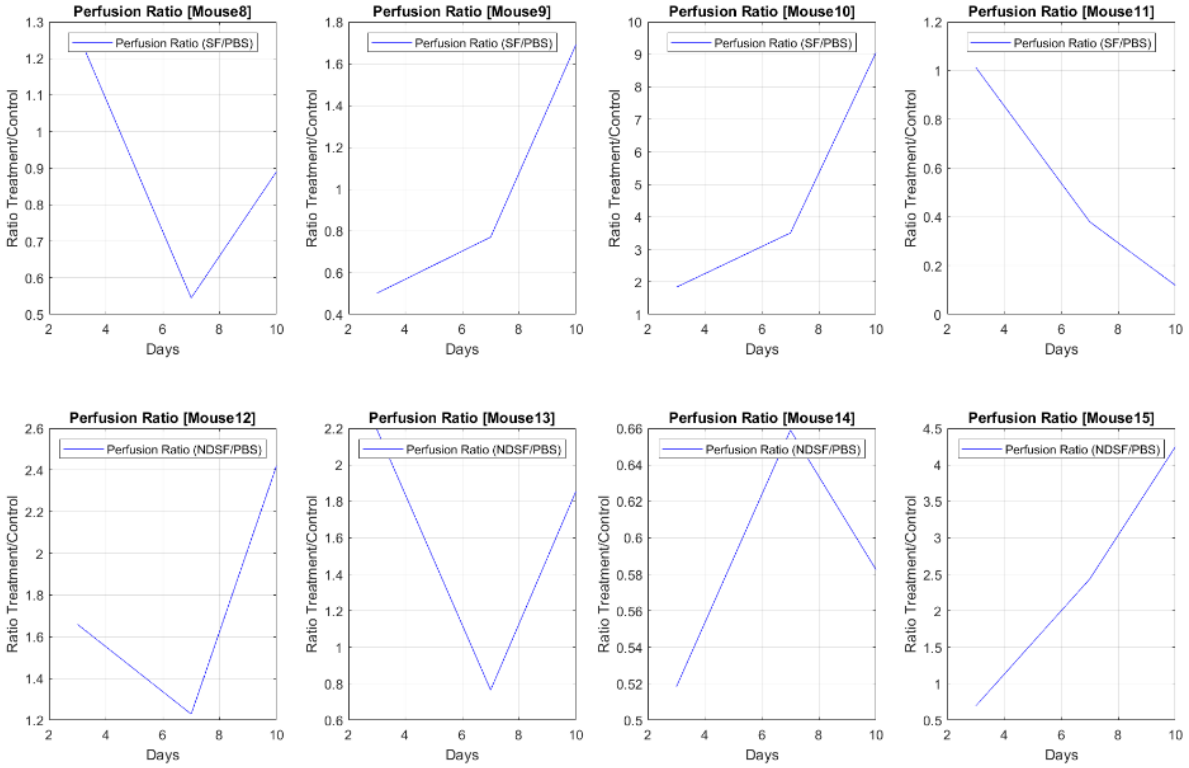


*Figure 13 - Doppler Perfusion Ratio*

After analysis of the normalised mean flux values of each animal over the experiment, there is no discernible relationship between the values within each specific group. Unfortunately, it is difficult to narrow down the source of the large variability seen in measurements considering the number of potential influencing factors for each individual specimen. This result is somewhat expected considering the small sample size and the time gaps between doppler measurements. The ideal result for these measurements would be a clear correlation

between the perfusion at treatment wounds, and observable trends in perfusion behaviour over the time line of the experiment.

At the end of the experiment, the scavenged wound tissues for each specimen were sliced and stained using H&E. Using a light microscope and Zeiss software, the wound cross sections were imaged as seen in  Figure 14 - Control Wound Cross Sections Figure 15 - Treatment Wound Cross Sections.

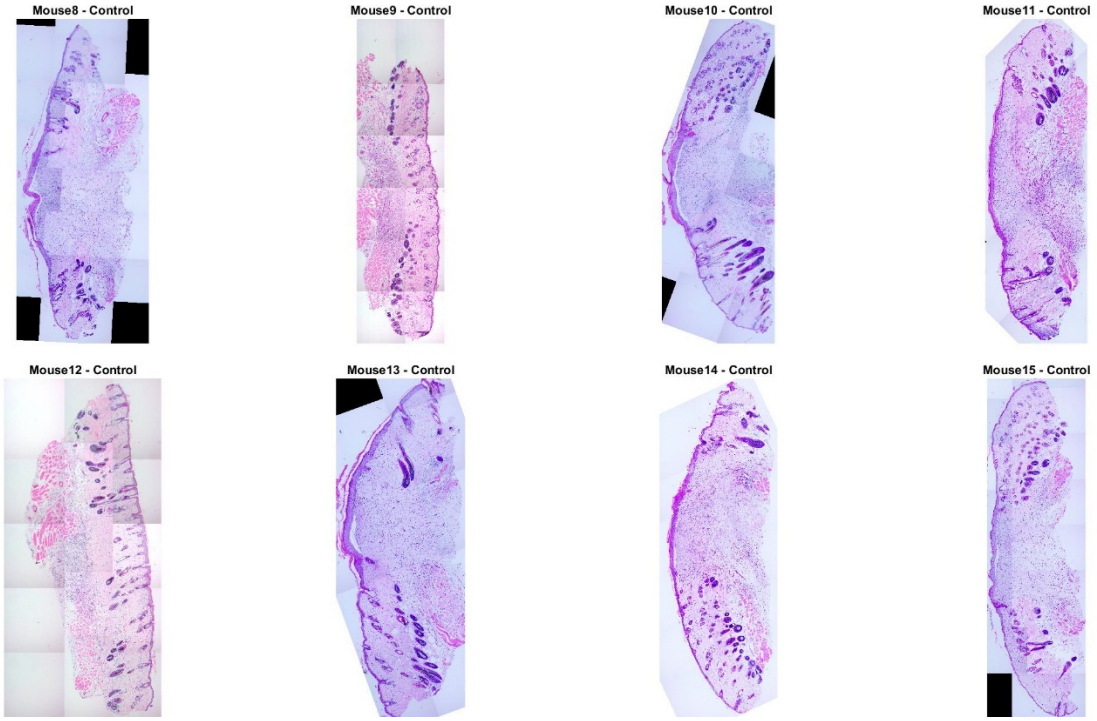


*Figure 14 - Control Wound Cross Sections*

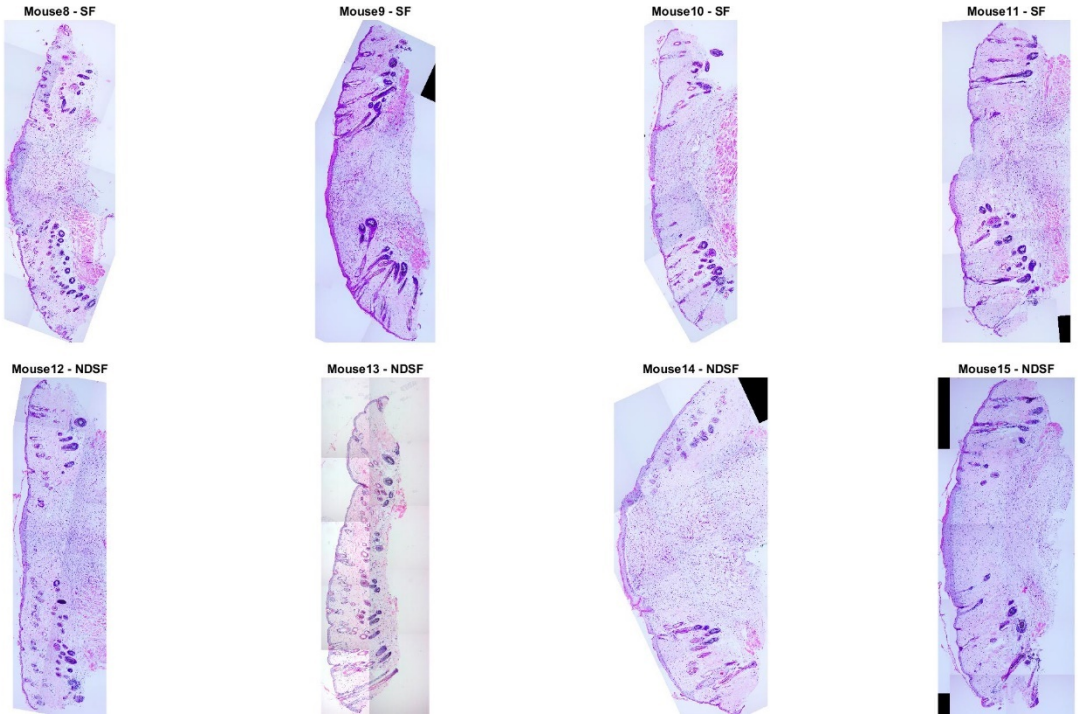


*Figure 15 - Treatment Wound Cross Sections*

The H&E method stains the nuclei and cytoplasmic cells of the wound tissue purple, the colour intensity of stained cells helps to differentiate between different cell types. The inflammatory cells in the cross section of the wound are the result of the immune response to the initial surgical cuts made and represent a strip of dark cells across the width of the cross section in the centre. The volume of cells in this region is an indication of how significant the immune response was to the presence of the treatment film, and the control wounds are analysed for normalization of each specimen.

The granulation zone of inflammatory cell infiltrate at the wound site is reflective of the biological activity and can be used as a tool to compare control wound activity relative to treatment activity. Due to the nature of cell slicing, the wound cross section is shaved into slices and consequently the granulation information erodes with each slice from the wound centre. Therefore, some of the stained cells do not contain the granulation zone of inflammatory cells for analysis. The viable cells are analysed using Image Pro Premier software by identifying a region of interest where the inflammatory cells exist. Figure 16 - Control Wound Granulation Zone Approximations and Figure 17 - Treatment Wound Granulation Zone Approximations shows the viable cell regions of interests (ROI).

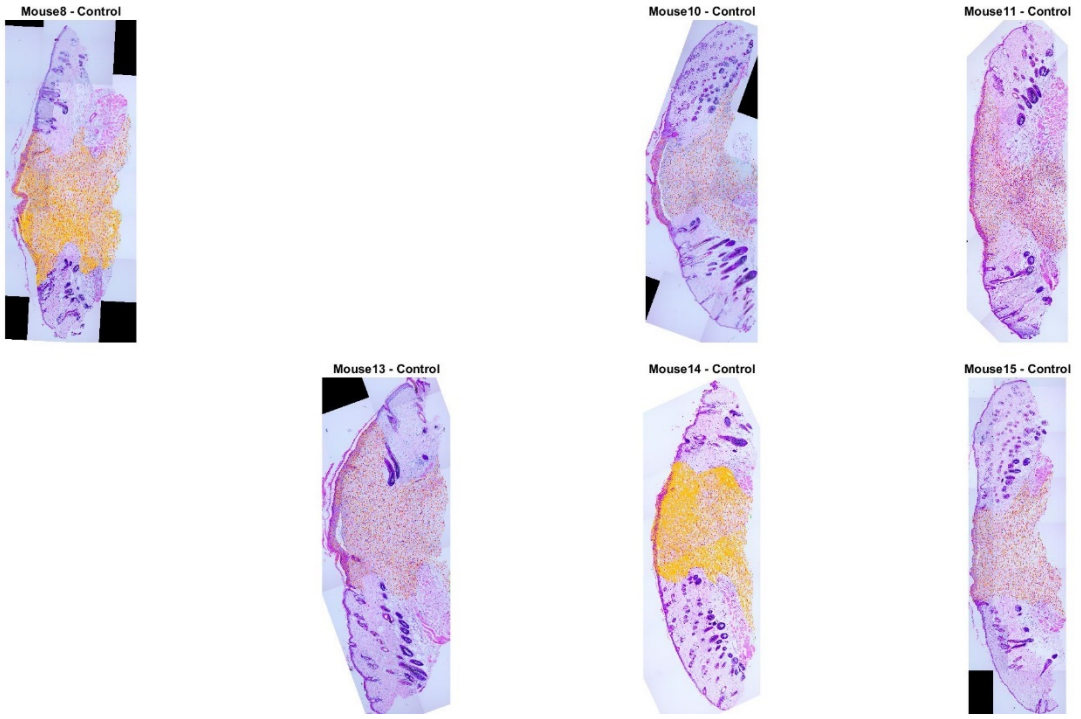


*Figure 16 - Control Wound Granulation Zone Approximations*

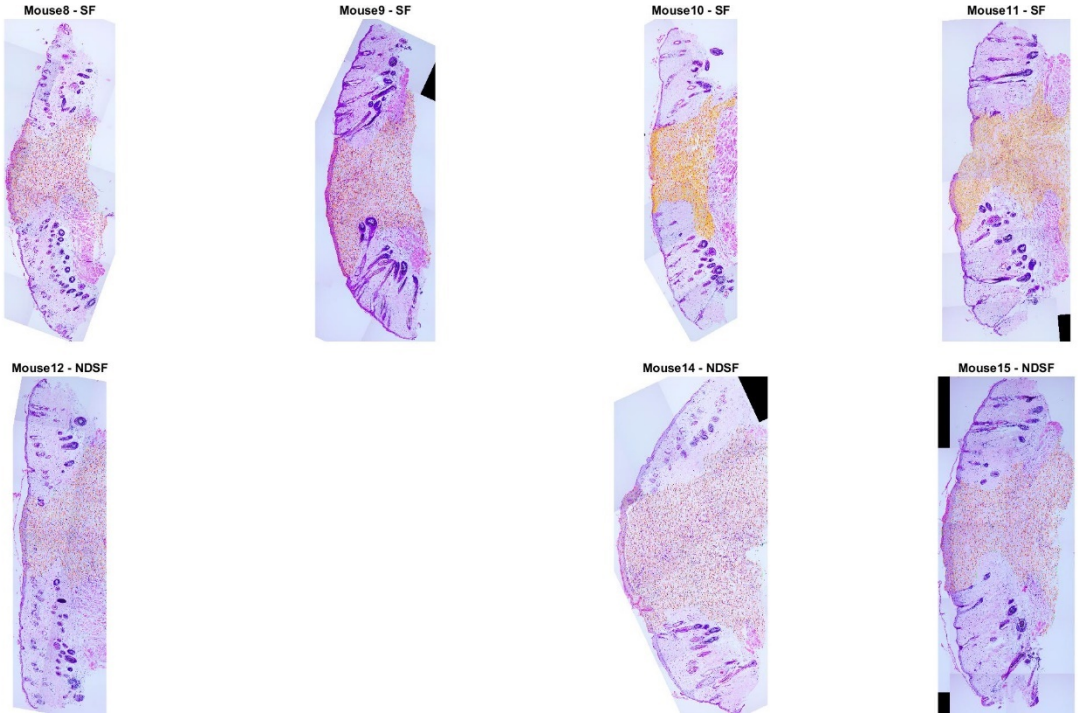


*Figure 17 - Treatment Wound Granulation Zone Approximations*

The Image Pro Premier software allows the granulation zone to be identified by the colour intensity relative to surrounding cells. The ROI is selected manually which best represents the trend of inflammatory cells at the centre of the cross section. With some processing, the approximate area, in pixel size, of the dark cell region is calculated as a ratio of inflammatory

cells to white space in the ROI, giving a percentage of the volume of inflammatory cells for the ROI. This gives a quantifiable result of which graphs can be generated to better understand the granulation zone size discrepancies between control and treatment wounds in each group. The treatment zone from each group is compared to the control zone for that group in Figure 18 - Infiltrate Ratios for Control and Treatment Wounds.

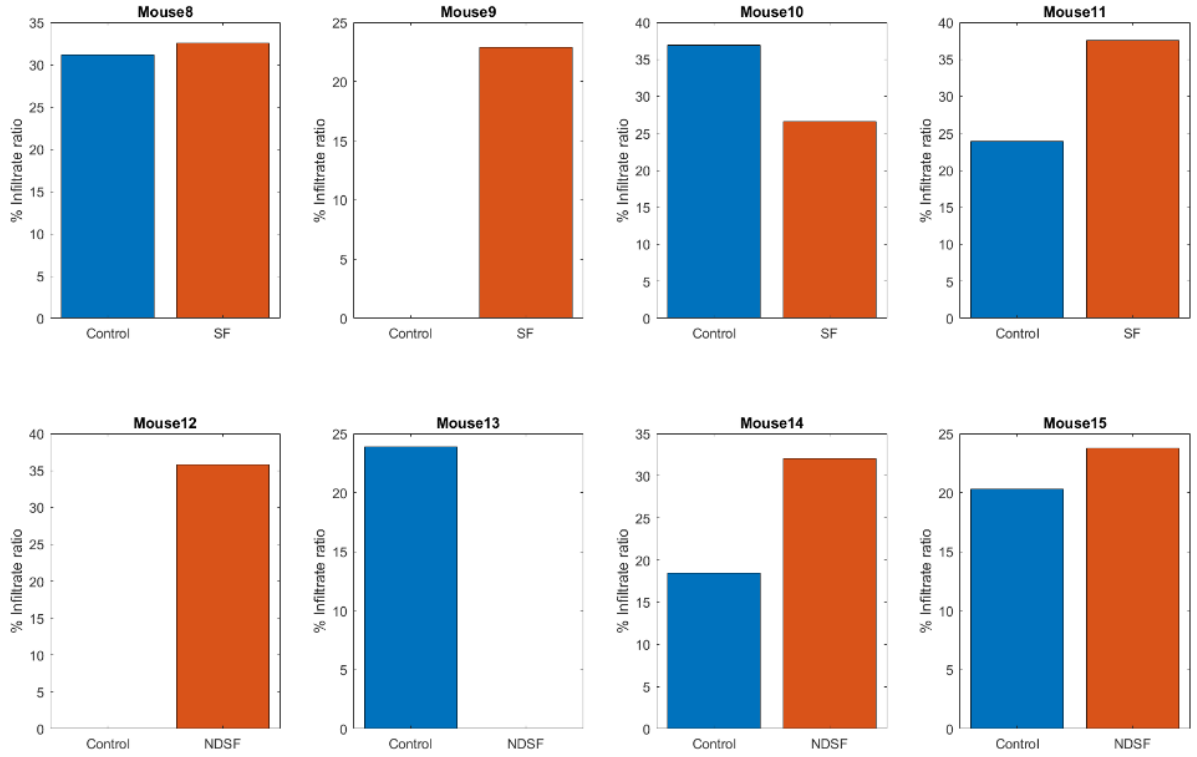


*Figure 18 - Infiltrate Ratios for Control and Treatment Wounds*

When analysing the individual infiltrate percentages for each animal, there is no clear consistency between the values in specific groups. From the NDSF group, it appears as though the treatment wound exhibits a higher granulation zone area in comparison to control however given that only 2/4 comparisons are available in this group, it can not be concluded with certainty.

# Discussion

The aims for this project were initially, validation of wound healing acceleration through topical SF film administration, and analysis into the biocompatibility and applicability of impregnating those films with NDs. Khalid et al., (2014) outlines the emission enhancement of $NV^-$ centres in NDs when coated in SF, therefore eluding to the idea that these hybrid films

are very useful for biomedical imaging applications given that the fluorescence is enhanced. Non-cytotoxicity was established through wound tissue analysis of the specimen, however a thorough analysis on systemic effects was not recorded.(Khalid et al., 2014) Given the rapidly growing research and development surrounding NDs for quantum sensors, the findings from Khalid et al., (2014) serve as a stepping stone for further research into the possibilities of NDSF given the inherent emission rate increase. The impressive properties of SF not only help enhance optical sensing of the NDs, but the material itself has the ability to be selectively tuned through electrospinning and integrates exceptionally with bodily tissues through degradation and signalling.(Zhou et al., 2019) Theoretically, the characteristics of each individual material can be exploited separately if implemented correctly. The added benefit of scaffold tuneability through porosity control, fibre alignment and size allow fabrication of location specific scaffolds to accommodate the porosity needed for vascularisation or structural integrity for ECM mimicking.(Zhou et al., 2019) Recent literature details the observations for silk treatment in rodent model full-thickness wounds, however the transferability is poor given the collateral contractile healing process.(Sugihara et al., 2000; Tahir et al., 2017; Vasconcelos et al., 2012) This study also investigates not only topical administration of SF in a humanised model, but single application of fabricated SF scaffolds immediately following surgical intervention, which is not heavily cited. The significance of analysing a SF scaffold in this manner, is that it looks at the effects of single application rather than continuous intervention, which in some practical applications is not viable clinically. Nevertheless, some of the complications surrounding this type of experiment can be traced back to the scaffold fabrication process. As mentioned, the freedom in scaffold design through electrospinning also amplifies the level of uncertainty, specifically with degradation times, fibre alignment and tissue integration.(Zhou et al., 2019) These parameters influence how appropriate the scaffold is for the trauma, and consequently add to the complexity of application specific scaffold design. For this reason there is currently heavy research being conducted into electrospinning of biomaterial scaffolds with controlled parameters.(Hong, 2016; Inagaki et al., 2014; Yuan et al., 2017)

The results agree with the studies conducted by Sugihara et al., (2000), and Vasconcelos et al., (2012) in the sense that SF did show accelerated wound healing in the majority of specimens as compared to control. Table 2 - Healing Data is constructed to analyse the overall healing percentages for the 10 mice used in the experiment.

| Healing Data for Control vs Treatment Wounds in Mouse Model | | | | | |
|---|---|---|---|---|---|
| Mouse ID | **Silk Fibroin Group** | | Mouse ID | **Nano-Diamond Silk Fibroin Group** | |
| | Control Wound Area % Healed | SF Wound Area % Healed | | Control Wound Area % Healed | NDSF Wound Area % Healed |
| Mouse8 | 53.96 | 76.91 | Mouse 12 | 72.98 | 66.06 |
| Mouse9 | 60.84 | 66.59 | Mouse 13 | 58.03 | 71.32 |
| Mouse10 | 33.25 | 50.12 | Mouse14 | 56.94 | 49.88 |
| Mouse11 | 66.57 | 54.25 | Mouse15 | 60.83 | 51.02 |
| **Average** | **53.66** | **61.97** | **Average** | **62.20** | **59.57** |

*Table 2 - Healing Data*

From Table 2 - Healing Data, the average healing percentage over the 10-day experiment in the SF group was 61.97%, and 59.57% in the NDSF group. The SF scaffold did show an 8.31% average increase in healing as compared to control, whereas the NDSF treatment showed a 2.63% reduction in average wound size as compared to control. It is difficult to compare to previous literature given that most experiments are conducted until complete healing has taken place, however the 10-day experiment does give an indication of the trend associated with each treatment. The variability in treatment structure used for these experiments makes it difficult to assess the appropriate time frame necessary to appropriately represent the behaviour of the material. Previous literature suggests that the peak action of SF will take place at the time of peak proteolytic degradation, and from observation the material seemed to completely degrade within 7 days upon implementation.(Cao and Wang, 2009) For this reason the average healing rate graphs from Figure 8 - Average Rate of Healing were approximated from logistic models, to identify whether a trend in the time of peak healing rate wound present itself. For the SF group the peak healing rate was consistently around the 6-7-day mark for treatment wound, whereas the NDSF peak healing time was inconclusive due to inaccuracies in mathematical modelling. Nevertheless, observations from these models must be conducted cautiously, given the loss of accuracy through the modelling process. Overall it appears as though the presence of NDs did impact the healing benefits exhibited by pure SF and didn't accelerate wound healing compared to control. This result could be due to several factors, and the variability between animals adds to the uncertainty. The size of the NDs used in fabrication is significant, given that the interactions between biological cells is

changed by relative size.(Doshi and Mitragotri, 2010) One possibility is that the presence of NDs in the SF matrix inhabited porous areas of the material and prevented cellular ingrowth and vascularisation at the same rate as pure SF films. Alternatively, the interactions between surrounding cells and NDs delayed the healing process due to foreign body reaction. This information would be suggested by the granulation zone area calculations, however due to the lost data it is difficult to make conclusions based on the NDSF group data. Higher granulation areas for NDSF wounds in comparison to control would suggest that the presence of NDs triggered a larger release of immune cells in response to the foreign object. (Anderson et al., 2008) Based on the outcomes of this study, the following experiments were going to be focussed on the image and biosensing capabilities of the impregnated NDs. Given the findings by Khalid et al. on the optical properties of NDSF films, it stands to reason that the next step is to explore potential imaging and biosensing applications of this material, given the advantage of enhanced emission count over pure NDs. The ND quantum biosensing field is rapidly increasing as new studies explore the possibilities of temperature, pH and electric field measurements through manipulation of $NV^-$ centre point defects. For example, (Fujisaku et al., 2019) very recently published a method of determining environmental pH by exploiting the optical and magnetic states of NDs. Similarly, ODMR is a well-known method of determining resonant frequencies of NV centre electrons using fluorescence intensity, which is dependent on environmental temperature.(Zhang et al., 2018) Thus the biosensing capabilities have been verified and continue to be explored as tools in the biomedical field, to extract physiological information in unique ways due to the inherent properties of NDs. (Schrand et al., 2009) The results of this study suggest that NDs may not have a place in the wound healing area, unless more research is done into the biological interactions between NDs and immune cells in full-thickness wounds, and the effects can be counteracted to promote natural or accelerated healing.

A more insightful study would be to analyse the effects of several different electro-spun SF films in order to identify the best spin parameters to produce a film which best integrates with native tissue. As discussed, the spinning parameters in addition to the solution used allow for some diverse scaffold designs, some of which are more suitable for different environments. Some of the important parameters in the field of biomaterial scaffold design are porosity, degradation time and mechanical strength.(Kaplan et al., 2010) In the case of wound healing, the biomaterial scaffold must have comparable properties to that of the lost ECM, such that native cells integrate and accept the material without a foreign body response.(Anderson et al., 2008) Due to the known benefits of natural SF, several studies have been conducted into

the healing acceleration of novel scaffolds consisting of SF polymer hybrids, such as elastin, PCL, chitosan, collagen and many more materials known to have positive effects on biological wound healing.(Altman et al., 2003) The addition of secondary materials into the scaffold structure aim to enhance the healing promotion, as well as improve acceptance and control degradation.(Altman et al., 2003) It is certainly a promising avenue for future medical procedures such as standardised tissue engineering scaffolds and bioresorbable wound dressings. As further research in conducted into the most effective polymer solutions for specific applications, the advances will have clinical significance and improve treatment methods for new tissue growth. However, understanding pure SF's effect on wound healing is a suitable stepping stone to deciding appropriate polymer hybrids.

# Further Research

Further investigation on SF biocompatibility can be conducted by analysing the blood samples from each specimen, in order to determine the concentration and type of immune cells present in the blood plasma as a result of material presence. Two wound tissue quarters were scavenged from each animal wound with the intention to perform protein and RNA analyses for more information. However, due to time constraints on the project, the blood and tissue analyses are omitted from this study but will be conducted later. An additional component to the progression of this study is in-vivo fluoresce imaging of the NDs embedded within the wound, to quantify the intensity of the signal received. In terms of a further investigation, an interesting follow on study would be to investigate the impact of conjugating bioactive molecules with the SF scaffold, to further accelerate the wound healing process by providing pre-cursors or growth factors necessary for the healing process. Research surrounding the benefits of these hybrid scaffolds has been conducted, and generally the healing acceleration of SF is enhanced with appropriate combinations.(Altman et al., 2003) As mentioned previously, the ND size may have contributed to poor interactions between cells and contributed to a larger influx due to poor acceptance. Further studies could be conducted into the discrepancies between native cells and NDs based on size, to better understand the results seen here. The initial perspectives for the study were to analyse the biocompatibility and diagnostic potential of NDSF hybrid films in wound healing. The motivation was targeting the current deficit in wound healing therapies to combat increasing rates of non-healing wounds and reduce amputation in these patients. The pursuit to find novel wound healing therapies is high among different researchers to combat increased rates

of disease related chronic wounds, and biomaterial scaffold are certainly an avenue which must be capitalised upon. In terms of biosensing, the idea of incorporating NDs was to open the door to diagnostics for patient wounds. Given that temperature and pH are both important parameters dictating the success of wound healing, a novel, real-time non-contact method of extracting that data would be of great benefit to physicians, to prevent frequent healing disturbance through replacing wound dressings. Methods of pH and temperature sensing with NDs have been established recently, with a promising forecast for future medical device development.(Fujisaku et al., 2019; Zhu et al., 2012) Given the recent uprising of ND research for quantum sensing, many of these methods are not at the stage of being incorporated smoothly with existing medical procedures, so with time and information the advances will continue. An application of NDs in wound healing is drug delivery, such as previously used ND vehicles for controlled insulin release.(Mengesha and Youan, 2013) The results of this study analysing the wound healing effects of topical ND administration suggest that NDs are more suited for other healing applications, due to the hindrance of SF's benefits in accelerated wound healing.

# Conclusion

The healing acceleration of the SF methanol treated films were confirmed in the humanised Murine model as compared to control, by achieving greater wound closure over the 10-day experiment. NDSF methanol treated films did not exhibit the same wound closure effects as pure treated SF, and no significant wound closure improvement was observed for NDSF wounds over control, suggesting that the presence of the NDs did affect the natural healing promotion of SF. Granulation zone area calculations and doppler blood perfusion results did not exhibit notable correlations for mice in specific groups, largely due to inherent variability and exogeneous factors for each specimen. Further blood plasma, RNA and protein tissue analysis on specimens will reveal more information to the tune of biocompatibility. SF verified the literature on its promotive effects on wound healing, and biocompatibility. NDSF wounds did not appear to exhibit large adverse effects in specimens, and wound closure was not significantly impacted relative to control, on this basis the NDSF films can be assumed biocompatible in the context of this healing model. Given that the wound healing acceleration benefits were somewhat mitigated by the presence of the NDs, it is suggested that the NDSF hybrid is explored for other medial applications to exploit the emission enhancement property.

# References


Altman, G.H., Diaz, F., Jakuba, C., Calabro, T., Horan, R.L., Chen, J., Lu, H., Richmond, J., Kaplan, D.L., 2003. Silk-based biomaterials. Biomaterials 24, 401–416. https://doi.org/10.1016/S0142-9612(02)00353-8

Anderson, J.M., Rodriguez, A., Chang, D.T., 2008. FOREIGN BODY REACTION TO BIOMATERIALS. Semin. Immunol. 20, 86–100. https://doi.org/10.1016/j.smim.2007.11.004

Arai, T., Freddi, G., Innocenti, R., Tsukada, M., 2004. Biodegradation of Bombyx mori silk fibroin fibers and films. J. Appl. Polym. Sci. 91, 2383–2390. https://doi.org/10.1002/app.13393

Australian Institute of Health and Welfare, 2013. Diabetes expenditure in Australia 2008-09.

Boughton, E., Mclennan, S.V., 2013. Biomimetic scaffolds for skin tissue and wound repair, in: Biomimetic Biomaterials. Elsevier, pp. 153–180. https://doi.org/10.1533/9780857098887.2.153

Brem, H., Tomic-Canic, M., 2007. Cellular and molecular basis of wound healing in diabetes. J. Clin. Invest. 117, 1219–1222. https://doi.org/10.1172/JCI32169

Cao, Y., Wang, B., 2009. Biodegradation of Silk Biomaterials. Int. J. Mol. Sci. 10, 1514–1524. https://doi.org/10.3390/ijms10041514

Doshi, N., Mitragotri, S., 2010. Macrophages Recognize Size and Shape of Their Targets. PLoS ONE 5. https://doi.org/10.1371/journal.pone.0010051

Dunn, L., Prosser, H.C.G., Tan, J.T.M., Vanags, L.Z., Ng, M.K.C., Bursill, C.A., 2013. Murine Model of Wound Healing. J. Vis. Exp. JoVE. https://doi.org/10.3791/50265

Emmerson, E., Campbell, L., Davies, F.C.J., Ross, N.L., Ashcroft, G.S., Krust, A., Chambon, P., Hardman, M.J., 2012. Insulin-like growth factor-1 promotes wound healing in estrogen-deprived mice: new insights into cutaneous IGF-1R/ERα cross talk. J. Invest. Dermatol. 132, 2838–2848. https://doi.org/10.1038/jid.2012.228

Fischer, A.H., Jacobson, K.A., Rose, J., Zeller, R., 2008. Hematoxylin and eosin staining of tissue and cell sections. CSH Protoc. 2008, pdb.prot4986. https://doi.org/10.1101/pdb.prot4986

Fujisaku, T., Tanabe, R., Onoda, S., Kubota, R., Segawa, T.F., So, F.T.-K., Ohshima, T., Hamachi, I., Shirakawa, M., Igarashi, R., 2019. pH Nanosensor Using Electronic Spins in Diamond. ACS Nano. https://doi.org/10.1021/acsnano.9b05342

Gethin, G., 2007. The significance of surface pH in chronic wounds. Wounds UK 3.

Giordano, N., 2009. College Physics: Reasoning and Relationships. Cengage Learning.

Gonzalez, A.C. de O., Costa, T.F., Andrade, Z. de A., Medrado, A.R.A.P., 2016. Wound healing - A literature review. An. Bras. Dermatol. 91, 614–620. https://doi.org/10.1590/abd1806-4841.20164741

Guo, S., DiPietro, L.A., 2010. Factors Affecting Wound Healing. J. Dent. Res. 89, 219–229. https://doi.org/10.1177/0022034509359125

Han, G., Ceilley, R., 2017. Chronic Wound Healing: A Review of Current Management and Treatments. Adv. Ther. 34, 599–610. https://doi.org/10.1007/s12325-017-0478-y

Hayashi, K., Matsuzaki, Y., Taniguchi, T., Shimo-Oka, T., Nakamura, I., Onoda, S., Ohshima, T., Morishita, H., Fujiwara, M., Saito, S., Mizuochi, N., 2018. Optimization of Temperature Sensitivity Using the Optically Detected Magnetic-Resonance Spectrum of a Nitrogen-Vacancy Center Ensemble. Phys. Rev. Appl. 10, 034009. https://doi.org/10.1103/PhysRevApplied.10.034009

Hong, Y., 2016. 19 - Electrospun fibrous polyurethane scaffolds in tissue engineering, in: Cooper, S.L., Guan, J. (Eds.), Advances in Polyurethane Biomaterials. Woodhead Publishing, pp. 543–559. https://doi.org/10.1016/B978-0-08-100614-6.00019-6

Howard, D., Buttery, L.D., Shakesheff, K.M., Roberts, S.J., 2008. Tissue engineering: strategies, stem cells and scaffolds. J. Anat. 213, 66–72. https://doi.org/10.1111/j.1469-7580.2008.00878.x

Inagaki, M., Kang, F., Toyoda, M., Konno, H., 2014. Chapter 8 - Carbon Nanofibers Via Electrospinning, in: Inagaki, M., Kang, F., Toyoda, M., Konno, H. (Eds.), Advanced Materials Science and Engineering of Carbon. Butterworth-Heinemann, Boston, pp. 165–188. https://doi.org/10.1016/B978-0-12-407789-8.00008-9

Kaplan, D.L., Jin, H.-J., Rutledge, G., Fridrikh, S., 2010. Silk biomaterials and methods of use thereof. US7674882B2.

Khalid, A., Lodin, R., Domachuk, P., Tao, H., Moreau, J.E., Kaplan, D.L., Omenetto, F.G., Gibson, B.C., Tomljenovic-Hanic, S., 2014. Synthesis and characterization of biocompatible nanodiamond-silk hybrid material. Biomed. Opt. Express 5, 596–608. https://doi.org/10.1364/BOE.5.000596

Kumari, P., Mk, C., Vp, V., 2013. Spider web ointment: A traditional based approach in Cutaneous wound healing 12, 7.

Lakkis, F.G., Lechler, R.I., 2013. Origin and Biology of the Allogeneic Response. Cold Spring Harb. Perspect. Med. 3. https://doi.org/10.1101/cshperspect.a014993

Legislation Revision and Publication Act, 2017. Best practice methodology in the use of animals for scientific purposes | NHMRC [WWW Document]. URL https://www.nhmrc.gov.au/about-us/publications/best-practice-methodology-use-animals-scientific-purposes (accessed 10.21.19).

Lima, M.H.M., Caricilli, A.M., de Abreu, L.L., Araújo, E.P., Pelegrinelli, F.F., Thirone, A.C.P., Tsukumo, D.M., Pessoa, A.F.M., dos Santos, M.F., de Moraes, M.A., Carvalheira, J.B.C., Velloso, L.A., Saad, M.J.A., 2012. Topical insulin accelerates wound healing in diabetes by enhancing the AKT and ERK pathways: a double-blind placebo-controlled clinical trial. PloS One 7, e36974. https://doi.org/10.1371/journal.pone.0036974

Lindsay S. Wray, Xiao Hu, Jabier Gallego, Irene Georgakoudi, Fiorenzo G. Omenetto, Daniel Schmidt, David L. Kaplan, 2011. Effect of processing on silk-based biomaterials: Reproducibility and biocompatibility - Wray - 2011 - Journal of Biomedical Materials Research Part B: Applied Biomaterials - Wiley Online Library [WWW Document]. URL https://onlinelibrary.wiley.com/doi/full/10.1002/jbm.b.31875 (accessed 9.23.19).

McGuiness, W., Vella, E., Harrison, D., 2004. Influence of dressing changes on wound temperature. J. Wound Care 13, 383–385. https://doi.org/10.12968/jowc.2004.13.9.26702

Mengesha, A.E., Youan, B.-B.C., 2013. Nanodiamonds for drug delivery systems, in: Diamond-Based Materials for Biomedical Applications. Elsevier, pp. 186–205. https://doi.org/10.1533/9780857093516.2.186

Micheels, J., Alsbjorn, B., Sorensen, B., 1984. Laser doppler flowmetry. A new non-invasive measurement of microcirculation in intensive care? Resuscitation 12, 31–39. https://doi.org/10.1016/0300-9572(84)90056-x

Neumann, P., Jakobi, I., Dolde, F., Burk, C., Reuter, R., Waldherr, G., Honert, J., Wolf, T., Brunner, A., Shim, J.H., Suter, D., Sumiya, H., Isoya, J., Wrachtrup, J., 2013. High-Precision Nanoscale Temperature Sensing Using Single Defects in Diamond. Nano Lett. 13, 2738–2742. https://doi.org/10.1021/nl401216y

NHMRC, 2002. Animal Welfare Act 1985 35.

Numata, K., Cebe, P., Kaplan, D.L., 2010. Mechanism of Enzymatic Degradation of Beta-sheet Crystals. Biomaterials 31, 2926. https://doi.org/10.1016/j.biomaterials.2009.12.026

O'Brien, F.J., 2011. Biomaterials & scaffolds for tissue engineering. Mater. Today 14, 88–95. https://doi.org/10.1016/S1369-7021(11)70058-X

Pendsey, S.P., 2010. Understanding diabetic foot. Int. J. Diabetes Dev. Ctries. 30, 75–79. https://doi.org/10.4103/0973-3930.62596

Pettker, C.M., Campbell, K.H., 2018. 14 - Antepartum Fetal Assessment, in: Gleason, C.A., Juul, S.E. (Eds.), Avery's Diseases of the Newborn (Tenth Edition). Content Repository Only!, Philadelphia, pp. 145-157.e3. https://doi.org/10.1016/B978-0-323-40139-5.00014-0

Scherer, S.S., Pietramaggiori, G., Mathews, J.C., Chan, R., Fiorina, P., Orgill, D.P., 2008. Wound healing kinetics of the genetically diabetic mouse. Wounds 20, 18–28.

Schneider, L.A., Korber, A., Grabbe, S., Dissemond, J., 2007. Influence of pH on wound-healing: a new perspective for wound-therapy? Arch. Dermatol. Res. 298, 413–420. https://doi.org/10.1007/s00403-006-0713-x

Schrand, A.M., Hens, S.A.C., Shenderova, O.A., 2009. Nanodiamond Particles: Properties and Perspectives for Bioapplications. Crit. Rev. Solid State Mater. Sci. 34, 18–74. https://doi.org/10.1080/10408430902831987

Sekiguchi, T., Sotoma, S., Harada, Y., 2018. Fluorescent nanodiamonds as a robust temperature sensor inside a single cell. Biophys. Physicobiology 15, 229–234. https://doi.org/10.2142/biophysico.15.0_229

Sugihara, A., Sugiura, K., Morita, H., Ninagawa, T., Tubouchi, K., Tobe, R., Izumiya, M., Horio, T., Abraham, N.G., Ikehara, S., 2000. Promotive Effects of a Silk Film on Epidermal Recovery from Full-Thickness Skin Wounds. Proc. Soc. Exp. Biol. Med. 225, 58–64. https://doi.org/10.1111/j.1525-1373.2000.22507.x

Tahir, H.M., Rakha, A., Mukhtar, M.K., Yaqoob, R., Samiullah, K., Ahsan, M.M., 2017. EVALUATION OF WOUND HEALING POTENTIAL OF SPIDER SILK USING MICE MODEL 7.

Vasconcelos, A., Gomes, A.C., Cavaco-Paulo, A., 2012. Novel silk fibroin/elastin wound dressings. Acta Biomater. 8, 3049–3060. https://doi.org/10.1016/j.actbio.2012.04.035

Vepari. C, Kaplan, D.L., 2007. Silk as a Biomaterial. Prog. Polym. Sci. 32, 991–1007. https://doi.org/10.1016/j.progpolymsci.2007.05.013

Wang, Y., Kim, H.-J., Vunjak-Novakovic, G., Kaplan, D.L., 2006. Stem cell-based tissue engineering with silk biomaterials. Biomaterials, Biomaterials and Stem Cells 27, 6064–6082. https://doi.org/10.1016/j.biomaterials.2006.07.008

Yang, Y., Chen, X., Ding, F., Zhang, P., Liu, J., Gu, X., 2007. Biocompatibility evaluation of silk fibroin with peripheral nerve tissues and cells in vitro. Biomaterials 28, 1643–1652. https://doi.org/10.1016/j.biomaterials.2006.12.004

Yuan, H., Zhou, Q., Zhang, Y., 2017. 6 - Improving fiber alignment during electrospinning, in: Afshari, M. (Ed.), Electrospun Nanofibers, Woodhead Publishing Series in Textiles. Woodhead Publishing, pp. 125–147. https://doi.org/10.1016/B978-0-08-100907-9.00006-4

Zhang, H., Belvin, C., Li, W., Wang, J., Wainwright, J., Berg, R., Bridger, J., 2018. Little bits of diamond: Optically detected magnetic resonance of nitrogen-vacancy centers. Am. J. Phys. 86, 225–236. https://doi.org/10.1119/1.5023389

Zhou, C.-J., Li, Y., Yao, S.-W., He, J.-H., 2019. Silkworm-based silk fibers by electrospinning. Results Phys. 15, 102646. https://doi.org/10.1016/j.rinp.2019.102646

Zhu, Y., Li, J., Li, W., Zhang, Y., Yang, X., Chen, N., Sun, Y., Zhao, Y., Fan, C., Huang, Q., 2012. The Biocompatibility of Nanodiamonds and Their Application in Drug Delivery Systems. Theranostics 2, 302–312. https://doi.org/10.7150/thno.3627

# Appendices

## Treatment Films

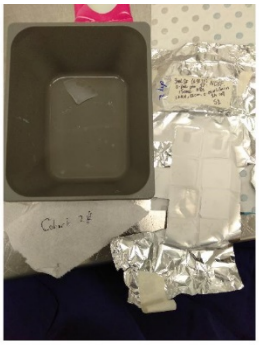

# Biocompatibility Study 1# Images

## Specimens 1-7: Surgical Intervention

Mouse1 - SF

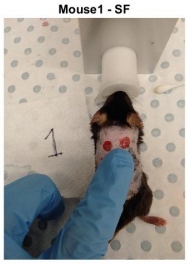


Mouse2 - SF

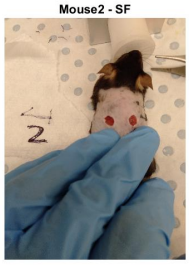


Mouse3 - SF


Mouse4 - NDSF


Mouse5 - NDSF


Mouse6 - NDSF

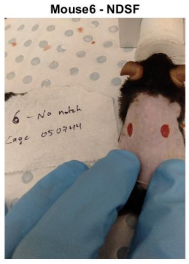


Mouse7 - NDSF

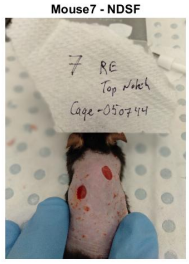


Mouse1 - SF


Mouse2 - SF

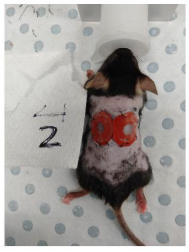


Mouse3 - SF

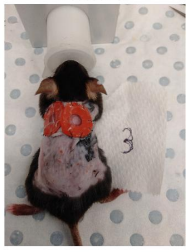


Mouse4 - NDSF

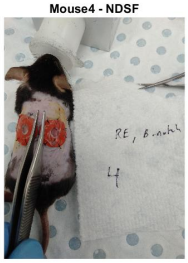


Mouse5 - NDSF

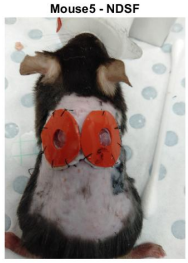

Mouse6 - NDSF

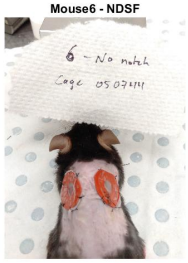


Mouse7 - NDSF

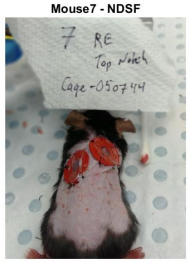

# Wound Closure

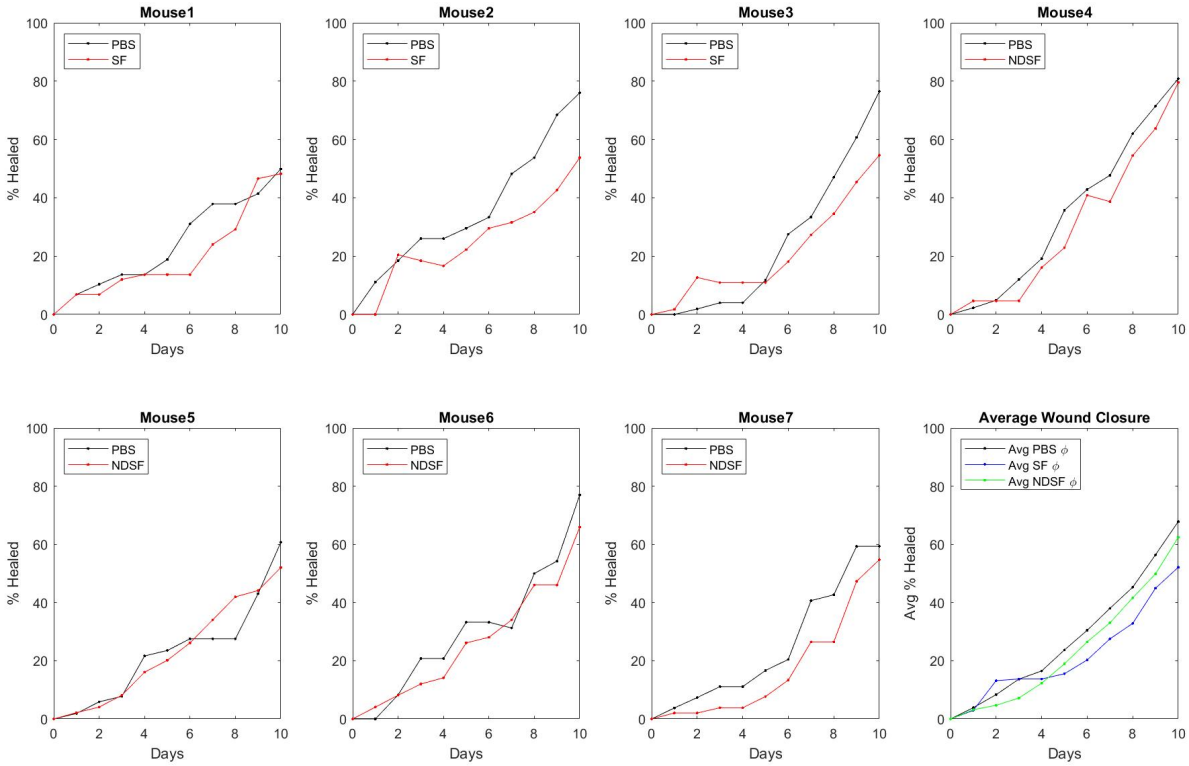


# Average Blood Perfusion

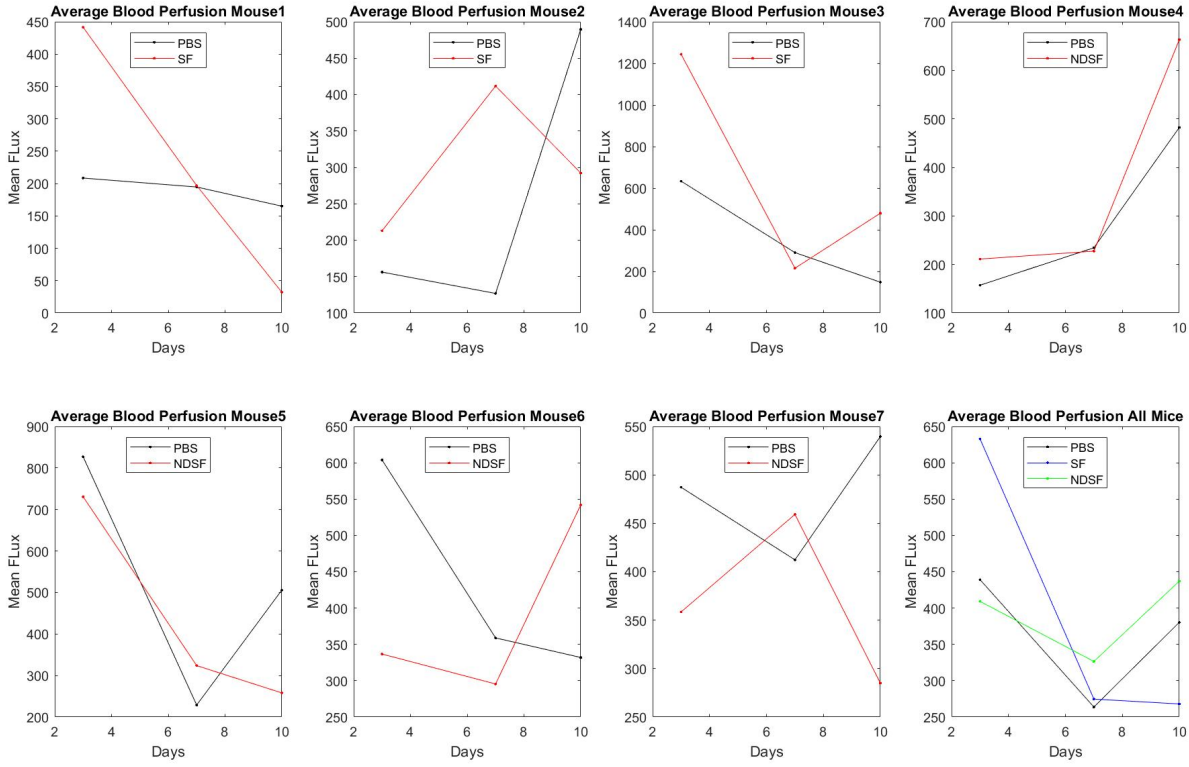

Mouse1

Control

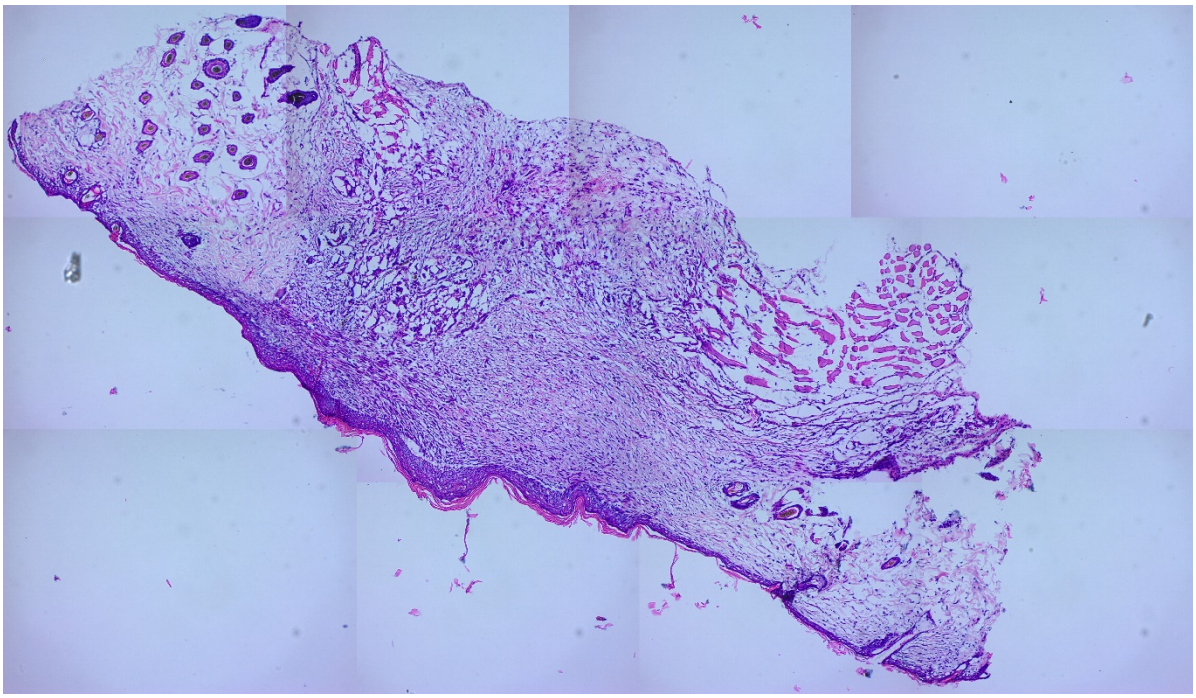

SF

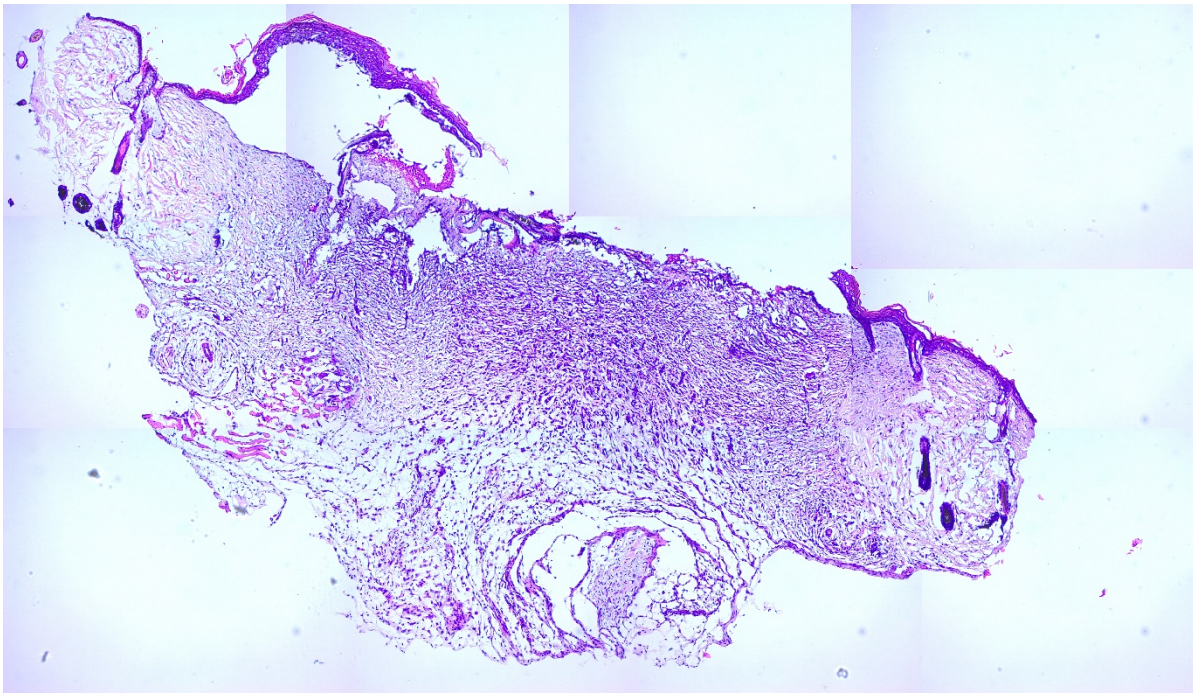

Mouse2

Control

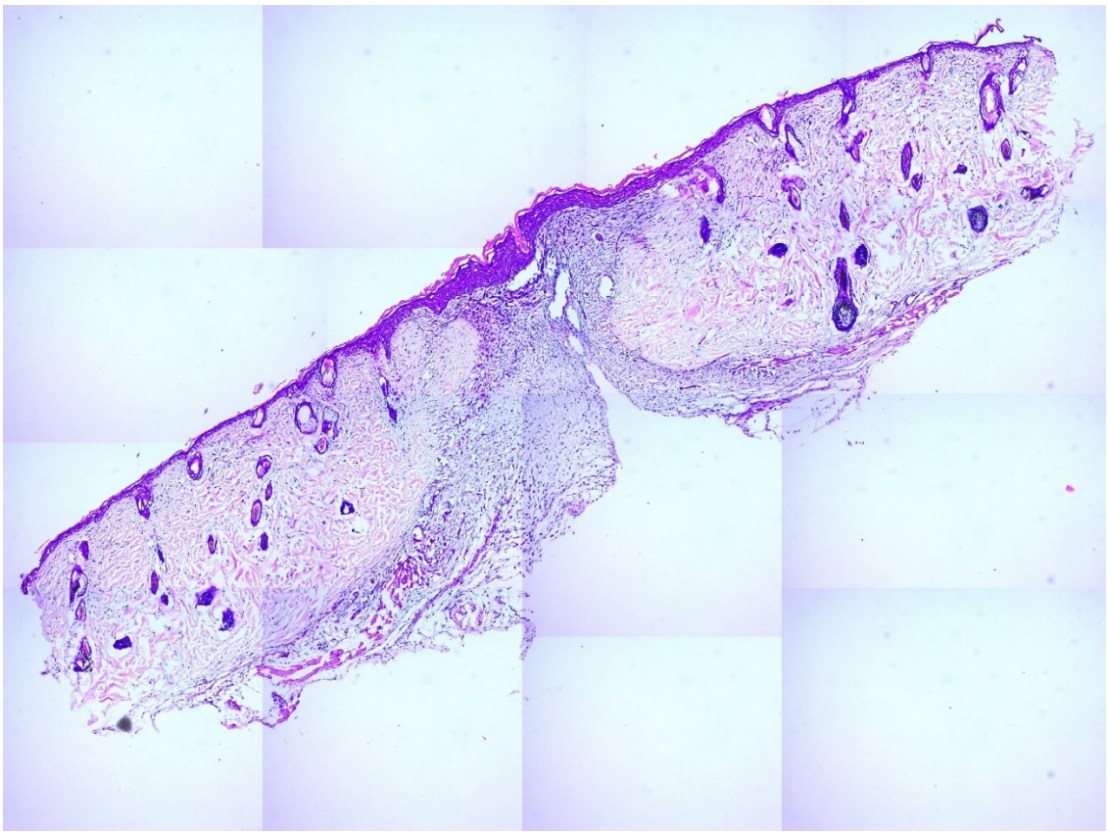

SF

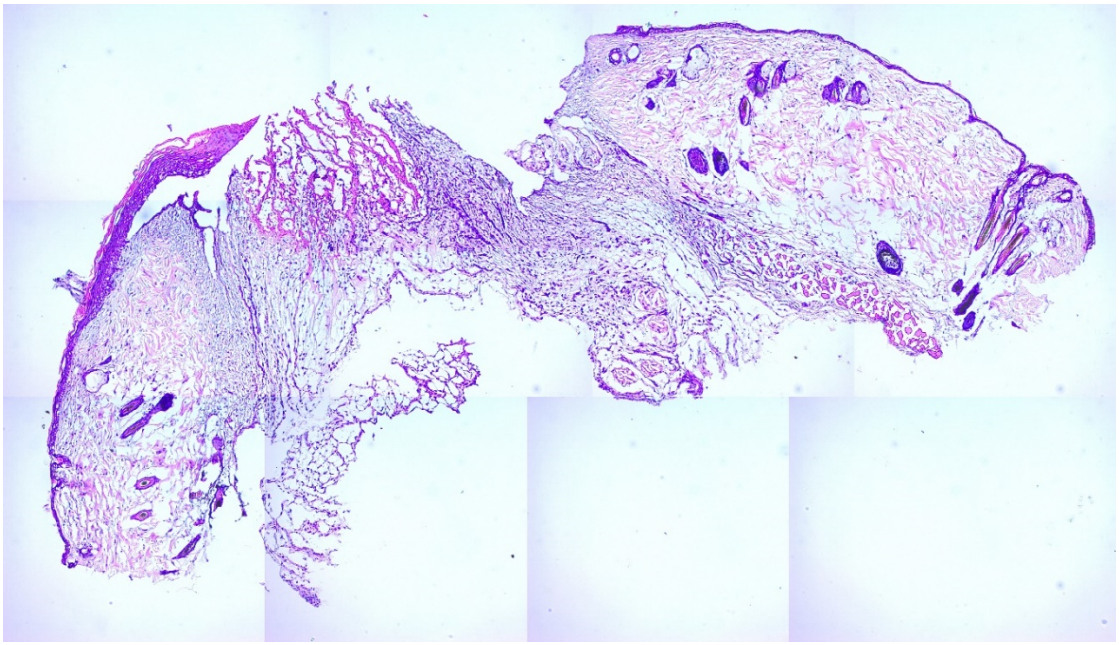

Mouse3

Control

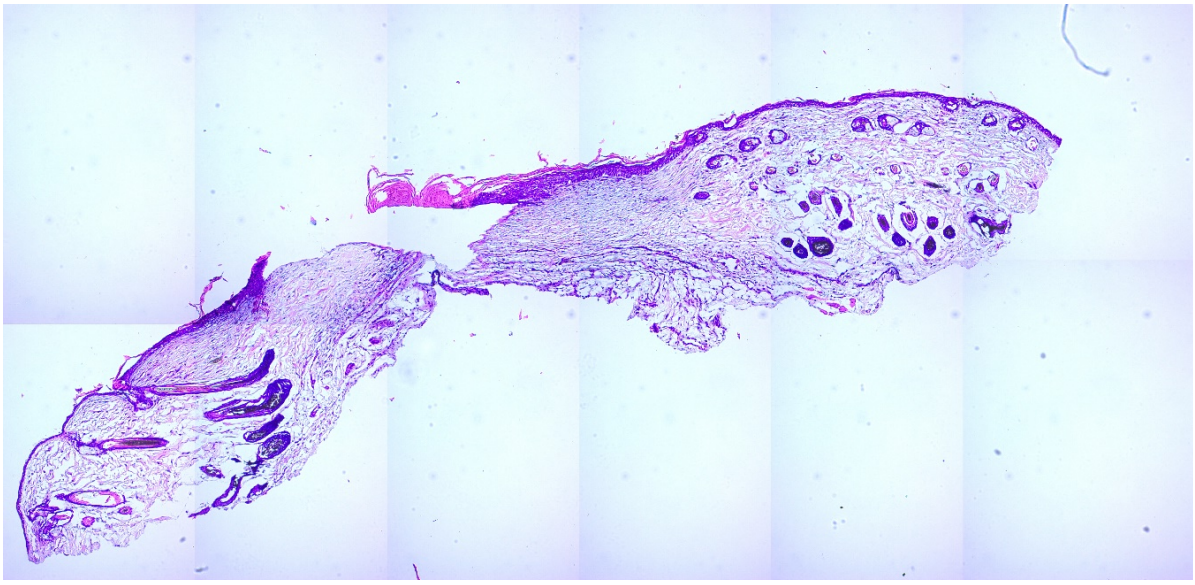

SF

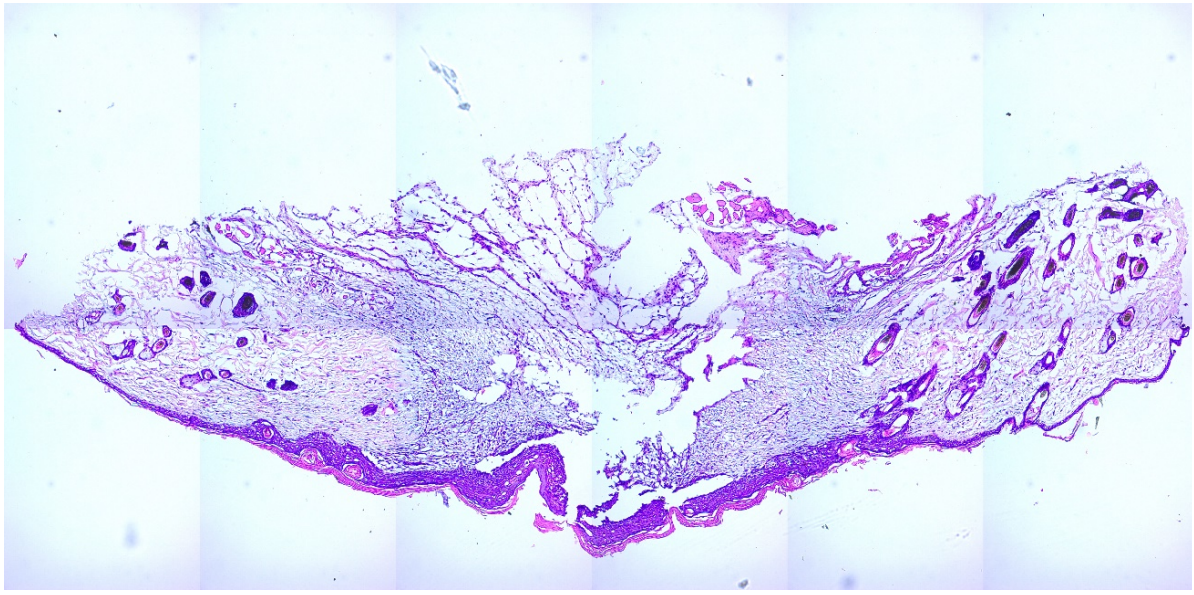

Mouse4

Control

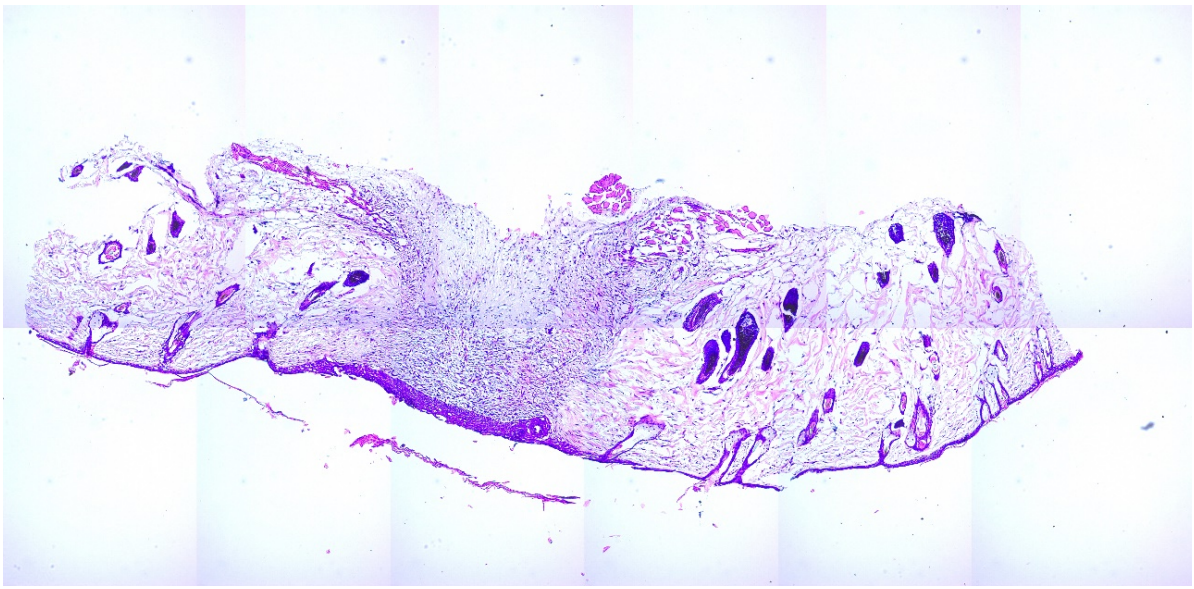

NDSF

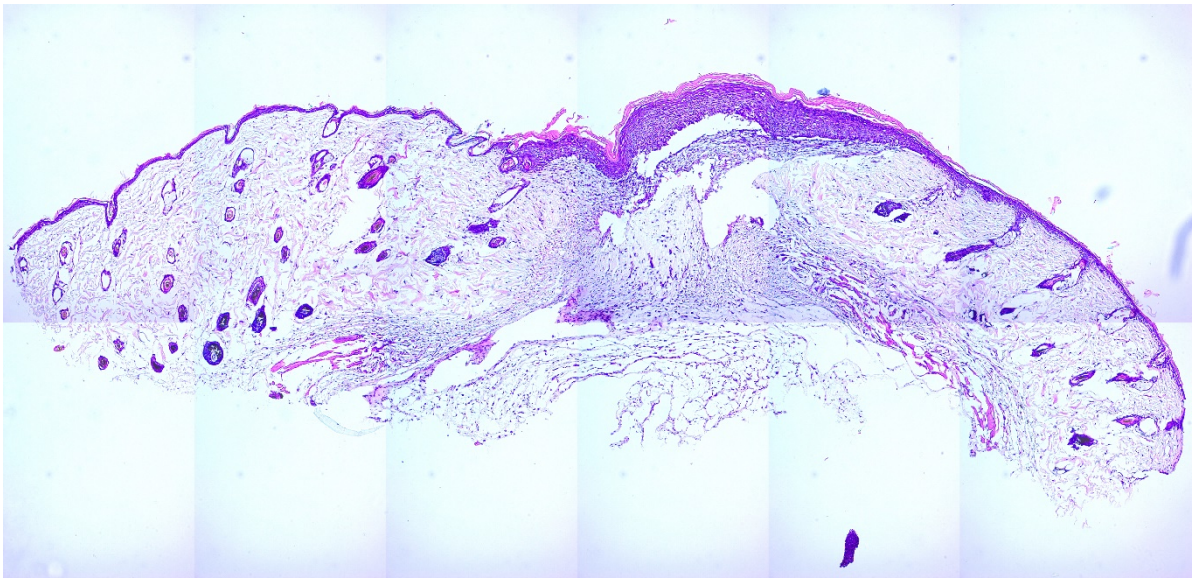

Mouse5

Control

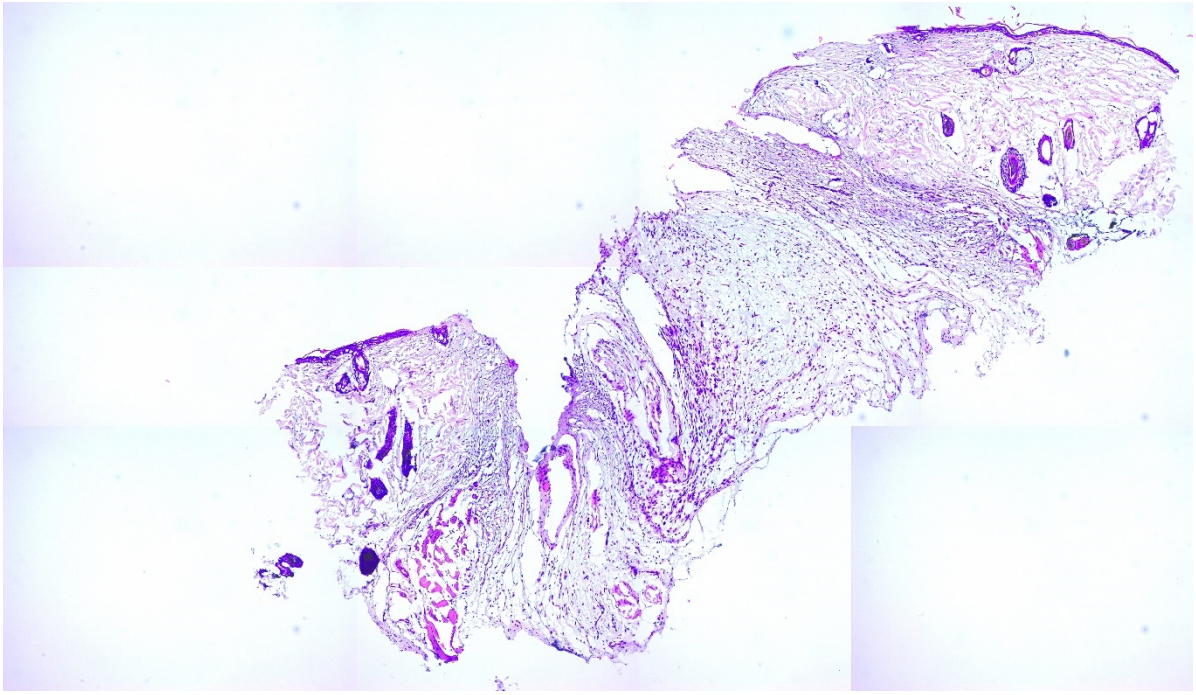

NDSF

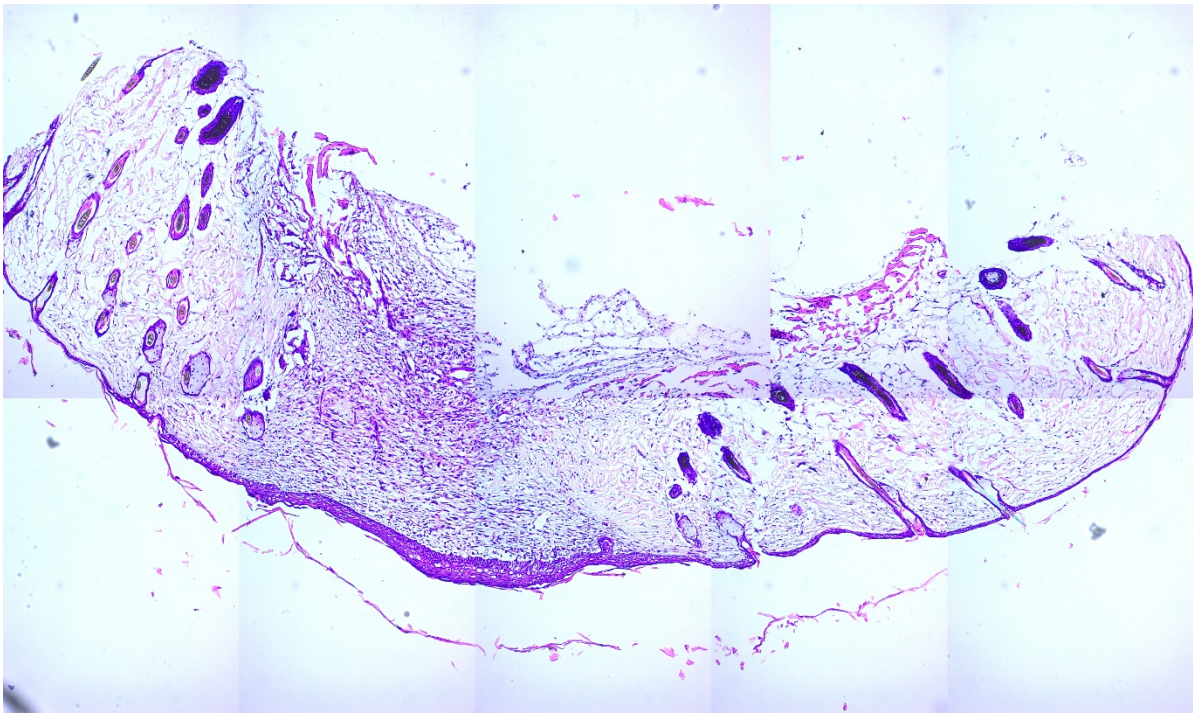

Mouse6

Control

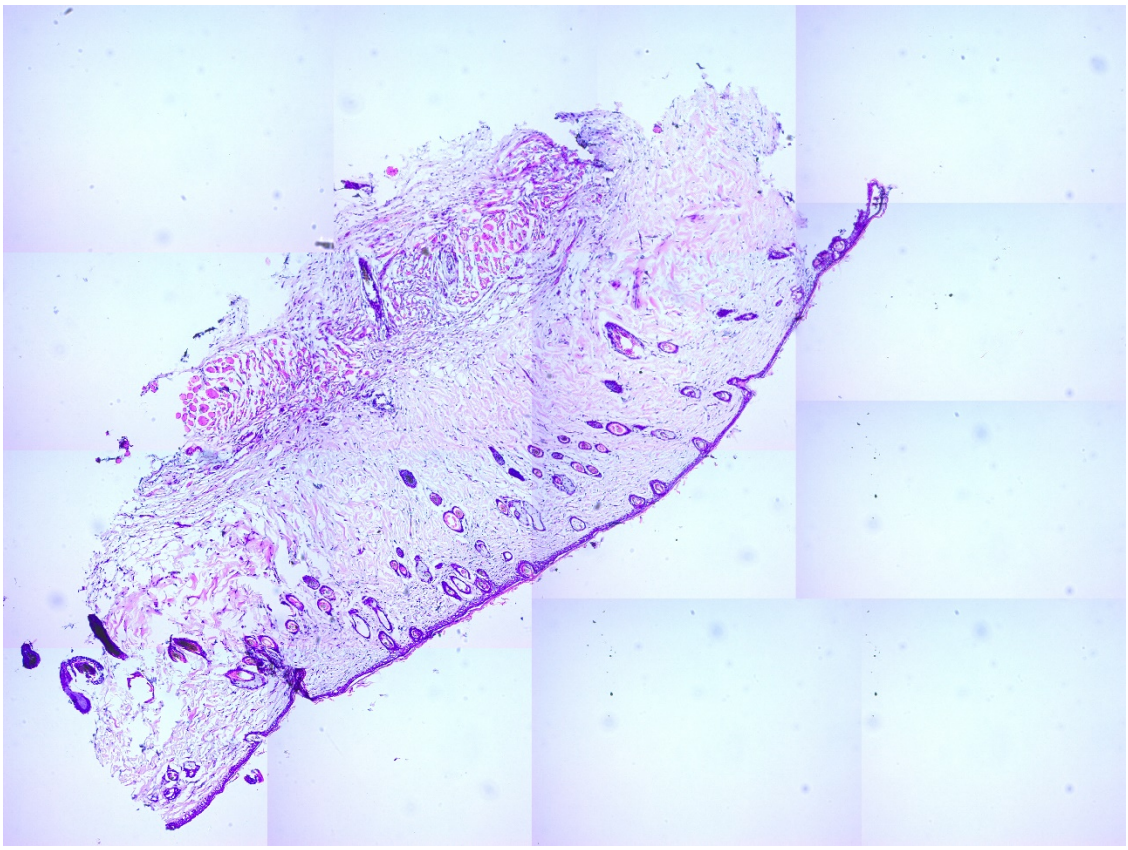

NDSF

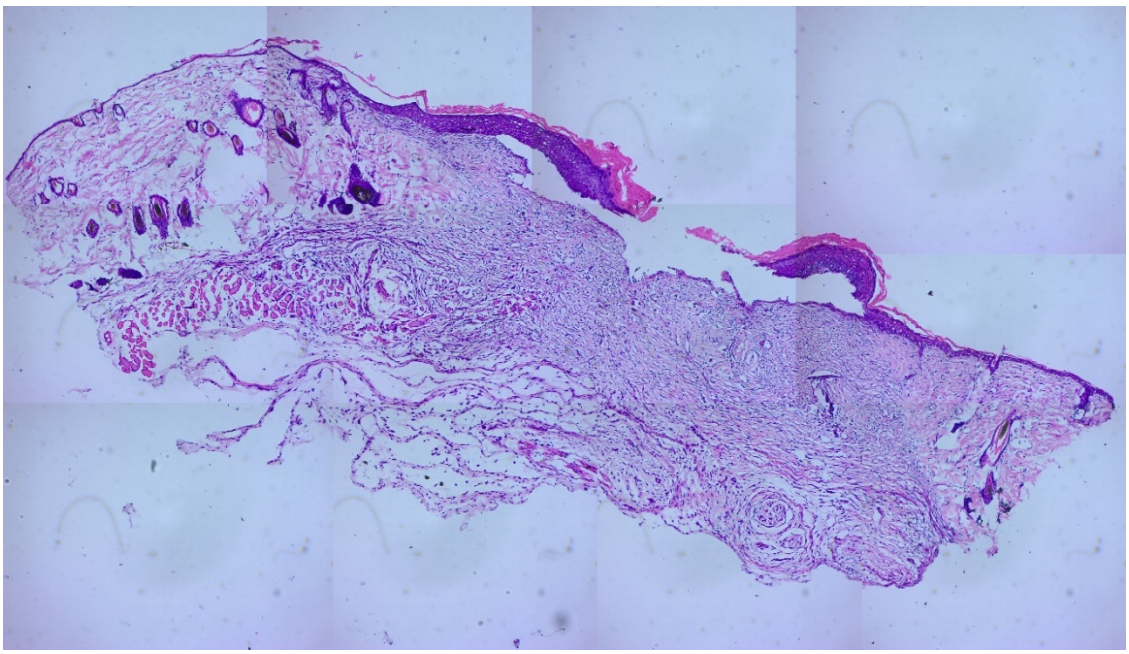

Mouse7

Control

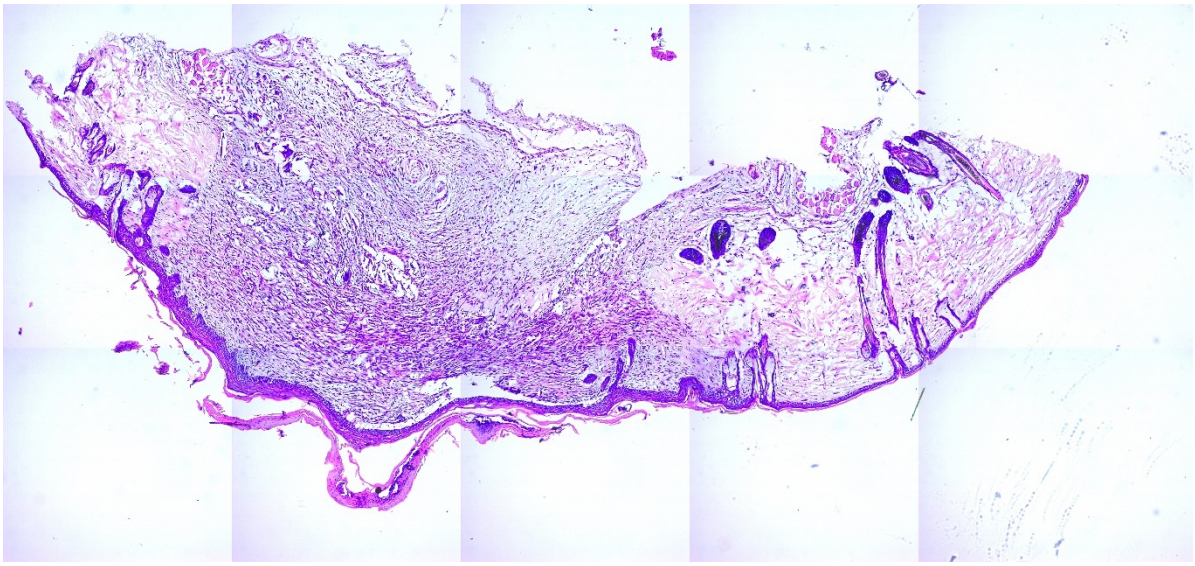

NDSF

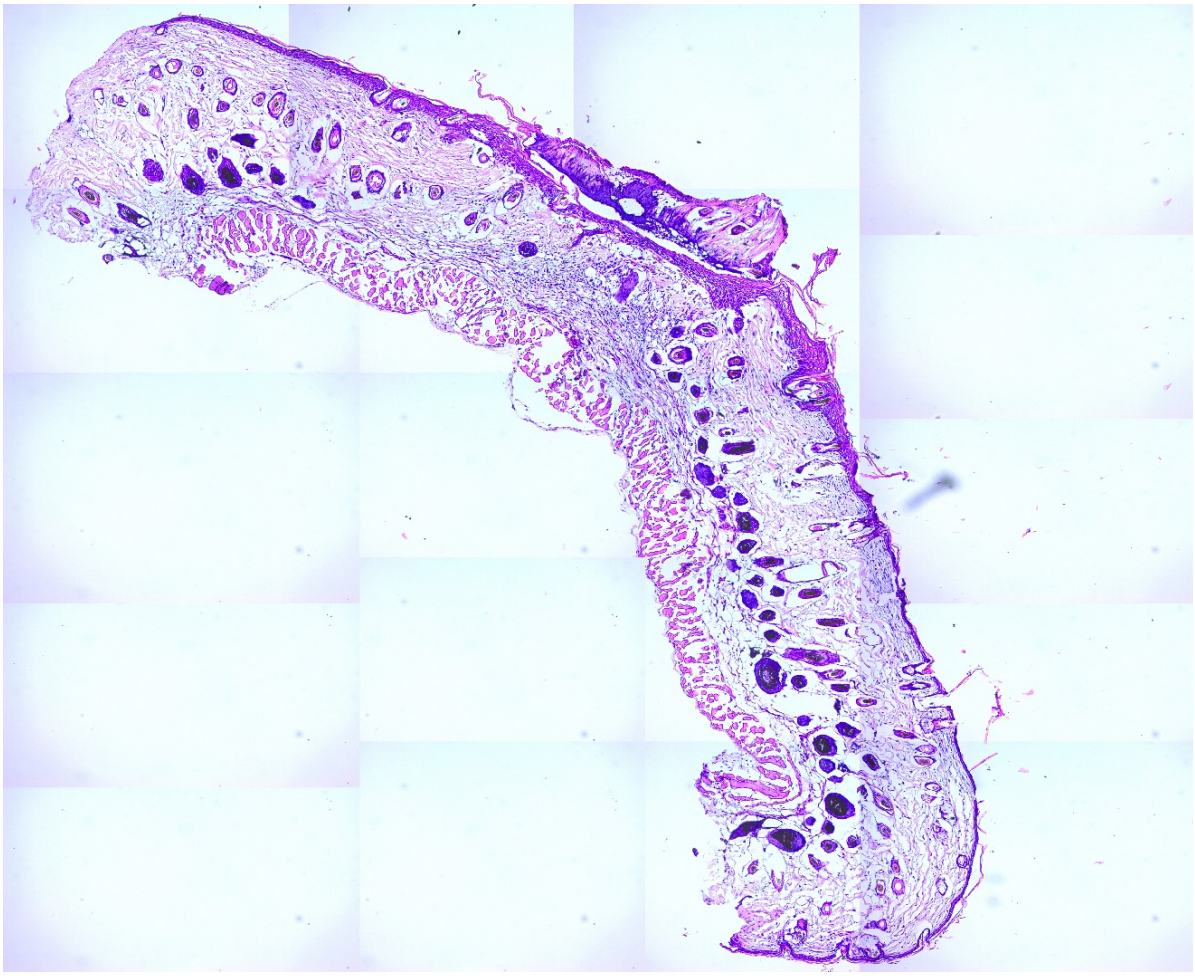

# Biocompatibility Study 2# Images

## Specimens 8-15: Surgical Intervention

Mouse8 - SF


Mouse9 - SF

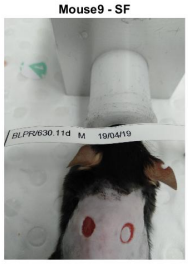

Mouse10 - SF

Mouse11 - SF

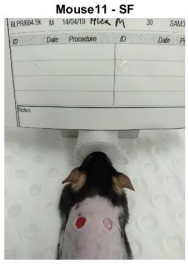

Mouse12 - NDSF

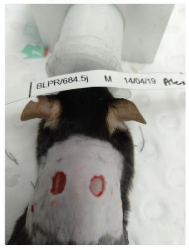

Mouse13 - NDSF

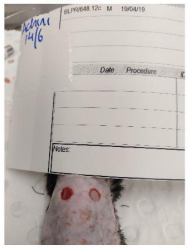

Mouse14 - NDSF

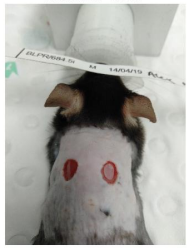

Mouse15 - NDSF

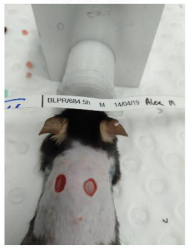

Mouse8 - SF


Mouse9 - SF

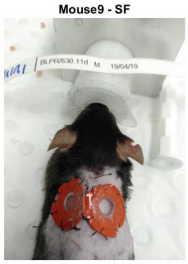

Mouse10 - SF

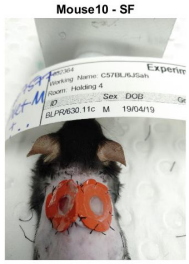

Mouse11 - SF

Mouse12 - NDSF

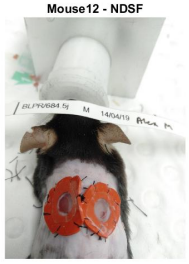

Mouse13 - NDSF

Mouse14 - NDSF

Mouse15 - NDSF

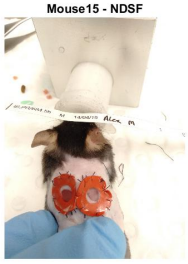

Mouse8

Control

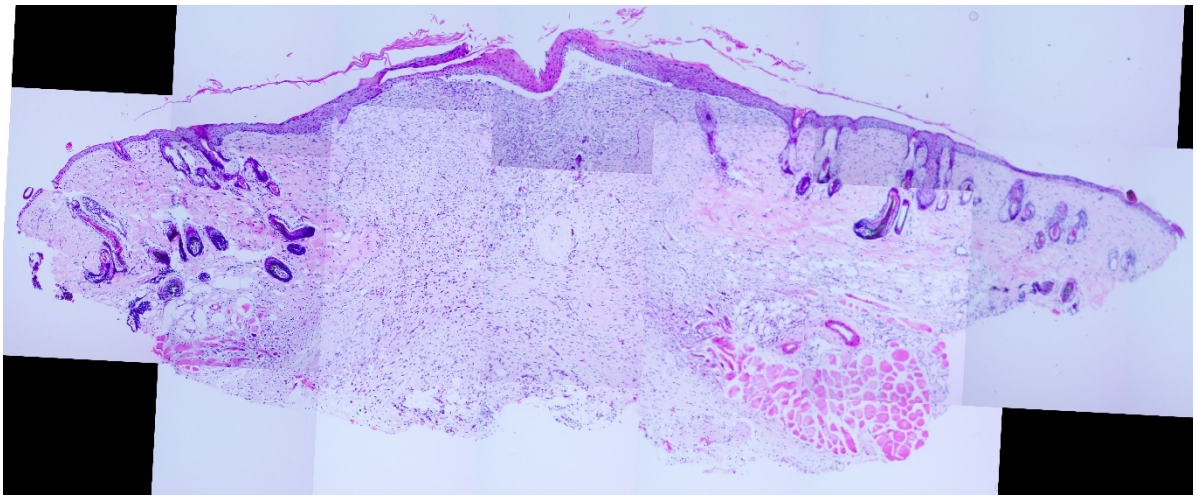

SF

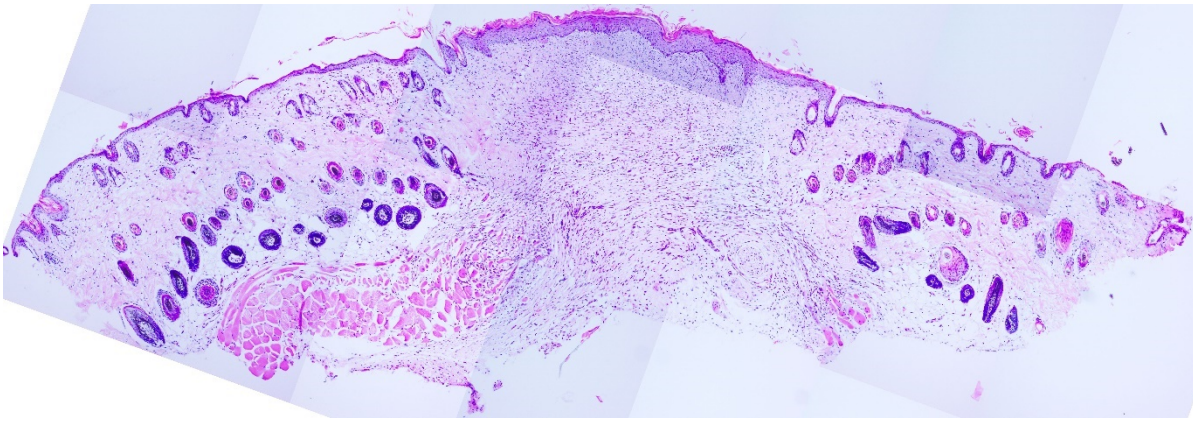

Mouse9

Control

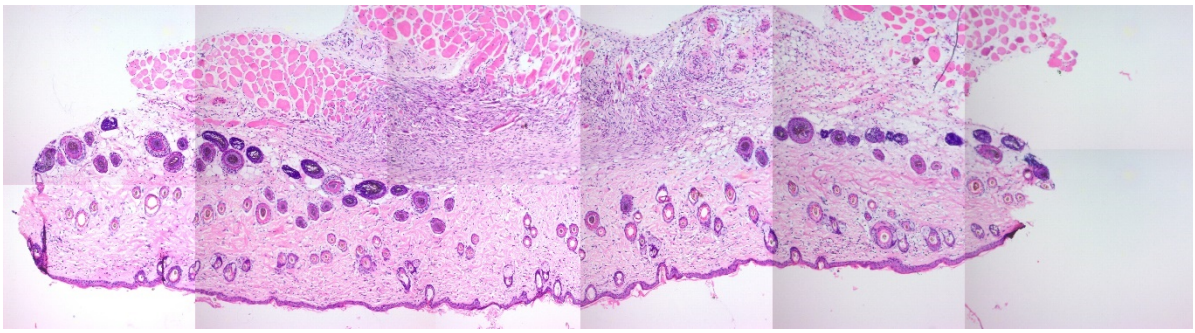

SF

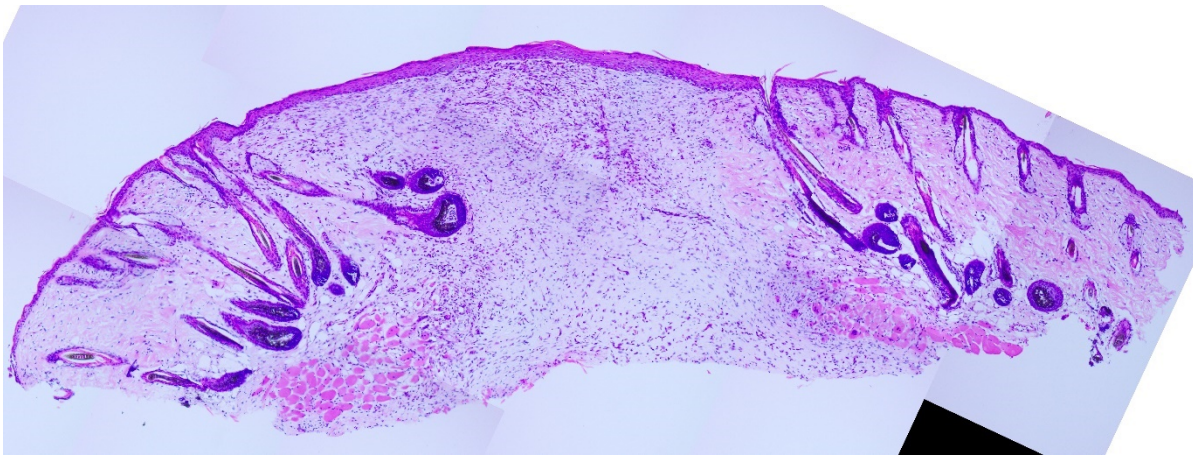

Mouse10

Control

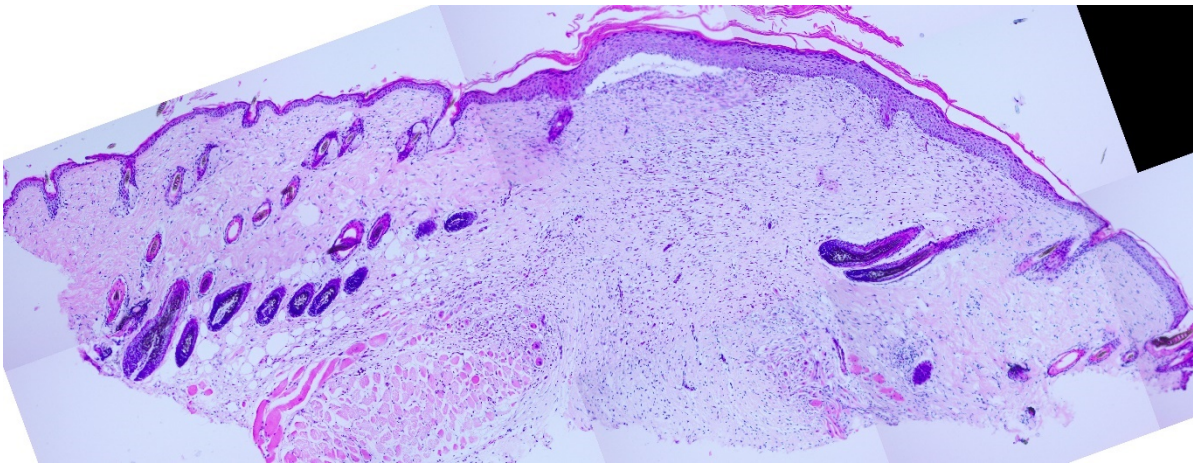

SF

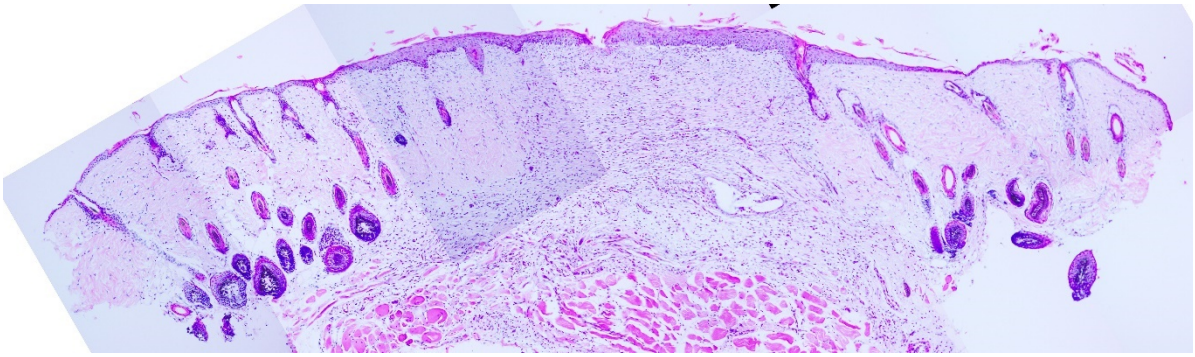

Mouse11

Control

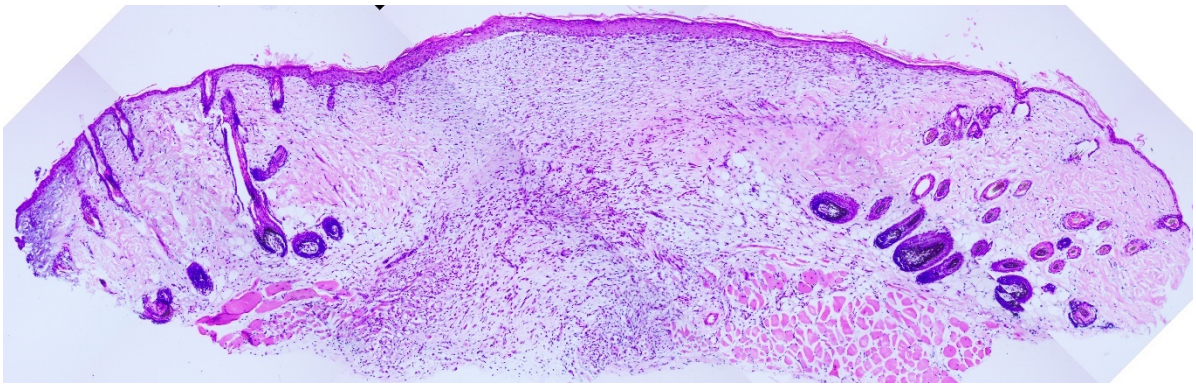

SF

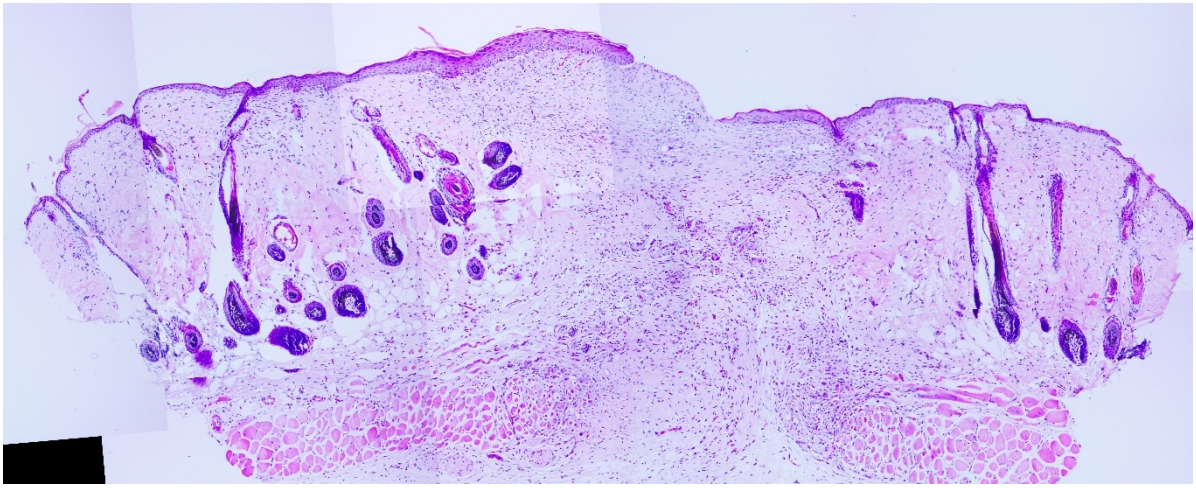

Mouse12

Control

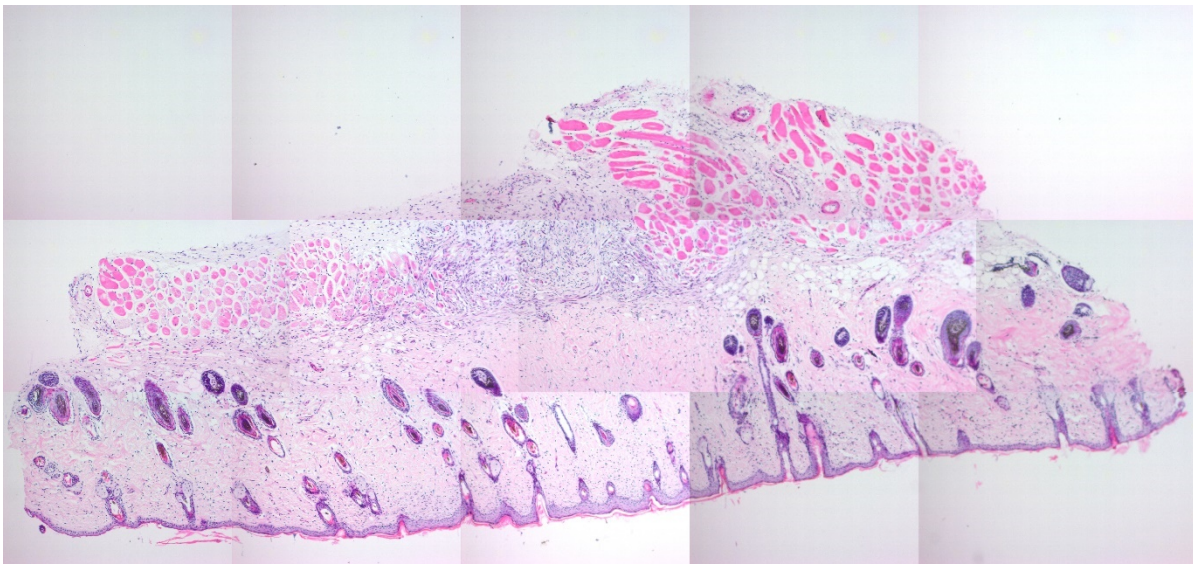

NDSF

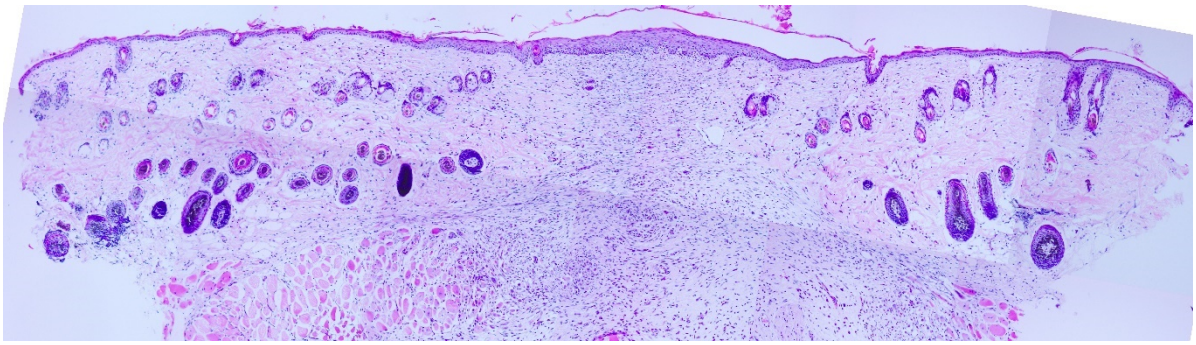

Mouse13

Control

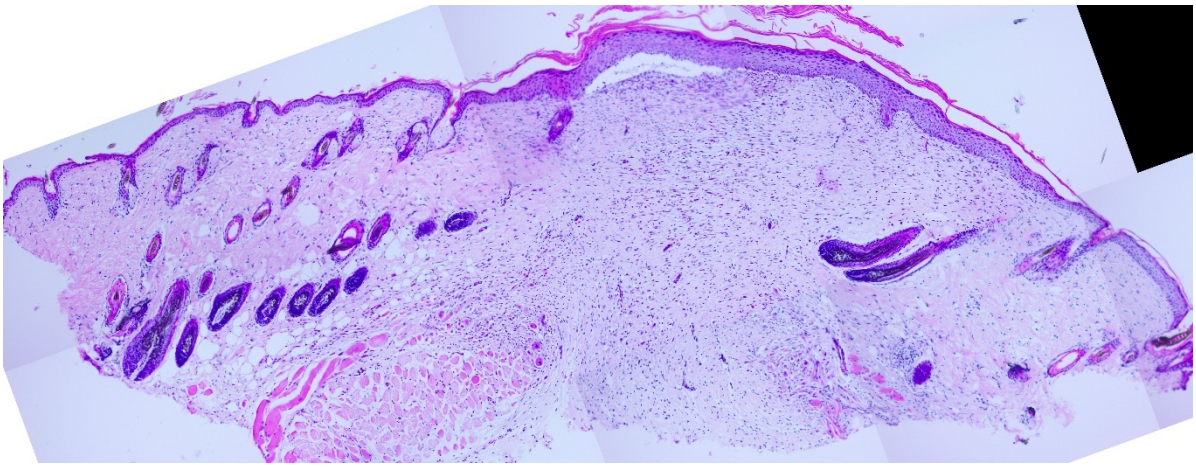

NDSF

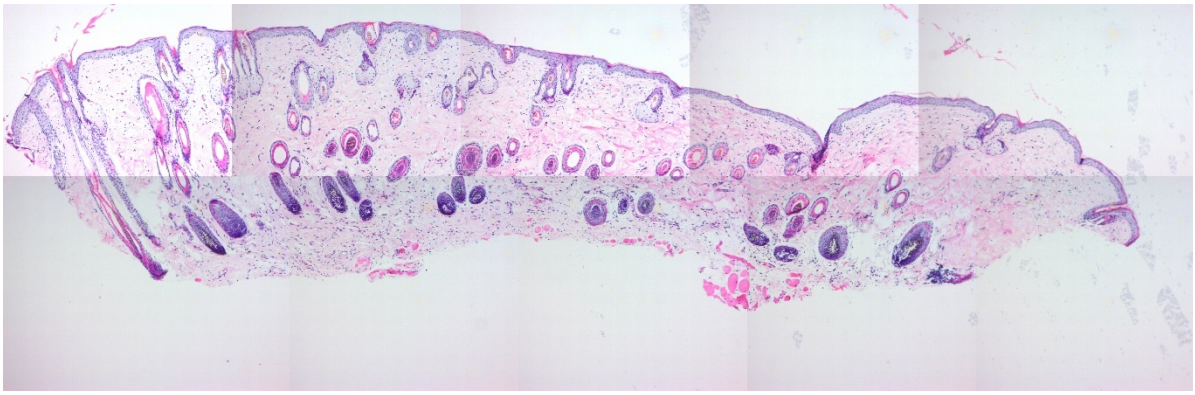

Mouse14

Control

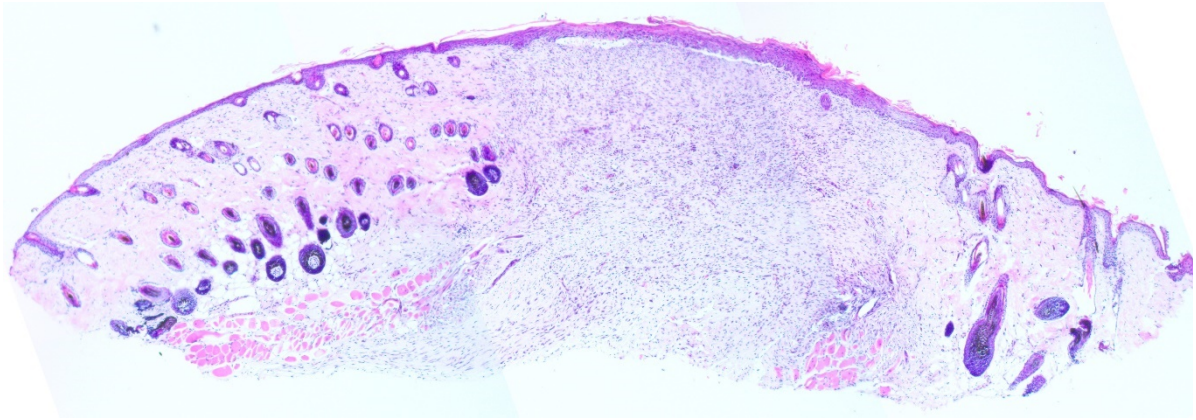

NDSF

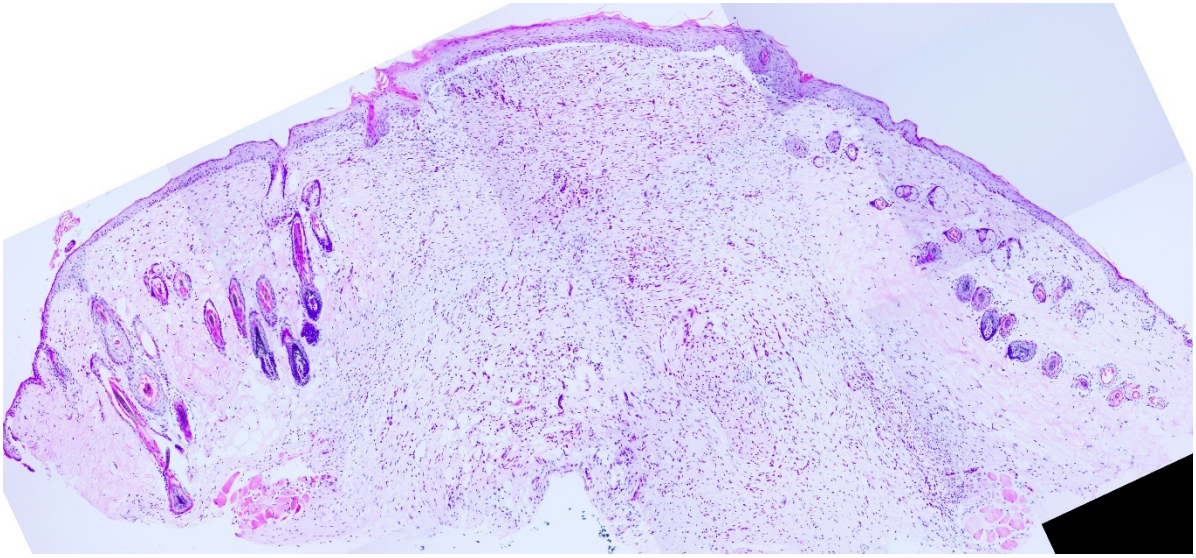

Mouse15

Control

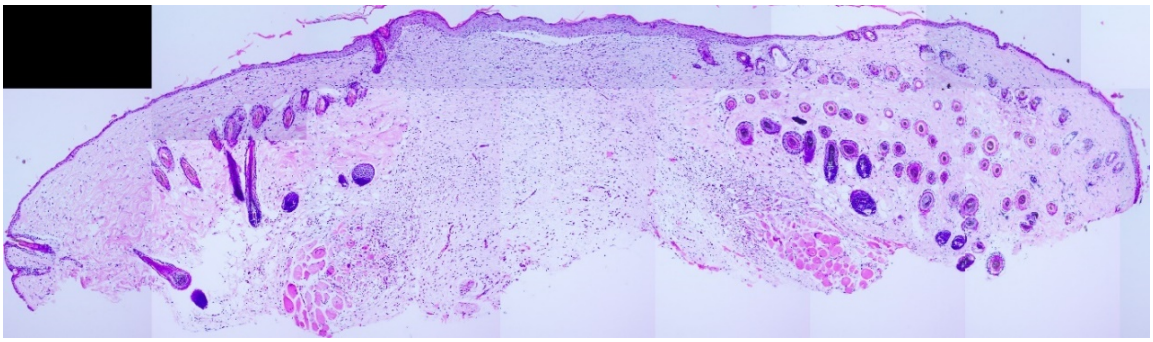

NDSF

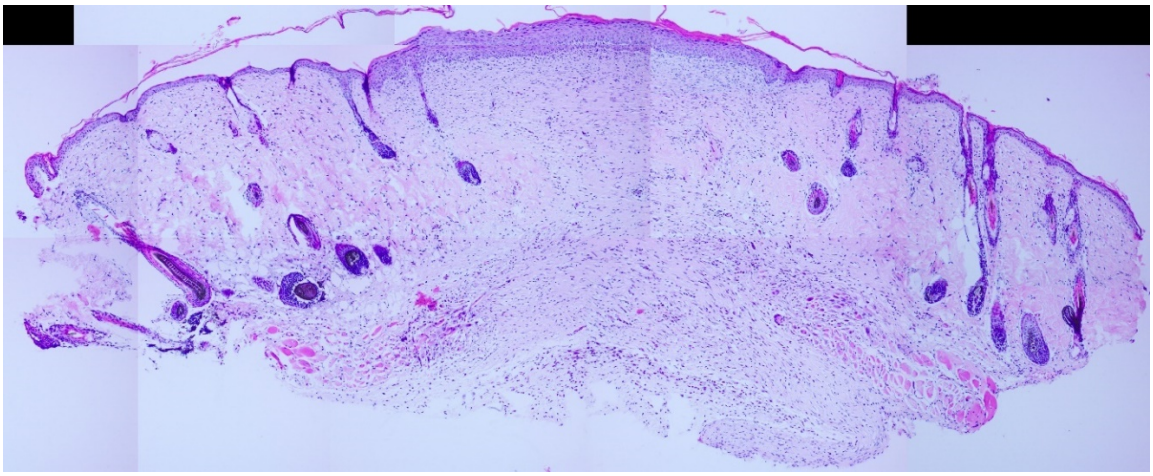

# MATLAB Code

```
%% Mouse Study Data Analysis %%

%% WOUND HEALING STUDY 1 %%

Days = [0,1,2,3,4,5,6,7,8,9,10];

Avg_Diam_Mouse1_SF =
[4.83,4.50,4.33,4.17,4.17,3.92,3.33,3.00,3.00,2.83,2.42...
    4.83,4.50,4.50,4.25,4.17,4.17,4.17,3.67,3.42,2.58,2.50
]; %holds avg diam for 10 days of both control and treatment {Cont. |
Treat.}
% ID: 700.1f
Avg_Diam_Mouse2_SF =
[4.50,4.00,3.67,3.33,3.33,3.17,3.00,2.33,2.08,1.42,1.08...
    4.50,4.50,3.58,3.67,3.75,3.50,3.17,3.08,2.92,2.58,2.08
]; % ID: 700.1b

Avg_Diam_Mouse3_SF =
[4.25,4.25,4.17,4.08,4.08,3.75,3.08,2.83,2.25,1.67,1.00...
    4.58,4.50,4.00,4.08,4.08,4.08,3.75,3.33,3.00,2.50,2.08
]; % ID: 700.1c

Avg_Diam_Mouse4_NDSF =
[3.50,3.42,3.33,3.08,2.83,2.25,2.00,1.83,1.33,1.00,0.67...
    3.67,3.50,3.50,3.50,3.08,2.83,2.17,2.25,1.67,1.33,0.75
]; % ID: 700.1d

Avg_Diam_Mouse5_NDSF =
[4.25,4.17,4.00,3.92,3.33,3.25,3.08,3.08,3.08,2.42,1.67...
    4.17,4.08,4.00,3.83,3.50,3.33,3.08,2.75,2.42,2.33,2.00
]; % ID: 700.1e

Avg_Diam_Mouse6_NDSF =
[4.00,4.00,3.67,3.17,3.17,2.67,2.67,2.75,2.00,1.83,0.92...
    4.17,4.00,3.83,3.67,3.58,3.08,3.00,2.75,2.25,2.25,1.42
]; % ID: 644.10b

Avg_Diam_Mouse7_NDSF =
[4.50,4.33,4.17,4.00,4.00,3.75,3.58,2.67,2.58,1.83,1.83...
```

```
    4.42,4.33,4.33,4.25,4.25,4.08,3.83,3.25,3.25,2.33,2.00
]; % ID: 644.10c

for i=1:11 % Concatenate each mouse's daily avg data
   Avg_Diam_Concat_PBS(i) =
(Avg_Diam_Mouse1_SF(i)+Avg_Diam_Mouse2_SF(i)+Avg_Diam_Mouse3_SF(i)+Avg_Diam
_Mouse4_NDSF(i)+...

Avg_Diam_Mouse5_NDSF(i)+Avg_Diam_Mouse6_NDSF(i)+Avg_Diam_Mouse7_NDSF(i))/7;

   Avg_Diam_Concat_SF(i) =
(Avg_Diam_Mouse1_SF(i+11)+Avg_Diam_Mouse2_SF(i+11)+Avg_Diam_Mouse3_SF(i+11)
)/3;

   Avg_Diam_Concat_NDSF(i) =
(Avg_Diam_Mouse4_NDSF(i+11)+Avg_Diam_Mouse5_NDSF(i+11)+Avg_Diam_Mouse6_NDSF
(i+11)+...
       Avg_Diam_Mouse7_NDSF(i+11))/4;
end

% Rate of Healing for each mouse STUDY 1
subplot(2,4,1), plot(Days,((Avg_Diam_Mouse1_SF(1)-
Avg_Diam_Mouse1_SF(1:11))/Avg_Diam_Mouse1_SF(1))*100,'k.-'),...
    hold on, plot(Days, ((Avg_Diam_Mouse1_SF(12)-
Avg_Diam_Mouse1_SF(12:end))/Avg_Diam_Mouse1_SF(12))*100,'r.-'),...
    legend('PBS','SF','Location','northwest'),title('Mouse1'), ylabel('%
Healed'),xlabel('Days'),ylim([0,100])

subplot(2,4,2), plot(Days,((Avg_Diam_Mouse2_SF(1)-
Avg_Diam_Mouse2_SF(1:11))/Avg_Diam_Mouse2_SF(1))*100,'k.-'),...
    hold on, plot(Days, ((Avg_Diam_Mouse2_SF(12)-
Avg_Diam_Mouse2_SF(12:end))/Avg_Diam_Mouse2_SF(12))*100,'r.-'),...
    legend('PBS','SF','Location','northwest'),title('Mouse2'), ylabel('%
Healed'),xlabel('Days'),ylim([0,100])

subplot(2,4,3), plot(Days,((Avg_Diam_Mouse3_SF(1)-
Avg_Diam_Mouse3_SF(1:11))/Avg_Diam_Mouse3_SF(1))*100,'k.-'),...
    hold on, plot(Days, ((Avg_Diam_Mouse3_SF(12)-
Avg_Diam_Mouse3_SF(12:end))/Avg_Diam_Mouse3_SF(12))*100,'r.-'),...
    legend('PBS','SF','Location','northwest'),title('Mouse3'), ylabel('%
Healed'),xlabel('Days'),ylim([0,100])
```

```
subplot(2,4,4), plot(Days,((Avg_Diam_Mouse4_NDSF(1)-
Avg_Diam_Mouse4_NDSF(1:11))/Avg_Diam_Mouse4_NDSF(1))*100,'k.-'),...
    hold on, plot(Days, ((Avg_Diam_Mouse4_NDSF(12)-
Avg_Diam_Mouse4_NDSF(12:end))/Avg_Diam_Mouse4_NDSF(12))*100,'r.-'),...
    legend('PBS','NDSF','Location','northwest'),title('Mouse4'), ylabel('%
Healed'),xlabel('Days'),ylim([0,100])

subplot(2,4,5), plot(Days,((Avg_Diam_Mouse5_NDSF(1)-
Avg_Diam_Mouse5_NDSF(1:11))/Avg_Diam_Mouse5_NDSF(1))*100,'k.-'),...
    hold on, plot(Days, ((Avg_Diam_Mouse5_NDSF(12)-
Avg_Diam_Mouse5_NDSF(12:end))/Avg_Diam_Mouse5_NDSF(12))*100,'r.-'),...
    legend('PBS','NDSF','Location','northwest'),title('Mouse5'), ylabel('%
Healed'),xlabel('Days'),ylim([0,100])

subplot(2,4,6), plot(Days,((Avg_Diam_Mouse6_NDSF(1)-
Avg_Diam_Mouse6_NDSF(1:11))/Avg_Diam_Mouse6_NDSF(1))*100,'k.-'),...
    hold on, plot(Days, ((Avg_Diam_Mouse6_NDSF(12)-
Avg_Diam_Mouse6_NDSF(12:end))/Avg_Diam_Mouse6_NDSF(12))*100,'r.-'),...
    legend('PBS','NDSF','Location','northwest'),title('Mouse6'), ylabel('%
Healed'),xlabel('Days'),ylim([0,100])

subplot(2,4,7), plot(Days,((Avg_Diam_Mouse7_NDSF(1)-
Avg_Diam_Mouse7_NDSF(1:11))/Avg_Diam_Mouse7_NDSF(1))*100,'k.-'),...
    hold on, plot(Days, ((Avg_Diam_Mouse7_NDSF(12)-
Avg_Diam_Mouse7_NDSF(12:end))/Avg_Diam_Mouse7_NDSF(12))*100,'r.-'),...
    legend('PBS','NDSF','Location','northwest'),title('Mouse7'), ylabel('%
Healed'),xlabel('Days'),ylim([0,100])

subplot(2,4,8), plot(Days,((Avg_Diam_Concat_PBS(1)-
Avg_Diam_Concat_PBS(1:11))/Avg_Diam_Concat_PBS(1))*100,'k.-'),hold on,...
    plot(Days,((Avg_Diam_Concat_SF(1)-
Avg_Diam_Concat_SF(1:11))/Avg_Diam_Concat_SF(1))*100,'b.-'),hold on,...
    plot(Days,((Avg_Diam_Concat_NDSF(1)-
Avg_Diam_Concat_NDSF(1:11))/Avg_Diam_Concat_NDSF(1))*100,'g.-'),...
    legend('Avg PBS \phi','Avg SF \phi','Avg NDSF
\phi','Location','northwest')...
    ,title('Average Wound Closure'), ylabel('Avg %
Healed'),xlabel('Days'),ylim([0,100])
```

```
%% WOUND HEALING STUDY 1 DOPPLER %%

% Mean Flux [Day3: Cont,Treat, Day7: Cont,Treat, Day10: Cont,Treat]
Doppler_7001c = [633.8,1243.9,290.4,215.5,148.3,479.7];
Doppler_7001f = [208.5,441.5,194.7,196.9,165.1,32.2];
Doppler_7001b = [156.2,213,126.9,411.7,489.6,292.2];
Doppler_7001d = [157.3,211.2,234.4,227.4,482.2,663.1];
Doppler_7001e = [826.8,730.6,228.9,323.9,505.8,258.1];
Doppler_64410b = [603.8,336.7,358.9,295.5,332,542];
Doppler_64410c = [487.2,358.5,412.3,459.2,539.6,285];

DopDays = [3,7,10];
count=1;
for i=1:2:6;
    AvgDop_PBS_Study1(count) =
(Doppler_7001c(i)+Doppler_7001f(i)+Doppler_7001b(i)+Doppler_7001d(i)+...
        Doppler_7001e(i)+Doppler_64410b(i)+Doppler_64410c(i))/7;
    count=count+1
end
count=1;
for i=2:2:6;
    AvgDop_SF_Study1(count) =
(Doppler_7001c(i)+Doppler_7001f(i)+Doppler_7001b(i))/3;
    AvgDop_NDSF_Study1(count) =
(Doppler_7001d(i)+Doppler_7001e(i)+Doppler_64410b(i)+Doppler_64410c(i))/4;
    count=count+1
end

% Blood Perfusion based on Mean Flux on Doppler Images
subplot(2,4,1), plot(DopDays,Doppler_7001f(1:2:end), 'k.-'),hold on,
plot(DopDays,Doppler_7001f(2:2:end), 'r.-'),...
    legend('PBS', 'SF','Location','north'),title('Average Blood Perfusion
Mouse1'),xlabel('Days'), ylabel('Mean FLux')

subplot(2,4,2), plot(DopDays,Doppler_7001b(1:2:end), 'k.-'),hold on,
plot(DopDays,Doppler_7001b(2:2:end), 'r.-'),...
    legend('PBS', 'SF','Location','north'),title('Average Blood Perfusion
Mouse2'),xlabel('Days'), ylabel('Mean FLux')

subplot(2,4,3), plot(DopDays,Doppler_7001c(1:2:end), 'k.-'),hold on,
plot(DopDays,Doppler_7001c(2:2:end), 'r.-'),...
```

```
    legend('PBS', 'SF','Location','north'),title('Average Blood Perfusion
Mouse3'),xlabel('Days'), ylabel('Mean FLux')

subplot(2,4,4), plot(DopDays,Doppler_7001d(1:2:end), 'k.-'),hold on,
plot(DopDays,Doppler_7001d(2:2:end), 'r.-'),...
    legend('PBS', 'NDSF','Location','north'),title('Average Blood Perfusion
Mouse4'),xlabel('Days'), ylabel('Mean FLux')

subplot(2,4,5), plot(DopDays,Doppler_7001e(1:2:end), 'k.-'),hold on,
plot(DopDays,Doppler_7001e(2:2:end), 'r.-'),...
    legend('PBS', 'NDSF','Location','north'),title('Average Blood Perfusion
Mouse5'),xlabel('Days'), ylabel('Mean FLux')

subplot(2,4,6), plot(DopDays,Doppler_64410b(1:2:end), 'k.-'),hold on,
plot(DopDays,Doppler_64410b(2:2:end), 'r.-'),...
    legend('PBS', 'NDSF','Location','north'),title('Average Blood Perfusion
Mouse6'),xlabel('Days'), ylabel('Mean FLux')

subplot(2,4,7), plot(DopDays,Doppler_64410c(1:2:end), 'k.-'),hold on,
plot(DopDays,Doppler_64410c(2:2:end), 'r.-'),...
    legend('PBS', 'NDSF','Location','north'),title('Average Blood Perfusion
Mouse7'),xlabel('Days'), ylabel('Mean FLux')

subplot(2,4,8), plot(DopDays,AvgDop_PBS_Study1, 'k.-'),hold on,
plot(DopDays,AvgDop_SF_Study1, 'b.-'),...
    hold on, plot(DopDays,AvgDop_NDSF_Study1, 'g.-
'),legend('PBS','SF','NDSF','Location','north'),...
    title('Average Blood Perfusion All Mice'),xlabel('Days'), ylabel('Mean
FLux')



%% WOUND HEALING STUDY 2 %%

Avg_Diam_Mouse8_SF =
[4.17,4.08,4.08,4.00,3.42,3.42,3.08,2.67,2.50,2.17,1.92,...
    4.33,4.25,4.25,4.17,3.92,3.33,2.83,1.17,1.17,1.17,1.00
]; %holds avg diam for 10 days of both control and treatment {Cont. |
Treat.}
```

```
Avg_Diam_Mouse9_SF =
[3.83,3.83,3.83,3.75,3.50,2.67,2.25,2.17,2.08,1.92,1.50,...
    4.25,4.17,4.08,4.08,3.33,3.33,2.33,1.67,1.67,1.58,1.42
];

Avg_Diam_Mouse10_SF =
[4.00,4.00,3.92,3.92,3.58,3.50,3.00,3.08,3.00,3.00,2.67,...
    4.17,4.33,4.08,4.17,3.83,3.83,2.75,2.42,2.33,2.08,2.08
];

Avg_Diam_Mouse11_SF =
[3.50,3.50,3.50,3.33,3.00,2.58,2.50,1.92,1.33,1.25,1.17,...
    4.00,3.92,3.92,3.50,3.25,2.83,2.67,2.33,2.00,2.00,1.83
];

Avg_Diam_Mouse12_NDSF =
[4.33,4.00,4.00,3.42,3.25,3.00,2.58,2.08,1.92,1.33,1.17,...
    4.42,4.33,4.33,4.08,3.83,3.25,3.25,2.92,2.58,1.83,1.50
];

Avg_Diam_Mouse13_NDSF =
[4.17,4.25,4.17,4.08,4.00,3.92,3.17,2.58,1.92,1.75,1.75,...
    4.08,4.17,4.17,3.92,3.50,3.42,2.83,1.92,1.17,1.17,1.17
];

Avg_Diam_Mouse14_NDSF =
[4.25,4.00,3.83,3.83,3.67,3.33,3.17,3.00,2.42,2.00,1.83,...
    4.33,4.17,3.92,3.92,3.75,3.67,3.33,3.25,3.25,3.17,2.17
];

Avg_Diam_Mouse15_NDSF =
[3.83,3.83,3.83,3.33,3.00,3.00,2.42,1.67,1.67,1.67,1.50,...
    3.92,3.92,3.83,3.83,3.58,3.33,2.67,2.50,2.50,2.00,1.92
];

for i=1:11 % Concatenate each mouse's daily avg data
   Avg_Diam_Concat_PBS_Study2(i) =
(Avg_Diam_Mouse8_SF(i)+Avg_Diam_Mouse9_SF(i)+Avg_Diam_Mouse10_SF(i)+Avg_Dia
m_Mouse11_SF(i)+...
```

```
Avg_Diam_Mouse12_NDSF(i)+Avg_Diam_Mouse13_NDSF(i)+Avg_Diam_Mouse14_NDSF(i)+
Avg_Diam_Mouse15_NDSF(i))/8;

   Avg_Diam_Concat_SF_Study2(i) =
(Avg_Diam_Mouse8_SF(i+11)+Avg_Diam_Mouse9_SF(i+11)+Avg_Diam_Mouse10_SF(i+11
)+Avg_Diam_Mouse11_SF(i+11))/4;

   Avg_Diam_Concat_NDSF_Study2(i) =
(Avg_Diam_Mouse12_NDSF(i+11)+Avg_Diam_Mouse13_NDSF(i+11)+Avg_Diam_Mouse14_N
DSF(i+11)+...
       Avg_Diam_Mouse15_NDSF(i+11))/4;
end

%Rate of Healing for each mouse STUDY 1
subplot(2,4,1), plot(Days,((Avg_Diam_Mouse8_SF(1)-
Avg_Diam_Mouse8_SF(1:11))/Avg_Diam_Mouse8_SF(1))*100,'k.-'),...
    hold on, plot(Days, ((Avg_Diam_Mouse8_SF(12)-
Avg_Diam_Mouse8_SF(12:end))/Avg_Diam_Mouse8_SF(12))*100,'r.-'),...
    legend('PBS','SF','Location','northwest'),title('Mouse8'), ylabel('%
Healed'),xlabel('Days'),ylim([0,100])

subplot(2,4,2), plot(Days,((Avg_Diam_Mouse9_SF(1)-
Avg_Diam_Mouse9_SF(1:11))/Avg_Diam_Mouse9_SF(1))*100,'k.-'),...
    hold on, plot(Days, ((Avg_Diam_Mouse9_SF(12)-
Avg_Diam_Mouse9_SF(12:end))/Avg_Diam_Mouse9_SF(12))*100,'r.-'),...
    legend('PBS','SF','Location','northwest'),title('Mouse9'), ylabel('%
Healed'),xlabel('Days'),ylim([0,100])

subplot(2,4,3), plot(Days,((Avg_Diam_Mouse10_SF(1)-
Avg_Diam_Mouse10_SF(1:11))/Avg_Diam_Mouse10_SF(1))*100,'k.-'),...
    hold on, plot(Days, ((Avg_Diam_Mouse10_SF(12)-
Avg_Diam_Mouse10_SF(12:end))/Avg_Diam_Mouse10_SF(12))*100,'r.-'),...
    legend('PBS','SF','Location','northwest'),title('Mouse10'), ylabel('%
Healed'),xlabel('Days'),ylim([0,100])

subplot(2,4,4), plot(Days,((Avg_Diam_Mouse11_SF(1)-
Avg_Diam_Mouse11_SF(1:11))/Avg_Diam_Mouse11_SF(1))*100,'k.-'),...
    hold on, plot(Days, ((Avg_Diam_Mouse11_SF(12)-
Avg_Diam_Mouse11_SF(12:end))/Avg_Diam_Mouse11_SF(12))*100,'r.-'),...
```

```
    legend('PBS','SF','Location','northwest'),title('Mouse11'), ylabel('%
Healed'),xlabel('Days'),ylim([0,100])

subplot(2,4,5), plot(Days,((Avg_Diam_Mouse12_NDSF(1)-
Avg_Diam_Mouse12_NDSF(1:11))/Avg_Diam_Mouse12_NDSF(1))*100,'k.-'),...
    hold on, plot(Days, ((Avg_Diam_Mouse12_NDSF(12)-
Avg_Diam_Mouse12_NDSF(12:end))/Avg_Diam_Mouse12_NDSF(12))*100,'r.-'),...
    legend('PBS','NDSF','Location','northwest'),title('Mouse12'), ylabel('%
Healed'),xlabel('Days'),ylim([0,100])

subplot(2,4,6), plot(Days,((Avg_Diam_Mouse13_NDSF(1)-
Avg_Diam_Mouse13_NDSF(1:11))/Avg_Diam_Mouse13_NDSF(1))*100,'k.-'),...
    hold on, plot(Days, ((Avg_Diam_Mouse13_NDSF(12)-
Avg_Diam_Mouse13_NDSF(12:end))/Avg_Diam_Mouse13_NDSF(12))*100,'r.-'),...
    legend('PBS','NDSF','Location','northwest'),title('Mouse13'), ylabel('%
Healed'),xlabel('Days'),ylim([0,100])

subplot(2,4,7), plot(Days,((Avg_Diam_Mouse14_NDSF(1)-
Avg_Diam_Mouse14_NDSF(1:11))/Avg_Diam_Mouse14_NDSF(1))*100,'k.-'),...
    hold on, plot(Days, ((Avg_Diam_Mouse14_NDSF(12)-
Avg_Diam_Mouse14_NDSF(12:end))/Avg_Diam_Mouse14_NDSF(12))*100,'r.-'),...
    legend('PBS','NDSF','Location','northwest'),title('Mouse14'), ylabel('%
Healed'),xlabel('Days'),ylim([0,100])

subplot(2,4,8), plot(Days,((Avg_Diam_Mouse15_NDSF(1)-
Avg_Diam_Mouse15_NDSF(1:11))/Avg_Diam_Mouse15_NDSF(1))*100,'k.-'),...
    hold on, plot(Days, ((Avg_Diam_Mouse15_NDSF(12)-
Avg_Diam_Mouse15_NDSF(12:end))/Avg_Diam_Mouse15_NDSF(12))*100,'r.-'),...
    legend('PBS','NDSF','Location','northwest'),title('Mouse15'), ylabel('%
Healed'),xlabel('Days'),ylim([0,100])

%% WOUND HEALING 2: LOGISTIC MODELLING OF TREATMENT DATA %%
y8 = ((Avg_Diam_Mouse8_SF(12)-
Avg_Diam_Mouse8_SF(12:end))/Avg_Diam_Mouse8_SF(12))*100;
[fit8,gof8] = fit(Days',y8','c./(1+exp(b1+b2*x))','start',[0,-1,1]);

y9 = ((Avg_Diam_Mouse9_SF(12)-
Avg_Diam_Mouse9_SF(12:end))/Avg_Diam_Mouse9_SF(12))*100;
[fit9,gof9] = fit(Days',y9','c./(1+exp(b1+b2*x))','start',[0,-1,1]);
```

```
y10 = ((Avg_Diam_Mouse10_SF(12)-
Avg_Diam_Mouse10_SF(12:end))/Avg_Diam_Mouse10_SF(12))*100;
[fit10,gof10] = fit(Days',y10','c./(1+exp(b1+b2*x))','start',[0,-1,1]);

y11 = ((Avg_Diam_Mouse11_SF(12)-
Avg_Diam_Mouse11_SF(12:end))/Avg_Diam_Mouse11_SF(12))*100;
[fit11,gof11] = fit(Days',y11','c./(1+exp(b1+b2*x))','start',[0,-1,1]);

y12 = ((Avg_Diam_Mouse12_NDSF(12)-
Avg_Diam_Mouse12_NDSF(12:end))/Avg_Diam_Mouse12_NDSF(12))*100;
[fit12,gof12] = fit(Days',y12','c./(1+exp(b1+b2*x))','start',[0,-1,1]);

y13 = ((Avg_Diam_Mouse13_NDSF(12)-
Avg_Diam_Mouse13_NDSF(12:end))/Avg_Diam_Mouse13_NDSF(12))*100;
[fit13,gof13] = fit(Days',y13','c./(1+exp(b1+b2*x))','start',[0,-1,1]);

y14 = ((Avg_Diam_Mouse14_NDSF(12)-
Avg_Diam_Mouse14_NDSF(12:end))/Avg_Diam_Mouse14_NDSF(12))*100;
[fit14,gof14] = fit(Days',y14','c./(1+exp(b1+b2*x))','start',[0,-1,1]);

y15 = ((Avg_Diam_Mouse15_NDSF(12)-
Avg_Diam_Mouse15_NDSF(12:end))/Avg_Diam_Mouse15_NDSF(12))*100;
[fit15,gof15] = fit(Days',y15','c./(1+exp(b1+b2*x))','start',[0,-1,1]);

% Plotting SF and NDSF Logistic Modells
subplot(2,4,1), plot(Days, ((Avg_Diam_Mouse8_SF(12)-
Avg_Diam_Mouse8_SF(12:end))/Avg_Diam_Mouse8_SF(12))*100, 'r'),...
    hold on,
plot(Days,Logistic8(Days,fit8.c,fit8.b1,fit8.b2),'b'),title("[Mouse8] rsqr
= " + gof8.rsquare(1)),xlabel('Days'),...
    ylabel('% Healed'),legend('Raw SF Data', 'Logistic Model', 'Location',
'northwest'), grid on

subplot(2,4,2), plot(Days, ((Avg_Diam_Mouse9_SF(12)-
Avg_Diam_Mouse9_SF(12:end))/Avg_Diam_Mouse9_SF(12))*100, 'r'),...
    hold on,
plot(Days,Logistic9(Days,fit9.c,fit9.b1,fit9.b2),'b'),title("[Mouse9] rsqr
= " + gof9.rsquare),xlabel('Days'),...
    ylabel('% Healed'),legend('Raw SF Data', 'Logistic Model', 'Location',
'northwest'), grid on
```

```
subplot(2,4,3), plot(Days, ((Avg_Diam_Mouse10_SF(12)-
Avg_Diam_Mouse10_SF(12:end))/Avg_Diam_Mouse10_SF(12))*100, 'r'),...
    hold on,
plot(Days,Logistic10(Days,fit10.c,fit10.b1,fit10.b2),'b'),title("[Mouse10]
rsqr = " + gof10.rsquare),xlabel('Days'),...
    ylabel('% Healed'),legend('Raw SF Data', 'Logistic Model', 'Location',
'northwest'), grid on

subplot(2,4,4), plot(Days, ((Avg_Diam_Mouse11_SF(12)-
Avg_Diam_Mouse11_SF(12:end))/Avg_Diam_Mouse11_SF(12))*100, 'r'),...
    hold on,
plot(Days,Logistic11(Days,fit11.c,fit11.b1,fit11.b2),'b'),title("[Mouse11]
rsqr = " + gof11.rsquare),xlabel('Days'),...
    ylabel('% Healed'),legend('Raw SF Data', 'Logistic Model', 'Location',
'northwest'), grid on

subplot(2,4,5), plot(Days, ((Avg_Diam_Mouse12_NDSF(12)-
Avg_Diam_Mouse12_NDSF(12:end))/Avg_Diam_Mouse12_NDSF(12))*100, 'r'),...
    hold on,
plot(Days,Logistic12(Days,fit12.c,fit12.b1,fit12.b2),'b'),title("[Mouse12]
rsqr = " + gof12.rsquare),xlabel('Days'),...
    ylabel('% Healed'),legend('Raw NDSF Data', 'Logistic Model',
'Location', 'northwest'), grid on

subplot(2,4,6), plot(Days, ((Avg_Diam_Mouse13_NDSF(12)-
Avg_Diam_Mouse13_NDSF(12:end))/Avg_Diam_Mouse13_NDSF(12))*100, 'r'),...
    hold on,
plot(Days,Logistic13(Days,fit13.c,fit13.b1,fit13.b2),'b'),title("[Mouse13]
rsqr = " + gof13.rsquare),xlabel('Days'),...
    ylabel('% Healed'),legend('Raw NDSF Data', 'Logistic Model',
'Location', 'northwest'), grid on

subplot(2,4,7), plot(Days, ((Avg_Diam_Mouse14_NDSF(12)-
Avg_Diam_Mouse14_NDSF(12:end))/Avg_Diam_Mouse14_NDSF(12))*100, 'r'),...
    hold on,
plot(Days,Logistic14(Days,fit14.c,fit14.b1,fit14.b2),'b'),title("[Mouse14]
rsqr = " + gof14.rsquare),xlabel('Days'),...
    ylabel('% Healed'),legend('Raw NDSF Data', 'Logistic Model',
'Location', 'northwest'), grid on
```

```
subplot(2,4,8), plot(Days, ((Avg_Diam_Mouse15_NDSF(12)-
Avg_Diam_Mouse15_NDSF(12:end))/Avg_Diam_Mouse15_NDSF(12))*100, 'r'),...
    hold on,
plot(Days,Logistic15(Days,fit15.c,fit15.b1,fit15.b2),'b'),title("[Mouse15]
rsqr = " + gof15.rsquare),xlabel('Days'),...
    ylabel('% Healed'),legend('Raw NDSF Data', 'Logistic Model',
'Location', 'northwest'), grid on


%% WOUND HEALING 2: LOGISTIC MODELLING OF CONTROL DATA %%

y8c = ((Avg_Diam_Mouse8_SF(1)-
Avg_Diam_Mouse8_SF(1:11))/Avg_Diam_Mouse8_SF(1))*100;
[fit8c,gof8c] = fit(Days',y8c','c./(1+exp(b1+b2*x))','start',[0,-1,1]);

y9c = ((Avg_Diam_Mouse9_SF(1)-
Avg_Diam_Mouse9_SF(1:11))/Avg_Diam_Mouse9_SF(1))*100;
[fit9c,gof9c] = fit(Days',y9c','c./(1+exp(b1+b2*x))','start',[0,-1,1]);

y10c = ((Avg_Diam_Mouse10_SF(1)-
Avg_Diam_Mouse10_SF(1:11))/Avg_Diam_Mouse10_SF(1))*100;
[fit10c,gof10c] = fit(Days',y10c','c./(1+exp(b1+b2*x))','start',[0,-1,1]);

y11c = ((Avg_Diam_Mouse11_SF(1)-
Avg_Diam_Mouse11_SF(1:11))/Avg_Diam_Mouse11_SF(1))*100;
[fit11c,gof11c] = fit(Days',y11c','c./(1+exp(b1+b2*x))','start',[0,-1,1]);

y12c = ((Avg_Diam_Mouse12_NDSF(1)-
Avg_Diam_Mouse12_NDSF(1:11))/Avg_Diam_Mouse12_NDSF(1))*100;
[fit12c,gof12c] = fit(Days',y12c','c./(1+exp(b1+b2*x))','start',[0,-1,1]);

y13c = ((Avg_Diam_Mouse13_NDSF(1)-
Avg_Diam_Mouse13_NDSF(1:11))/Avg_Diam_Mouse13_NDSF(1))*100;
[fit13c,gof13c] = fit(Days',y13c','c./(1+exp(b1+b2*x))','start',[0,-1,1]);

y14c = ((Avg_Diam_Mouse14_NDSF(1)-
Avg_Diam_Mouse14_NDSF(1:11))/Avg_Diam_Mouse14_NDSF(1))*100;
[fit14c,gof14c] = fit(Days',y14c','c./(1+exp(b1+b2*x))','start',[0,-1,1]);

y15c = ((Avg_Diam_Mouse15_NDSF(1)-
Avg_Diam_Mouse15_NDSF(1:11))/Avg_Diam_Mouse15_NDSF(1))*100;
```

```
[fit15c,gof15c] = fit(Days',y15c','c./(1+exp(b1+b2*x))','start',[0,-1,1]);

% Plotting PBS Logistic Models
subplot(2,4,1), plot(Days, ((Avg_Diam_Mouse8_SF(1)-
Avg_Diam_Mouse8_SF(1:11))/Avg_Diam_Mouse8_SF(1))*100, 'r'),...
    hold on,
plot(Days,Logistic8c(Days,fit8c.c,fit8c.b1,fit8c.b2),'b'),title("[Mouse8]
rsqr = " + gof8c.rsquare(1)),xlabel('Days'),...
    ylabel('% Healed'),legend('Raw PBS Data', 'Logistic Model', 'Location',
'northwest'), grid on

subplot(2,4,2), plot(Days, ((Avg_Diam_Mouse9_SF(1)-
Avg_Diam_Mouse9_SF(1:11))/Avg_Diam_Mouse9_SF(1))*100, 'r'),...
    hold on,
plot(Days,Logistic9c(Days,fit9c.c,fit9c.b1,fit9c.b2),'b'),title("[Mouse9]
rsqr = " + gof9c.rsquare),xlabel('Days'),...
    ylabel('% Healed'),legend('Raw PBS Data', 'Logistic Model', 'Location',
'northwest'), grid on

subplot(2,4,3), plot(Days, ((Avg_Diam_Mouse10_SF(1)-
Avg_Diam_Mouse10_SF(1:11))/Avg_Diam_Mouse10_SF(1))*100, 'r'),...
    hold on,
plot(Days,Logistic10c(Days,fit10c.c,fit10c.b1,fit10c.b2),'b'),title("[Mouse
10] rsqr = " + gof10c.rsquare),xlabel('Days'),...
    ylabel('% Healed'),legend('Raw PBS Data', 'Logistic Model', 'Location',
'northwest'), grid on

subplot(2,4,4), plot(Days, ((Avg_Diam_Mouse11_SF(1)-
Avg_Diam_Mouse11_SF(1:11))/Avg_Diam_Mouse11_SF(1))*100, 'r'),...
    hold on,
plot(Days,Logistic11c(Days,fit11c.c,fit11c.b1,fit11c.b2),'b'),title("[Mouse
11] rsqr = " + gof11c.rsquare),xlabel('Days'),...
    ylabel('% Healed'),legend('Raw PBS Data', 'Logistic Model', 'Location',
'northwest'), grid on

subplot(2,4,5), plot(Days, ((Avg_Diam_Mouse12_NDSF(1)-
Avg_Diam_Mouse12_NDSF(1:11))/Avg_Diam_Mouse12_NDSF(1))*100, 'r'),...
    hold on,
plot(Days,Logistic12c(Days,fit12c.c,fit12c.b1,fit12c.b2),'b'),title("[Mouse
12] rsqr = " + gof12c.rsquare),xlabel('Days'),...
```

```
    ylabel('% Healed'),legend('Raw PBS Data', 'Logistic Model', 'Location',
'northwest'), grid on

subplot(2,4,6), plot(Days, ((Avg_Diam_Mouse13_NDSF(1)-
Avg_Diam_Mouse13_NDSF(1:11))/Avg_Diam_Mouse13_NDSF(1))*100, 'r'),...
    hold on,
plot(Days,Logistic13c(Days,fit13c.c,fit13c.b1,fit13c.b2),'b'),title("[Mouse
13] rsqr = " + gof13c.rsquare),xlabel('Days'),...
    ylabel('% Healed'),legend('Raw PBS Data', 'Logistic Model', 'Location',
'northwest'), grid on

subplot(2,4,7), plot(Days, ((Avg_Diam_Mouse14_NDSF(1)-
Avg_Diam_Mouse14_NDSF(1:11))/Avg_Diam_Mouse14_NDSF(1))*100, 'r'),...
    hold on,
plot(Days,Logistic14c(Days,fit14c.c,fit14c.b1,fit14c.b2),'b'),title("[Mouse
14] rsqr = " + gof14c.rsquare),xlabel('Days'),...
    ylabel('% Healed'),legend('Raw PBS Data', 'Logistic Model', 'Location',
'northwest'), grid on

subplot(2,4,8), plot(Days, ((Avg_Diam_Mouse15_NDSF(1)-
Avg_Diam_Mouse15_NDSF(1:11))/Avg_Diam_Mouse15_NDSF(1))*100, 'r'),...
    hold on,
plot(Days,Logistic15c(Days,fit15c.c,fit15c.b1,fit15c.b2),'b'),title("[Mouse
15] rsqr = " + gof15c.rsquare),xlabel('Days'),...
    ylabel('% Healed'),legend('Raw PBS Data', 'Logistic Model', 'Location',
'northwest'), grid on


%% HEALING RATE (LOGISTIC): CONT. VS TREAT

% Healing Rate Comparison: Treat. vs Cont.
subplot(2,4,1),
plot(Days(2:end),diff(Logistic8(Days,fit8.c,fit8.b1,fit8.b2)),'r'), hold
on,...

plot(Days(2:end),diff(Logistic8c(Days,fit8c.c,fit8c.b1,fit8c.b2)),'k'),titl
e("Avg Healing Rate [Mouse8]"),xlabel('Days'),...
    ylabel('Rate Of Healing (mm^2/Day)'),legend('SF','PBS', 'Location',
'northwest'), grid on
```

```
subplot(2,4,2),
plot(Days(2:end),diff(Logistic9(Days,fit9.c,fit9.b1,fit9.b2)),'r'), hold
on,...

plot(Days(2:end),diff(Logistic9c(Days,fit9c.c,fit9c.b1,fit9c.b2)),'k'),titl
e("Avg Healing Rate [Mouse9]"),xlabel('Days'),...
    ylabel('Rate Of Healing (mm^2/Day)'),legend('SF','PBS', 'Location',
'northwest'), grid on

subplot(2,4,3),
plot(Days(2:end),diff(Logistic10(Days,fit10.c,fit10.b1,fit10.b2)),'r'),
hold on,...

plot(Days(2:end),diff(Logistic10c(Days,fit10c.c,fit10c.b1,fit10c.b2)),'k'),
title("Avg Healing Rate [Mouse10]"),xlabel('Days'),...
    ylabel('Rate Of Healing (mm^2/Day)'),legend('SF','PBS', 'Location',
'northwest'), grid on

subplot(2,4,4),
plot(Days(2:end),diff(Logistic11(Days,fit11.c,fit11.b1,fit11.b2)),'r'),
hold on,...

plot(Days(2:end),diff(Logistic11c(Days,fit11c.c,fit11c.b1,fit11c.b2)),'k'),
title("Avg Healing Rate [Mouse11]"),xlabel('Days'),...
    ylabel('Rate Of Healing (mm^2/Day)'),legend('SF','PBS', 'Location',
'northwest'), grid on

subplot(2,4,5),
plot(Days(2:end),diff(Logistic12(Days,fit12.c,fit12.b1,fit12.b2)),'r'),
hold on,...

plot(Days(2:end),diff(Logistic12c(Days,fit12c.c,fit12c.b1,fit12c.b2)),'k'),
title("Avg Healing Rate [Mouse12]"),xlabel('Days'),...
    ylabel('Rate Of Healing (mm^2/Day)'),legend('NDSF','PBS', 'Location',
'northwest'), grid on

subplot(2,4,6),
plot(Days(2:end),diff(Logistic13(Days,fit13.c,fit13.b1,fit13.b2)),'r'),
hold on,...
```

```
plot(Days(2:end),diff(Logistic13c(Days,fit13c.c,fit13c.b1,fit13c.b2)),'k'),
title("Avg Healing Rate [Mouse13]"),xlabel('Days'),...
    ylabel('Rate Of Healing (mm^2/Day)'),legend('NDSF','PBS', 'Location',
'northwest'), grid on

subplot(2,4,7),
plot(Days(2:end),diff(Logistic14(Days,fit14.c,fit14.b1,fit14.b2)),'r'),
hold on,...

plot(Days(2:end),diff(Logistic14c(Days,fit14c.c,fit14c.b1,fit14c.b2)),'k'),
title("Avg Healing Rate [Mouse14]"),xlabel('Days'),...
    ylabel('Rate Of Healing (mm^2/Day)'),legend('NDSF','PBS', 'Location',
'northwest'), grid on

subplot(2,4,8),
plot(Days(2:end),diff(Logistic15(Days,fit15.c,fit15.b1,fit15.b2)),'r'),
hold on,...

plot(Days(2:end),diff(Logistic15c(Days,fit15c.c,fit15c.b1,fit15c.b2)),'k'),
title("Avg Healing Rate [Mouse15]"),xlabel('Days'),...
    ylabel('Rate Of Healing (mm^2/Day)'),legend('NDSF','PBS', 'Location',
'northwest'), grid on

%% STUDY 2: GRANULATION AREA CALCS, INFILLTRATE RATIO

% Area = [cont,treat]
xb = 1:1:2;
Area_12c = [23.88, 0];
Area_11d = [0, 22.88];
Area_5h = [20.31, 23.78];
Area_5i = [18.47, 32.07];
Area_5j = [0, 35.84];
Area_5k = [23.93, 37.60];
Area_11c = [36.94, 26.58];
Area_5g = [31.15, 32.56];


subplot(2,4,1),X = categorical({'Control','SF'}),X =
reordercats(X,{'Control','SF'}),...
```

```
    b = bar(X,Area_5g','FaceColor','flat'),b.CData(2,:) = [0.8500 0.3250
0.0980],title('Mouse8'),...
    ylabel('% Infiltrate ratio')
subplot(2,4,2),X = categorical({'Control','SF'}),X =
reordercats(X,{'Control','SF'}),...
    b = bar(X,Area_11d','FaceColor','flat'),b.CData(2,:) = [0.8500 0.3250
0.0980],title('Mouse9'),...
    ylabel('% Infiltrate ratio')
subplot(2,4,3),X = categorical({'Control','SF'}),X =
reordercats(X,{'Control','SF'}),...
    b = bar(X,Area_11c','FaceColor','flat'),b.CData(2,:) = [0.8500 0.3250
0.0980],title('Mouse10'),...
    ylabel('% Infiltrate ratio')
subplot(2,4,4),X = categorical({'Control','SF'}),X =
reordercats(X,{'Control','SF'}),...
    b = bar(X,Area_5k','FaceColor','flat'),b.CData(2,:) = [0.8500 0.3250
0.0980],title('Mouse11'),...
    ylabel('% Infiltrate ratio')
subplot(2,4,5),X = categorical({'Control','NDSF'}),X =
reordercats(X,{'Control','NDSF'}),...
    b = bar(X,Area_5j','FaceColor','flat'),b.CData(2,:) = [0.8500 0.3250
0.0980],title('Mouse12'),...
    ylabel('% Infiltrate ratio')
subplot(2,4,6),X = categorical({'Control','NDSF'}),X =
reordercats(X,{'Control','NDSF'}),...
    b = bar(X,Area_12c','FaceColor','flat'),b.CData(2,:) = [0.8500 0.3250
0.0980],title('Mouse13'),...
    ylabel('% Infiltrate ratio')
subplot(2,4,7),X = categorical({'Control','NDSF'}),X =
reordercats(X,{'Control','NDSF'}),...
    b = bar(X,Area_5i','FaceColor','flat'),b.CData(2,:) = [0.8500 0.3250
0.0980],title('Mouse14'),...
    ylabel('% Infiltrate ratio')
subplot(2,4,8),X = categorical({'Control','NDSF'}),X =
reordercats(X,{'Control','NDSF'}),...
    b = bar(X,Area_5h','FaceColor','flat'),b.CData(2,:) = [0.8500 0.3250
0.0980],title('Mouse15'),...
    ylabel('% Infiltrate ratio')


%% WOUND HEALING STUDY 2 DOPPLER %%
```

```
% Mean Flux [Day3: Cont,Treat, Day7: Cont,Treat, Day10: Cont,Treat]

Doppler_5g = [320.40,406.80,678.10,369.60,171.30,152.50]  %SF
Doppler_5k = [434.10,439.80,506.60,192.10,478.50,57.00]   %SF
Doppler_11c = [322.00,591.40,145.90,511.50,36.90,334.00]  %SF
Doppler_11d = [767.80,384.80,353.40,272.00,75.20,127.10]  %SF
Doppler_5h = [395.40,274.90,141.60,345.00,27.20,115.50]   %NDSF
Doppler_5i = [349.40,181.10,531.30,350.10,69.70,40.60]    %NDSF
Doppler_5j = [344.00,570.90,272.60,335.00,183.10,443.10]  %NDSF
Doppler_12c = [189.40,415.40,343.90,263.20,137.50,254.90] %NDSF

count=1;
for i=1:2:6;
    AvgDop_PBS_Study2(count) =
(Doppler_5g(i)+Doppler_5k(i)+Doppler_11c(i)+Doppler_11d(i)+...
        Doppler_5h(i)+Doppler_5i(i)+Doppler_5j(i)+Doppler_12c(i))/8;
    count=count+1
end
count=1;
for i=2:2:6;
    AvgDop_SF_Study2(count) =
(Doppler_5g(i)+Doppler_5k(i)+Doppler_11c(i)+Doppler_11d(i))/4;
    AvgDop_NDSF_Study2(count) =
(Doppler_5h(i)+Doppler_5i(i)+Doppler_5j(i)+Doppler_12c(i))/4;
    count=count+1
end

% Blood Perfusion based on Mean Flux on Doppler Images
subplot(2,4,1), plot(DopDays,Doppler_5g(1:2:end), 'k.-'),hold on,
plot(DopDays,Doppler_5g(2:2:end), 'r.-'),...
    legend('PBS', 'SF','Location','north'),title('Average Blood Perfusion
684.5g'),xlabel('Days'), ylabel('Mean FLux')

subplot(2,4,2), plot(DopDays,Doppler_5k(1:2:end), 'k.-'),hold on,
plot(DopDays,Doppler_5k(2:2:end), 'r.-'),...
    legend('PBS', 'SF','Location','north'),title('Average Blood Perfusion
684.5k'),xlabel('Days'), ylabel('Mean FLux')

subplot(2,4,3), plot(DopDays,Doppler_11c(1:2:end), 'k.-'),hold on,
plot(DopDays,Doppler_11c(2:2:end), 'r.-'),...
```

```
    legend('PBS', 'SF','Location','north'),title('Average Blood Perfusion
630.11c'),xlabel('Days'), ylabel('Mean FLux')

subplot(2,4,4), plot(DopDays,Doppler_11d(1:2:end), 'k.-'),hold on,
plot(DopDays,Doppler_11d(2:2:end), 'r.-'),...
    legend('PBS', 'SF','Location','north'),title('Average Blood Perfusion
630.11d'),xlabel('Days'), ylabel('Mean FLux')

subplot(2,4,5), plot(DopDays,Doppler_5h(1:2:end), 'k.-'),hold on,
plot(DopDays,Doppler_5h(2:2:end), 'r.-'),...
    legend('PBS', 'NDSF','Location','north'),title('Average Blood Perfusion
684.5h'),xlabel('Days'), ylabel('Mean FLux')

subplot(2,4,6), plot(DopDays,Doppler_5i(1:2:end), 'k.-'),hold on,
plot(DopDays,Doppler_5i(2:2:end), 'r.-'),...
    legend('PBS', 'NDSF','Location','north'),title('Average Blood Perfusion
684.5i'),xlabel('Days'), ylabel('Mean FLux')

subplot(2,4,7), plot(DopDays,Doppler_5j(1:2:end), 'k.-'),hold on,
plot(DopDays,Doppler_5j(2:2:end), 'r.-'),...
    legend('PBS', 'NDSF','Location','north'),title('Average Blood Perfusion
684.5j'),xlabel('Days'), ylabel('Mean FLux')

subplot(2,4,8), plot(DopDays,Doppler_12c(1:2:end), 'k.-'),hold on,
plot(DopDays,Doppler_12c(2:2:end), 'r.-'),...
    legend('PBS', 'NDSF','Location','north'),title('Average Blood Perfusion
684.12c'),xlabel('Days'), ylabel('Mean FLux')

%% STUDY 2: DOPPLER PERFUSION RATIO

% Perfusion ratio = [Day 3:]
j=1;
for i=1:2:6
    Dop_5g_rat(j) = Doppler_5g(i+1)/Doppler_5g(i);
    Dop_5k_rat(j) = Doppler_5k(i+1)/Doppler_5k(i);
    Dop_11c_rat(j) = Doppler_11c(i+1)/Doppler_11c(i);
    Dop_11d_rat(j) = Doppler_11d(i+1)/Doppler_11d(i);
    Dop_5h_rat(j) = Doppler_5h(i+1)/Doppler_5h(i);
    Dop_5i_rat(j) = Doppler_5i(i+1)/Doppler_5i(i);
    Dop_5j_rat(j) = Doppler_5j(i+1)/Doppler_5j(i);
    Dop_12c_rat(j) = Doppler_12c(i+1)/Doppler_12c(i);
```

```
    j=j+1;
end

% Blood Perfusion ratio treat/cont

subplot(2,4,1), plot(DopDays,Dop_5g_rat, 'b-'),legend('Perfusion Ratio
(SF/PBS)','Location','north'),...
    title('Perfusion Ratio [Mouse8]'),xlabel('Days'), ylabel('Ratio
Treatment/Control'),grid on

subplot(2,4,2), plot(DopDays,Dop_11d_rat, 'b-'),legend('Perfusion Ratio
(SF/PBS)','Location','north'),...
    title('Perfusion Ratio [Mouse9]'),xlabel('Days'), ylabel('Ratio
Treatment/Control'),grid on

subplot(2,4,3), plot(DopDays,Dop_11c_rat, 'b-'),legend('Perfusion Ratio
(SF/PBS)','Location','north'),...
    title('Perfusion Ratio [Mouse10]'),xlabel('Days'), ylabel('Ratio
Treatment/Control'),grid on

subplot(2,4,4), plot(DopDays,Dop_5k_rat, 'b-'),legend('Perfusion Ratio
(SF/PBS)','Location','north'),...
    title('Perfusion Ratio [Mouse11]'),xlabel('Days'), ylabel('Ratio
Treatment/Control'),grid on

subplot(2,4,5), plot(DopDays,Dop_5j_rat, 'b-'),legend('Perfusion Ratio
(NDSF/PBS)','Location','north'),...
    title('Perfusion Ratio [Mouse12]'),xlabel('Days'), ylabel('Ratio
Treatment/Control'),grid on

subplot(2,4,6), plot(DopDays,Dop_12c_rat, 'b-'),legend('Perfusion Ratio
(NDSF/PBS)','Location','north'),...
    title('Perfusion Ratio [Mouse13]'),xlabel('Days'), ylabel('Ratio
Treatment/Control'),grid on

subplot(2,4,7), plot(DopDays,Dop_5i_rat, 'b-'),legend('Perfusion Ratio
(NDSF/PBS)','Location','north'),...
    title('Perfusion Ratio [Mouse14]'),xlabel('Days'), ylabel('Ratio
Treatment/Control'),grid on
```

```
subplot(2,4,8), plot(DopDays,Dop_5h_rat, 'b-'),legend('Perfusion Ratio
(NDSF/PBS)','Location','north'),...
    title('Perfusion Ratio [Mouse15]'),xlabel('Days'), ylabel('Ratio
Treatment/Control'),grid on


%% Functions Logistic Study 2: TREATMENT %%

function fun8 = Logistic8(x,c,b1,b2)
    fun8 = (c)./(1+exp(b1+b2*x));
end
function fun9 = Logistic9(x,c,b1,b2)
    fun9 = (c)./(1+exp(b1+b2*x));
end
function fun10 = Logistic10(x,c,b1,b2)
    fun10 = (c)./(1+exp(b1+b2*x));
end
function fun11 = Logistic11(x,c,b1,b2)
    fun11 = (c)./(1+exp(b1+b2*x));
end
function fun12 = Logistic12(x,c,b1,b2)
    fun12 = (c)./(1+exp(b1+b2*x));
end
function fun13 = Logistic13(x,c,b1,b2)
    fun13 = (c)./(1+exp(b1+b2*x));
end
function fun14 = Logistic14(x,c,b1,b2)
    fun14 = (c)./(1+exp(b1+b2*x));
end
function fun15 = Logistic15(x,c,b1,b2)
    fun15 = (c)./(1+exp(b1+b2*x));
end

%% Functions Logistic Study 2: CONTROL %%

function fun8c = Logistic8c(x,c,b1,b2)
    fun8c = (c)./(1+exp(b1+b2*x));
end
function fun9c = Logistic9c(x,c,b1,b2)
    fun9c = (c)./(1+exp(b1+b2*x));
end
```

```
function fun10c = Logistic10c(x,c,b1,b2)
    fun10c = (c)./(1+exp(b1+b2*x));
end
function fun11c = Logistic11c(x,c,b1,b2)
    fun11c = (c)./(1+exp(b1+b2*x));
end
function fun12c = Logistic12c(x,c,b1,b2)
    fun12c = (c)./(1+exp(b1+b2*x));
end
function fun13c = Logistic13c(x,c,b1,b2)
    fun13c = (c)./(1+exp(b1+b2*x));
end
function fun14c = Logistic14c(x,c,b1,b2)
    fun14c = (c)./(1+exp(b1+b2*x));
end
function fun15c = Logistic15c(x,c,b1,b2)
    fun15c = (c)./(1+exp(b1+b2*x));
end
```